# EXCITON DYNAMICS IN SEMICONDUCTOR CONFINED SYSTEMS

THÈSE N° 1908 (1998)

PRÉSENTÉE AU DÉPARTEMENT DE PHYSIQUE

ÉCOLE POLYTECHNIQUE FÉDÉRALE DE LAUSANNE

POUR L'OBTENTION DU GRADE DE DOCTEUR ÈS SCIENCES

PAR

Carlo PIERMAROCCHI

Laurea in fisica, Università degli Studi di Pisa, Italie

de nationalité italienne

acceptée sur proposition du jury:

Prof. A: Quattropani, directeur de thèse
Prof. F. Bechstedt, rapporteur
Prof. B. Deveaud-Plédran, rapporteur
Dr P. Schwendimann, rapporteur

Lausanne, EPFL
1998

# Contents

# Version Abrégée

Je propose dans cette thèse une analyse théorique de la dynamique des porteurs excités par pompage optique dans des semiconducteurs confinés. J'ai examiné en détail les conséquences de l'interaction coulombienne entre électrons et trous, qui conduit à la formation d'états liés, appelés excitons, avec des caractéristiques analogues aux atomes d'hydrogène. J'ai considéré la dynamique des excitons dans des puits quantiques simples, dans des puits quantiques placés à l'interieur d'une cavité optique (microcavité), et dans des fils quantiques.

J'ai examiné la dynamique de relaxation des excitons dans des puits quantiques et j'ai simulé l'évolution temporelle de la photoluminescence. Les effets combinés des populations d' excitons radiatifs et non radiatifs expliquent les temps de déclin observés, qui sont beaucoup plus longs que le temps de recombinaison radiative d'un exciton isolé. En plus, de fortes déviations de l'équilibre thermique donnent une dépendence charactéristique de ces temps de déclin en fonction de la température.

Dans les experiences à excitation non résonnante, les porteurs sont initialement créés dans des états à faible corrélation coulombienne. La relaxation est responsable de la formation des états liés. J'ai examiné la formation des excitons assistée par émission de phonons acoustiques et optiques, et j'ai calculé les temps characteristiques de ce processus dans des puits quantiques de GaAs. La formation peut être géminée ou bimoleculaire. Dans la formation géminée, l'exciton est créé directement par la pompe optique par émission d'un phonon optique. Par contre, dans la formation bimoleculaire l'exciton est créé à partir de couples electron trou à l'équilibre thermique. La première donne une contribution seulement pendant le pompage optique, la deuxième, par contre, dépend seulement de la densité de porteurs libres à disposition. Les effets de la formation assistée par phonons sur la dynamique des porteurs, des excitons, et de l'intensité de la photoluminescence ont été examinés en detail.

Les excitons confinés dans un puits quantique à l'intérieur d'une microcavité donnent des modes couplés appelés polaritons. Ces polaritons présentent une relation de dispersion avec une branche supérieure et une branche inférieure, et leur interaction avec les

phonons est très différente de celle des excitons dans des puits simples. En particulier, on remarque une région de la dispersion des polaritons où ceux-ci s'accumulent. Cette région ne correspond pas au minimum de la dispersion polaritonique, donc on assiste à une forte déviation de l'équilibre thermodynamique. En plus, la diffusion par phonon acoustique est fortement supprimée pour les polaritons de la branche inférieure, par conséquence l'élargissement des raies optiques associé à l'excitation thermique diminue.

Finalement, la dynamique des spectres dans des fils quantiques à semiconducteurs a été examinée. En effet, la recombinaison radiative baisse la densité totale des porteurs, qui évoluent adiabatiquement, et donc restent presque en équilibre thermique. J'ai utilisé une technique de fonctions de Green, avec un potentiel effectif de contact pour l'interaction coulombienne. Pour obtenir une description correcte du rôle joué par les porteurs liés et non liés, j'ai résolu l'équation de Bethe Salpeter pour la fonction de Green à deux particules. Cette méthode a donné la possibilité d'observer dans les spectres d'absorption du gain optique en même temps que la résonance excitonique. En plus, les effets de la corrélation électron trou, calculés par une méthode auto consistante par l'équation de Bethe Salpeter, compensent la renormalisation de l'énergie de la bande interdite et expliquent l'absence d'un déplacement du sommet de la photoluminescence.

# Summary

The purpose of my thesis is to provide a theoretical analysis of the dynamics of optically excited carriers in semiconductor confined systems. In particular, I will focus the investigations on the effects due to the presence of a strong electron-hole Coulomb correlation. The Coulomb interaction leads to the formation of hydrogen-like bound states called excitons. The dynamics of these states is investigated in bare and cavity embedded quantum wells, and in quantum wires.

I have investigated the dynamics of the relaxation of excitons in quantum wells due to the interaction with acoustic phonons and I have reproduced the temporal evolution of the photoluminescence emission. I have explained why the decay times observed in non resonant photoluminescence experiments are much slower than the radiative recombination time of a single exciton. Furthermore, deviations from the thermal equilibrium gives a characteristic dependence of these decay times on the temperature.

The build-up of the photoluminescence is related to the relaxation by phonon emission of the excited electron-hole pairs. Initially, the pairs created at high energy are not bound, and the formation of bound excitons occurs during the relaxation. I have described the exciton formation due to the emission of acoustic and optical phonons, and I have calculated the characteristic times for this process in GaAs quantum wells. The formation can be geminate or bimolecular. In the geminate formation, the exciton is directly created by the photon of the external pump by simultaneous emission of an optical phonon, while in the bimolecular formation the exciton is created from thermalized electron-hole pairs. In the first case the formation occurs only during the laser pump, while in the second case the formation depends on the total density of carriers available in the crystal. The effects of the phonon assisted formation on the overall dynamics of free carriers, excitons and of the photoluminescence are discussed.

Excitons confined in a quantum well coupled with the photons modes of a semiconductor microcavity give mixed exciton-photon states called microcavity polaritons. The dynamics of the population of polaritons, which present an energy dispersion with an upper and lower branch, shows peculiar characteristics. In particular, a bottleneck

region above the minimum of the lower polariton dispersion exists. In this region the population of polaritons is accumulated, and strong deviations from the thermal equilibrium are thus produced. Moreover, for the lower polariton states, a suppression of the scattering by acoustic phonons produces a strong inhibition of the thermal broadening.

Finally, the dynamics of the photoluminescence spectra in semiconductor quantum wires is investigated. The time resolved photoluminescence experiments, the radiative recombination modifies adiabatically the total density, and the hypothesis quasi-thermal equilibrium can be applied. The optical spectra probes a system which ranges from a regime of ionized electron hole plasma to a gas of weakly interacting bound excitons. In order to describe such a complex system, I have used a Green's functions technique, and I have modeled the Coulomb interaction using a contact potential. This approach allows to observe in the absorption spectra a gain region close to the excitonic resonance. Moreover, the effects of the electron-hole correlations, calculated in a numerical self consistent way, explain the absence of the shift of the photoluminescence emission due to Coulomb induced band gap renormalization.

# Chapter 1

# Introduction

In this thesis we will give a theoretical description of the carrier dynamics in optically excited semiconductors. In particular, we will focus on the effects of the carrier populations on the optical properties of quantum wells, quantum wires, and semiconductor microcavities. These properties are experimentally investigated both in time resolved and density dependent experiments, and the related theoretical analysis leads to a very complex problem where the effects of acoustic and optical phonons have to be taken into account. Moreover, in typical experimental conditions, the Coulomb interaction between the excited carriers affects the optical spectra. One of the strongest effect is provided by the electron-hole correlation, which may give rise to an enhancement of the light emission in particular regimes of density and temperature.

At low densities, the electron-hole Coulomb correlation can be modeled using the excitonic picture [Wannier, 1937]. The photoexcited electron and hole bind together and propagate through the crystal in a state with a well defined center of mass wave vector $\mathbf{q}$. This excited state corresponds to an elementary excitation of the crystal in the case of optical measurements, and is thus called *exciton*. The exciton can be built up from a basis of Hartree-Fock states. Each element of this basis represents a single *non interacting* electron hole pair with a given center of mass momentum $\mathbf{q}$, and relative momentum $\mathbf{k}$: $|\phi_{HF}(\mathbf{q},\mathbf{k})\rangle$. When a photon is absorbed in the sample the most general excited state of the crystal is given by a linear superposition of these Hartree-Fock states

$$|\phi^{\lambda}_{Ex}(\mathbf{q})\rangle = \sum_{\mathbf{k}} A^{\lambda}_{\mathbf{q}}(\mathbf{k})|\phi_{HF}(\mathbf{q},\mathbf{k})\rangle \ . \tag{1.1}$$

Due to the periodicity of the crystal, the center of mass wave vector $\mathbf{q}$ is a good quantum number. The state $|\phi^{\lambda}_{Ex}(\mathbf{q})\rangle$ is an eigenstate of the the total Hamiltonian of the system (which contains the electron hole Coulomb interaction), and the coefficients $A^{\lambda}_{\mathbf{q}}(\mathbf{k})$ must be obtained from a Schrödinger equation [Knox, 1963],[Bassani, 1975]. This equation

can be simplified as to obtain a simple hydrogen-like equation (the Wannier equation), and an hydrogenic envelope function for the electron hole relative motion. The index $\lambda$ labels the states of the Coulomb problem. It has been explicitly shown [Sham, 1966] that the presence of the complex structure of the electronic states in the crystal is correctly taken into account considering the electron and the hole effective masses and the static dielectric constant in the Coulomb interaction.

The absorption coefficient calculated using the state in Eq.1.1 as the final state is exact for a single electron-hole pair excited in the sample [Elliott, 1957]. It can be compared with the experimental spectra only when the external laser pump is a weak probe of a crystal which is initially in the vacuum state. However, in a typical continuous wave or time resolved experiment, the condition of single photon excitation of the system is fairly distant from the physical reality. This is especially true for photoluminescence experiments, in which the spontaneous emission of photons is collected from a system with a great number of excited electron-hole pairs. Actually, when several electron-hole pairs are created in a crystal, the optical properties have to be obtained by solving a many body problem. The dynamics of interaction with the photon and phonon field is also not the same as for a single electron-hole pair. In order to take into account these many body effects, two approaches have been taken. We will refer to them as the *excitonic*, and the *fermionic* approaches. In principle the two approaches are differentiated by the choice of the starting basis which is used in the calculation, but are equivalent. The problem, however, cannot be solved exactly and approximations which are appropriate for different physical situations may be conveniently introduced using both the approaches.

The excitonic approach states that when $N$ photons excite the crystal, $N$ excitons are created in the sample. In this approach the concept of exciton as a new particle in the system is introduced

$$|\phi_{Ex}^{\lambda}(\mathbf{q})\rangle = b_{\lambda,\mathbf{q}}^{\dagger}|vac\rangle \ , \tag{1.2}$$

where $b_{\lambda,\mathbf{q}}^{\dagger}$ is the exciton creation operator. This approach is particularly convenient when for some physical reason the analysis of a single excitonic branch can be considered. When a quasi thermal equilibrium is reached with a carrier thermal energy $k_BT$ much smaller than the exciton binding energy $E_b$, or when the external pump excitation is resonant with the lowest $1s$ excitonic level, the stationary and time resolved optical properties of the system are correctly modeled restricting the discussion to the only $1s$ exciton branch. In fact, the full fermionic Hamiltonian, including the electron and hole operators, can be rewritten as a microscopic excitonic Hamiltonian which includes a hierarchy of terms to all (even) orders in bosonic operators [Hanamura, 1972]. In

the investigation of the dynamics of carrier population, the natural parameter for the truncation of this hierarchy is $n_{exc}a_B$, where $a_B$ is the Bohr radius of the hydrogenic problem, and $n_{exc}$ is the total exciton density. Therefore, in the lowest approximation, excitons in bound states can be considered as pure bosons at low density since

$$[b^{\dagger}_{1s,\mathbf{q}} b_{1s,\mathbf{q}'}] = \delta_{\mathbf{q},\mathbf{q}'} - O(na_B^d) \ . \tag{1.3}$$

This approximation will be used in this thesis for the description of the effects on the carrier dynamics due to the interaction with acoustic and optical phonons. The excitonic approach can also be used for the calculation of collision broadening of the excitons in several semiconductor systems [Bobrysheva, 1980], [Manzke, 1984], [Braun, 1998], [Ciuti, 1998]. We want just to notice that in the calculation of the non linear optical response, the correct parameter for the hierarchy truncation becomes the field intensity. Non linear optical properties have been calculated using the excitonic approach in different systems [Hanamura, 1977], [Combescot, 1989], [Hiroshima, 1989], [Savasta, 1996], [Östreich, 1998].

In the fermionic approach the crystal excited by $N$ photons contains $N$ electrons and $N$ holes. The simplest approximation is the mean-field or Hartree-Fock approximation, where the correlations between the carriers is taken into account on average only. The Coulomb correlation effects can be included in the absorption and emission of photons through the dynamical response of the interband polarization to the external electromagnetic field. In this way, the excitonic resonance at low carrier density is correctly reproduced, since it turn out that the dynamics equation of motion is equivalent to the Wannier equation. This approach is used for instance in the semiconductor Bloch equations [Lindberg, 1988] and in the semiconductor luminescence equations [Kira, 1998]. We want to stress that the optical properties are calculated in a different way with respect to the original Elliott approach. In the Elliott approach, the first step was to calculate the correct state of the system (the exciton) using the Wannier equation. Then the optical properties are calculated with Fermi's golden rule. On the other hand, in the fermionic approach the state of the crystal will still be in the Hartree-Fock approximation, but the explicit introduction of an external perturbation in the dynamical equations yields optical spectra where the electron-hole correlations are included up to the excitonic level. Obviously, for a single electron hole pair the two approaches coincide. However, when effects related to the density are considered, some physics is missed in the Hartree-Fock approximation. This is because the occupation of the pair population is distributed over the Hartree-Fock spectrum which is given by the free electron-hole energies with a density dependent band gap renormalization. However, in the $k_BT \ll E_b$ regime the pair population occupies the bound states levels which do

not appear as eigenstates of the crystal at the Hartree-Fock level. Thus, new and interesting phenomena such as the boser effect in semiconductor microcavities [Yura, 1994], [Imamoglu, 1996], excitonic gain in semiconductor quantum wells [Kozlov, 1996], and Bose-Einstein condensation of excitons, cannot be investigated. Furthermore, some thermodynamic relations, e. g. the Saha (action mass) law describing the equilibrium between the populations of bound exciton pairs and unbound free carriers, require a treatment beyond the Hartree-Fock approximation [Stolz, 1979].

In this thesis we will use both the excitonic and fermionic approaches, and in the latter case we will go beyond the Hartree-Fock approximation. In the description of the interaction of carriers with the phonon (acoustic and optical) field we will adopt the excitonic picture. In time resolved photoluminescence experiments in quantum well samples the light is collected at the exciton resonance, and the effects of the exciton population are essential for an understanding of the characteristic times. In fact, even if the radiative recombination time of the exciton in quantum wells is very short (of the order of 10 ps) [Andreani, 1991], the photoluminescence emission at the exciton energy decays with a characteristic time that is much slower (several hundreds of ps) [Martinez-Pastor, 1993], [Yu, 1995]. This can be explained considering an excitonic population distributed over radiative and non radiative states. The slow decay of the photoluminescence time is then understood in terms of the relaxation of excitons by emission of acoustic phonons. We investigate this point in Chap.2, where the effects of the relaxation by acoustic phonons and of the radiative recombination rate on the evolution of the excitonic population are explicitly taken into account. We have discovered that as the excitons in the semiconductor structure are coupled to the external world through the electromagnetic interaction, strong deviations from the thermal equilibrium appear. Consequences on the temperature dependence of the photoluminescence decay time are predicted.

In non-resonant experiments the sample is excited well above the exciton resonance, in the continuum of the electron-hole hydrogenic spectrum. We consider in Chap.3 the relaxation of the electron-hole pairs through emission and absorption of acoustic and optical phonons starting from states in the continuum. This relaxation process leads to the formation of bound $1s$ electron-hole pairs and we refer to it as an exciton formation process. The dynamics of this process is investigated, and the effects on the rise of the photoluminescence signal due to the relaxation by acoustic and optical phonon identified. The Coulomb correlation of the electron-hole states in the continuum does not strongly affect the carrier-phonon interaction, and the formation rates are calculated by approximating the envelope functions in the continuum with plane waves. Finally,

the thermal equilibrium between the states in the continuum and the bound states is considered. We have found that, when the lattice thermal energy is lower than $E_b$, the thermalization through phonon scattering is very slow, and an excess of unbound states with respect to the thermal case may persist up to several hundreds of picoseconds.

One of the advantages of the excitonic basis is that the exciton-photon problem can be solved exactly and the useful concept of polariton introduced [Hopfield, 1958]. Polaritons are the real excited states of the crystal and consist of mixed exciton-photon states with a characteristic dispersion. In the investigation of the mechanisms of relaxation by phonons it is the dynamics of polaritons which must be considered. The peculiar dispersion of the polaritons in bulk samples has lead to the discovery of the bottleneck effect in the relaxation dynamics in such systems [Toyozawa, 1959], [Sumi, 1975], [Weisbuch, 1979]. This effect can also be evidenced in the two-dimensional equivalent of bulk polaritons, i.e., in microcavity polaritons. Microcavity polaritons are the states resulting from the exact diagonalization of two-dimensional excitons confined in a quantum well with two-dimensional cavity photons. The latter being obtained by confinement of the photon through a planar Fabry-Pérot system [Savona, 1996], [Savona, 1998]. In the case of quantum wells embedded in microcavities the dimensionality of the excitons in the quantum well matches, as for the bulk case, the dimensionality of the cavity confined photon modes. We investigate the dynamics of the population of microcavity polaritons in Chap.4. The peculiar shape of the cavity polariton dispersion also provides a physical interpretation for the absence of thermal broadening of the lower polariton peak at low temperatures. In fact, for lower polaritons close to the $q = 0$ region, scattering with acoustic phonons is strongly inhibited. We will give a comparison of the theory predicting this effect with recent experimental results.

Our aim in Chap.5 is to go beyond the usual Hartree-Fock approximation for the fermionic basis used in the calculation of the optical properties. We will propose a treatment where excitons are considered as composite fermions. We will take into account both the populations of strongly correlated electron-hole bound pairs and of the weakly correlated "free" carriers on the same footing. We will use a nonequilibrium Green's functions technique which allows a self consistent numerical treatment of the equations. The model leads to a set of very complex integral equations that can be simplified by choosing a contact potential model for the carrier interaction, and same masses for the electrons and the holes. This approximation represents the simplest model which enables the study of both bound and free carrier populations, and can be exploited for the analysis of new effects. Up to now, the onset of optical gain has been considered in the regime of a degenerate e-h plasma. On the other hand, an excitonic approach results

in a population of bosonic particles, and a gain is not expected. Using our approach we will show that an "excitonic" gain can be obtained in a low temperature regime. This gain is well distinguished from the usual electron-hole plasma gain because it is obtained at lower excitation densities and presents peculiar spectral characteristics. The self consistent calculation of the broadening and of the excitonic effects leads also to a physical interpretation for the absence of a direct evidence of band gap renormalization in photoluminescence spectra from quantum wires. In fact, the effects of the excitonic correlation persist even in the regime of degenerate electron-hole plasma, and mask, together with the broadening of the states, the band gap renormalization.

# Chapter 2

# Dynamics of exciton relaxation in quantum wells

In this chapter we give some details on the interaction of the confined excitons with acoustic phonons and we investigate the dynamics of exciton relaxation within the $1s$ exciton band. We calculate the exciton scattering rate due to acoustic phonons, and we solve the Boltzmann equation for the exciton population, considering also the exciton radiative recombination. Since we want to describe relaxation processes within the $1s$ exciton band only, optical phonons will not contribute because the exchanged energy is always smaller than the characteristic optical phonon energy ($\hbar\omega_{LO}$ =36 meV in GaAs and 47 meV in AlAs). In the investigation of the exciton relaxation, we will assume an initial distribution for the excitonic population. Some features of the exciton dynamics do not depend on the choice of the initial distribution, while others, mainly at short times, are affected by its shape. The shape of the initial distribution is related to the process of exciton formation, and will be treated in Chap.3. We better focus in this chapter on the properties which do not depend on the initial condition. The most interesting measurable quantity which results to be independent on the initial condition is the photoluminescence decay time. This characteristic time describes the dynamics of the exciton recombination after a stationary distribution function for the exciton population has been reached. For a temperature $k_BT \ll E_b$ the stationary distribution function is not affected by the presence of excited excitonic levels ( the $2s$ level is at $8/9E_b$), and by the presence of the light hole subband which is well above the continuum edge in quantum wells of width less than 12 nm. The dynamics within the $1s$ band only is thus a good approximation for the modelling of the characteristic times. It has been shown theoretically [Andreani, 1991] and experimentally [Deveaud, 1991a]

that the exciton radiative lifetime is very short in quantum wells. However, this short lifetime do not reflect itself in a short photoluminescence decay time in non resonant experiments. This is due to the distribution of excitons over radiative and non radiative states, which also give rise to a dependence of the decay times on the lattice temperature. The temperature dependence of the decay time has been the subject of many theoretical and experimental investigations, [Feldmann, 1987], [Andreani, 1991], [Citrin, 1993], [Martinez-Pastor, 1993]. In all the previous theoretical investigation the assumption of a thermal distribution for the exciton population has been considered. Solving the full Boltzmann equation, we have found instead that strong deviation from a thermal distribution can be found, mainly in the regime of low temperature. These deviations from the thermal equilibrium affect the temperature dependence of the decay time [Piermarocchi, 1996, Piermarocchi, 1995].

## 2.1 Deformation potential interaction

The main scattering mechanism for excitons interacting with acoustic phonons is provided by the deformation potential interaction. When an external pressure is applied to a semiconductor, the lattice constant and thus the eigenstates and eigenvalues of the crystal are modified. The effect of the pressure on the crystal is described by the symmetric stress tensor $\epsilon_{ij}$

$$\epsilon_{ij}(\underline{\mathbf{x}}) = \frac{1}{2}\left(\frac{\partial u_i}{\partial x_j} + \frac{\partial u_j}{\partial x_i}\right) , \tag{2.1}$$

where the $\underline{\mathbf{u}}(\underline{\mathbf{x}})$ [1] is the displacement vector. Let us consider an infinitesimal volume $dV$, the expression of this element of volume after the deformation become

$$dV' = dV(1 + Tr\epsilon_{ij}). \tag{2.2}$$

The change in energy for the electronic states at the bottom of the conduction band and at the top of valence band due to the deformation of the crystal is proportional to the relative variation of the volume

$$Tr\epsilon_{ij} = \frac{dV' - dV}{dV} , \tag{2.3}$$

and can be written as

$$\Delta Ec = a_c Tr\epsilon_{ij} \tag{2.4}$$

$$\Delta Ev = a_v Tr\epsilon_{ij} . \tag{2.5}$$

[1] We will use the notation $\underline{\mathbf{x}}$ for 3D vectors, $\mathbf{x}$ for 2D vectors, and $x$ for 1D vectors

The quantity $a_c - a_v$ is measured looking at the variation of the band gap under an hydrostatic pressure to the sample. The experimental values for the pressure dependence of the direct band gap in bulk GaAs range from 10.6 to 15.3 meV/kbar [Landolt, 1982], [Chang, 1984], and are in agreement with the theoretical calculation [Chang, 1984]. Using a Bulk modulus of 0.77 Mbar, we obtain a range for $a_c - a_v$ from 8.6 eV to 11.8 eV. On the other hand, the band edge deformation potentials $a_c$ and $a_v$ can not be measured separately. In the absence of direct measurements, the conduction and valence band deformation potential have been determined by fitting theoretical calculations to the existing free carrier mobility data. For bulk GaAs, fitting procedures has provided a range from -7.0 eV [Wolfe, 1970] to -15.3 eV [Pfeffer, 1984] for $a_c$. We have calculated the exciton acoustic phonons scattering rates using different values for the for $a_c$ and $a_v$, and we have remarked that the scattering rates are mostly sensitive to the $a_c - a_v$ parameter. In the following we will use $a_c - a_v$ =-9.7 eV [Welber, 1975], and $a_c$ =-7.0 eV [Wolfe, 1970].

Phonons represents elastic waves in the system due to the lattice vibration. The elastic wave with a given wavevector $\underline{\mathbf{q}}$, and polarization $\underline{\boldsymbol{\varepsilon}}(\underline{\mathbf{q}})$ read

$$\underline{\mathbf{u}}(\underline{\mathbf{x}}) = \sqrt{\frac{\hbar}{2\rho V u|\underline{\mathbf{q}}|}}\underline{\boldsymbol{\varepsilon}}(\underline{\mathbf{q}})(c_{\underline{\mathbf{q}}}e^{i\underline{\mathbf{q}}\cdot\underline{\mathbf{x}}} + c^{\dagger}_{\underline{\mathbf{q}}}e^{-i\underline{\mathbf{q}}\cdot\underline{\mathbf{x}}}) \tag{2.6}$$

Here $\rho$ and $u$ are the density and the longitudinal sound velocity in GaAs respectively and $V$ is the quantization volume. The relative compression of the volume associated with this elastic wave is given by

$$Tr\epsilon_{ij} = \nabla \cdot \underline{\mathbf{u}}(\underline{\mathbf{x}}) = i\sqrt{\frac{\hbar}{2\rho V u|\underline{\mathbf{q}}|}}\underline{\mathbf{q}} \cdot \underline{\boldsymbol{\varepsilon}}(\underline{\mathbf{q}})(c_{\underline{\mathbf{q}}}e^{i\underline{\mathbf{q}}\cdot\underline{\mathbf{x}}} - c^{\dagger}_{\underline{\mathbf{q}}}e^{-i\underline{\mathbf{q}}\cdot\underline{\mathbf{x}}}) \ . \tag{2.7}$$

Therefore, the deformation potential interaction is due to the coupling with longitudinal acoustic phonon modes only, and the matrix elements is proportional to $\sqrt{|\underline{\mathbf{q}}|}$.

Acoustic phonons interact with electronic states also through piezoeletric scattering. The electric field induced by the piezoelectric effect is proportional through the piezoelectric constant to the displacent vector $\underline{\mathbf{u}}(\underline{\mathbf{x}})$ . This field in the crystal interacts with the carriers, and the dependence of the piezolectric coupling on the phonon wavevector is thus $1/\sqrt{|\underline{\mathbf{q}}|}$. Furthermore, the pizoelectric interaction couples with both longitudinal and transverse acoustic phonon modes. However, it has been shown that in typical III-V materials the piezoelectric constant is very small and the resulting scattering rates due to this interaction are more than one order of magnitude smaller than the rates due to the deformation potential interaction [Stolz, 1989].

The deformation potential interaction for an electron hole pair is written in the form:

$$U(r_e, r_h) = \Delta(r_e)a_e - \Delta(r_h)a_h \ , \tag{2.8}$$

where $\Delta(r_e) = \nabla \cdot \underline{\mathbf{u}}(\underline{\mathbf{x}})|_{x=r_e}$ and $\Delta(r_h) = \nabla \cdot \underline{\mathbf{u}}(\underline{\mathbf{x}})|_{x=r_h}$ are the relative deformations of the lattice induced by phonons at the points where the electron and the hole are located. The exciton phonon interaction results from the sum of the phonon-electron and phonon-hole interaction. The Eq.2.8 can be rewritten in term of center of mass and relative variable of the electron hole pair, and is calculated for an exciton confined in the quantum wells. Using a separable envelope function for the exciton, the exciton-phonon Hamiltonian corresponding to the deformation potential interaction of Eq.2.8 is given by

$$H_{exc-ph} = \sum_{q_z} \sum_{\mathbf{q},\mathbf{k},\mathbf{k}'} G(\mathbf{q}, q_z)\delta_{\mathbf{k}',\mathbf{k}+\mathbf{q}}(c_{\mathbf{q},q_z} - c^{\dagger}_{-\mathbf{q},q_z})b^{\dagger}_{\mathbf{k}'}b_{\mathbf{k}} \ , \tag{2.9}$$

where $b^{\dagger}_{\mathbf{k}}$ ($b_{\mathbf{k}}$) is the creation (annihilation) operator of 2D excitons with in-plane wave vector $\mathbf{k}$, and $c^{\dagger}_{\mathbf{q},q_z}$ ($c_{\mathbf{q},q_z}$) is the creation (annihilation) of 3D phonons with wave vector $\underline{\mathbf{q}} = (\mathbf{q}, q_z)$ ($z$ is the growth direction). Translational invariance along the quantum well plane implies the conservation of the in-plane momentum $\mathbf{k}$, as explicitly shown in Eq.2.9 by the presence of the Kronecker delta function. The z component of the wave vector in not conserved and a sum over $q_z$ appears in Eq.2.9. The term $G(\mathbf{q}, q_z)$ contains all the parameters of the interaction and reads

$$\begin{aligned} G(\mathbf{q}, q_z) &= i\sqrt{\frac{\hbar(|\mathbf{q}|^2 + q_z^2)^{1/2}}{2\rho V u}}[a_e I_e^{\parallel}(|\mathbf{q}|)I_e^{\perp}(q_z) \\ &\quad -a_h I_h^{\parallel}(|\mathbf{q}|)I_h^{\perp}(q_z)] \ . \end{aligned} \tag{2.10}$$

The terms $I^{\parallel}_{e\ (h)}(|\mathbf{q}|)$ and $I^{\perp}_{e\ (h)}(q_z)$ are the superposition integrals of the exciton envelope function with the phonon wave function (plane wave) in the in-plane and z directions respectively. Using the exciton envelope function

$$F(\boldsymbol{\rho}, z_e, z_h) = \sqrt{\frac{2}{\pi a_B^2}} e^{-|\boldsymbol{\rho}|/a_B} f_e(z_e) f_h(z_h) \ , \tag{2.11}$$

where $\boldsymbol{\rho}$ is the in-plane electron-hole relative position, $a_B$ is the exciton Bohr radius, and $f_{e\ (h)}(z)$ are the electron (hole) envelope functions in the growth direction, the superposition integrals read

$$I^{\parallel}_{e\ (h)}(|\mathbf{q}|) = \left(1 + \left(\frac{m_{h\ (e)}}{2M}|\mathbf{q}|a_B\right)^2\right)^{-3/2} \ , \tag{2.12}$$

$$I^{\perp}_{e\ (h)}(q_z) = \int dz |f_{e\ (h)}(z)|^2 e^{iq_z z} \ , \tag{2.13}$$

where $M = m_e + m_h$. These integrals introduce cutoffs in the term $G(\mathbf{q}, q_z)$ for $|\mathbf{q}| > 1/a_B$, and for $q_z > 2\pi/L_{QW}$ where $L_{QW}$ is the QW width. The latter cutoff originates

from the electron and hole localization in the QW region described by the envelope functions $f_{e\ (h)}(z)$. This dependence of the cutoff in $I^{\perp}_{e\ (h)}(q_z)$ on $L_{QW}$ indicates that the exciton-phonon interaction decreases for larger QWs. This cutoff becomes critical for small QWs. In this case, the penetration in the barriers of the exciton wave function has to be correctly included in $f_{e\ (h)}(z)$, otherwise the scattering rates are overestimated. The cut-off in the perpendicular direction implies that the exciton phonon coupling vanishes when the acoustic phonon wavelength is much smaller than the spatial extension of the exciton confinement wavefunction in the growth direction. A similar interpretation can be given for the in plane superposition integrals, in this case the comparison of the phonon wavelength with the in plane electron hole relative position, related to the Borh radius, determines the cut off.

## 2.2 Exciton acoustic phonon scattering rates

The intraband transition rate for excitons scattered by acoustic phonons is calculated in the Born approximation. We obtain in the case of transitions involving absorption of a phonon

$$W^{abs}_{\mathbf{k}\to\mathbf{k}'} = \frac{2\pi}{\hbar}\sum_{q_z} |\langle \mathbf{k}'|\langle n_{\mathbf{q},q_z}|H_{exc-ph}|n_{\mathbf{q},q_z}+1\rangle|\mathbf{k}\rangle|^2 \\ \delta\left(E_{exc}(\mathbf{k}') - E_{exc}(\mathbf{k}) - E_{ph}(\mathbf{q},q_z)\right) \ . \tag{2.14}$$

Here $|\mathbf{k}\rangle$, $|\mathbf{k}'\rangle$ are the initial and final exciton states, and $|n_{\mathbf{q},q_z}\rangle$, $|n_{\mathbf{q},q_z}+1\rangle$ are the initial and final phonons states. $E_{exc}(\mathbf{k}) = \hbar\omega_{exc}+\hbar^2k^2/2M$, and $E_{ph}(\mathbf{q},q_z) = \hbar u(|\mathbf{q}|^2+q_z^2)^{1/2}$, are the exciton and phonons energies respectively. The rate $W^{abs}_{\mathbf{k}\to\mathbf{k}'}$ is then averaged over the whole phonon ensemble, which is assumed to be in thermal equilibrium (phonon bath). Since the in-plane wave vector is conserved in the interaction, only phonons having $\mathbf{q} = \mathbf{k}'-\mathbf{k}$ contribute to the ensemble average. The sum over $q_z$ may be performed exactly in the continuum limit because of the delta function in Eq.2.14. We finally obtain

$$W^{abs}_{\mathbf{k}\to\mathbf{k}'} = \frac{4\pi}{\hbar}\frac{L_z}{2\pi}\frac{\hbar}{2\rho V u}\frac{(|\mathbf{k}-\mathbf{k}'|^2+(q_z^0(\theta))^2)}{|\hbar u q_z^0(\theta)|} \\ \times\left(a_e I^{\parallel}_e(|\mathbf{k}'-\mathbf{k}|)I^{\perp}_e(q_z^0) - a_h I^{\parallel}_h(|\mathbf{k}'-\mathbf{k}|)I^{\perp}_h(q_z^0)\right)^2 \\ \times n_{ph}(E_{exc}(\mathbf{k}')-E_{exc}(\mathbf{k}))\ , \tag{2.15}$$

where $q_z^0$ is the root of the argument of the delta function

$$q_z^0 = \left(\left(\frac{E(\mathbf{k}')-E(\mathbf{k})}{\hbar u}\right)^2 - |\mathbf{k}-\mathbf{k}'|^2\right)^{1/2}\ , \tag{2.16}$$

and $n_{ph}(E)$ is the Bose distribution function of the phonon population. The transitions assisted by phonon emission are calculated in a similar way, and contain a term $(n_{ph}+1)$ instead of $n_{ph}$. We notice that $W^{abs}_{\mathbf{k}\to\mathbf{k}'}$ depends only on $|\mathbf{k}|$, $|\mathbf{k}'|$, and the relative angle $\theta$ because the interaction is isotropic. We remark that solutions of Eq.2.16 do not exist for arbitrary values of $|\mathbf{k}|$, $|\mathbf{k}'|$ and $\theta$. The equation 2.16 defines a phase space for the scattering process. If the initial exciton is at $|\mathbf{k}| = 0$ the final $|\mathbf{k}'|$ must have a kinetic energy such as

$$\frac{\hbar^2 k'^2}{2M} > \hbar u k' \tag{2.17}$$

which corresponds to

$$k' > \frac{2Mu}{\hbar} = k_{min} \ . \tag{2.18}$$

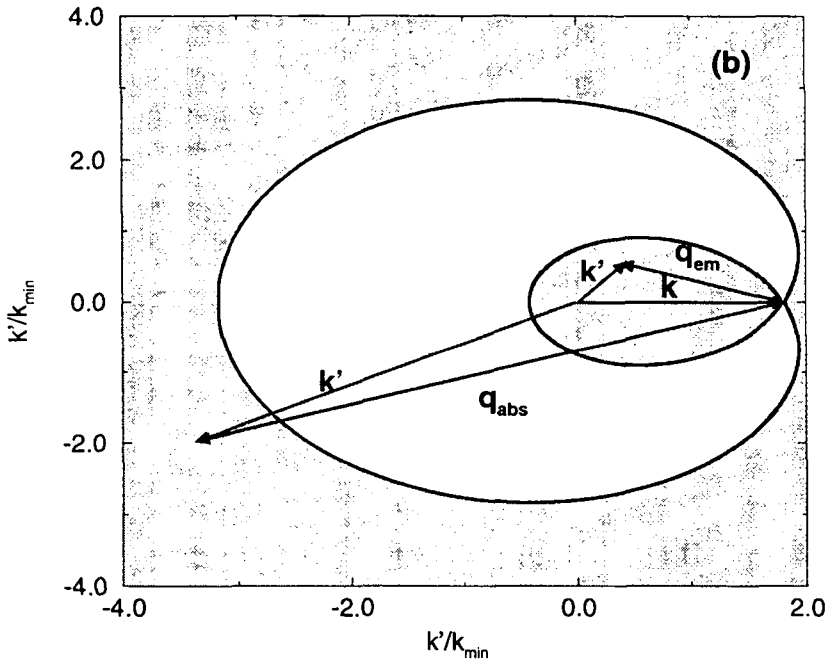


Figure 2.1: Scattering phase space for an exciton with fixed $\mathbf{k}$.

We give in Fig.2.1 the phase space for the scattering of an exciton for a given initial $\mathbf{k} \neq 0$. The shadowed region corresponds to the allowed $\mathbf{k}'$. The in plane component of the emitted ($q_{em}$) and absorbed phonon ($q_{abs}$) are shown. We remark that forward scattering has a larger phase space with respect to backward scattering. The form of a

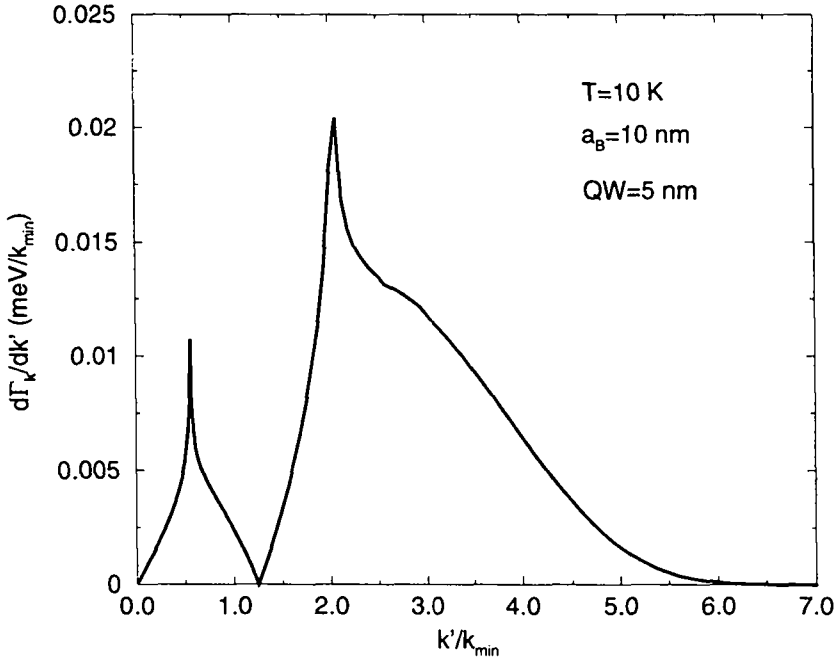


Figure 2.2: Scattering rate

characteristic scattering rate is given in Fig.2.2 where we plot the quantity

$$\frac{d\Gamma_{\mathbf{k}}}{dk'} = \int d\theta k' (W^{abs}_{\mathbf{k}\to\mathbf{k}'} + W^{em}_{\mathbf{k}\to\mathbf{k}'})$$

as a function of $k'$. The initial value of $|\mathbf{k}| = 1.3\ k_{min}$, the temperature is 10 K and the quantum well width is 50 Å. The emission and absorption correspond to the region above and below the initial $k$ respectively. The scattering rate has two peaks in the absorption and emission region corresponding to $q_z^0 = 0$. This means that emission of phonons along the quantum well plane is enhanced. The rate decreases at high energies, this is due to the cut off in the superposition integrals. In the materials considered here it is the cut off in $I_e^{\perp}(q_z^0)$ the which dominates over $I_h^{\parallel}(|\mathbf{k}' - \mathbf{k}|)$.

## 2.3 Boltzmann equation

The Boltzmann equation for the population $n_{\mathbf{k}}$ at a given in-plane $\mathbf{k}$ using the scattering rates $W_{\mathbf{k}\to\mathbf{k}'}$ reads

$$\dot{n}_{\mathbf{k}} = \sum_{\mathbf{k}'} W_{\mathbf{k}'\to\mathbf{k}} n_{\mathbf{k}'}(n_{\mathbf{k}} + 1) - \sum_{\mathbf{k}'} W_{\mathbf{k}\to\mathbf{k}'} n_{\mathbf{k}}(n_{\mathbf{k}'} + 1) - \Gamma_{\mathbf{k}} n_{\mathbf{k}} \ . \tag{2.19}$$

$\Gamma_{\mathbf{k}}$ is the radiative recombination rate. In the QW, a 2D exciton with in plane wave vector $\mathbf{k}$ interacts with photons having the same in plane wave vector, but with all possible values of $k_z$. This gives rise to a large radiative recombination rate with respect to the bulk case where the radiative recombination occurrs only through propagation to the crystal surface [Agranovich, 1966]. We have a density of states for the radiative decay

$$\rho(|\mathbf{k}|,\omega) = \sum_{k_z} \delta(E(\mathbf{k}) - \hbar\frac{c}{n}\sqrt{|\mathbf{k}|^2 + k_z^2}) =$$

$$= \frac{L_z}{2\pi}\frac{n}{\hbar c}\frac{2k_0}{\sqrt{k_0^2 - |\mathbf{k}|^2}}\theta(k_0 - |\mathbf{k}|) \ , \tag{2.20}$$

where $k_0$ is $n\omega_{exc}/c$, and $n$ is the refraction index. The function $\theta(k)$ is the Heavyside function. We remark that the radiative recombination occurs only for states with $|\mathbf{k}| < k_0$. This defines the radiative zone. The radiative recombination rate for transverse excitons with a given $\mathbf{k}$ is calculated by the Fermi's golden rule using the exciton-photon interaction Hamiltonian [Andreani, 1991], and reads

$$\Gamma_{\mathbf{k}}^T = \frac{2\pi}{n}\frac{e^2}{m_0 c}\frac{f_{xy}}{S}\frac{k_0}{k_z} \ , \tag{2.21}$$

where $f_{xy}/S$ is the oscillator strength per unit surface for transverse excitons, and $k_z = \sqrt{k_0^2 - |\mathbf{k}|^2}$. For longitudinal excitons a factor $k_z/k_0$ replaces $k_0/k_z$ in Eq.2.21. We average the recombination rate in the whole radiative region in order to eliminate the infrared divergence of $\Gamma_{\mathbf{k}}$. We obtain

$$< \Gamma_{\mathbf{k}}^T >= \frac{2\Gamma_0}{\Delta\mathbf{k}_{rad}}\int_{rad}\frac{k_0}{k_z}d\mathbf{k} = 4\Gamma_0 \tag{2.22}$$

$$< \Gamma_{\mathbf{k}}^L >= \frac{2\Gamma_0}{\Delta\mathbf{k}_{rad}}\int_{rad}\frac{k_z}{k_0}d\mathbf{k} = \frac{4}{3}\Gamma_0 \ , \tag{2.23}$$

where $\Gamma_0 = (\pi e^2/nm_0c)(f_{xy}/S)$, $\Delta\mathbf{k}_{rad}$ is the area of the radiative zone in the $\mathbf{k}$ space, and L and T indicate longitudinal and transverse excitons respectively. Assuming an initial isotropic distribution and taking into account that $W_{\mathbf{k}\to\mathbf{k}'}$ depends only on $|\mathbf{k}|$, $|\mathbf{k}'|$, and the angle $\theta$ between them, one readily sees that the distribution remains isotropic for all times. All the exciton parameters as Bohr radius, binding energies, oscillator strengths, and masses, are taken from theoretical calculations [Andreani, 1989], [Andreani, 1990]. We solve the Eq.2.19 by Runge-Kutta numerical integration, using a grid of 800 $|\mathbf{k}|$ points in the region from 0 up to 20 $k_0$, and 250 femtoseconds of temporal step. The terms $(n_{\mathbf{k}} + 1)$ are related to the bosonic character of excitons, and correspond to stimulated emission and absorption processes in the dynamics. However

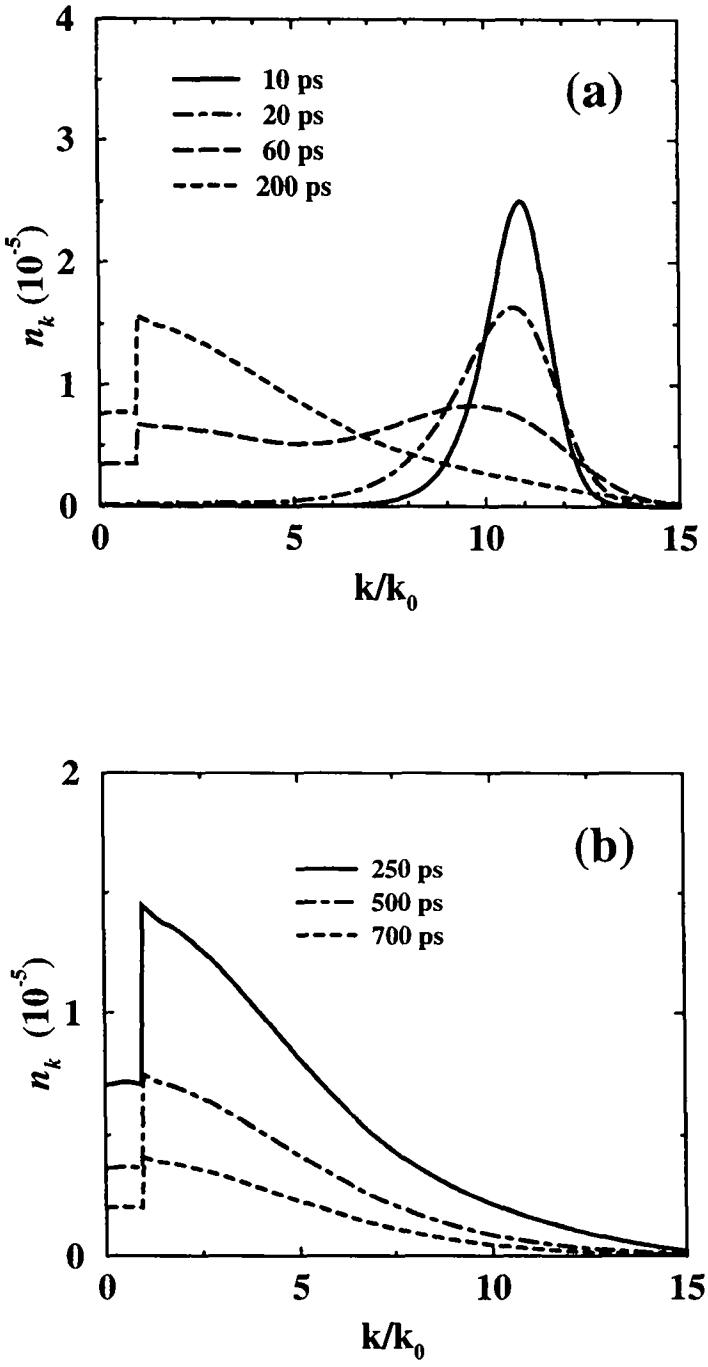


Figure 2.3: Time evolution of the exciton population $n_{\mathbf{k}}$ at T=50 K. The QW width is 40 Å. (a) Evolution up to 200 ps. (b) Evolution after 250 ps.

at low exciton densities, when $n_{\mathbf{k}} \ll 1$, their contributions is negligible. We study the dynamics of a realistic QW system of GaAs with $Ga_{0.6}Al_{0.4}As$ barriers and QW width of 40 Å. We also use $m_e = 0.067m_0$ for the electron mass, and $m_h = 0.18m_0$ for the heavy hole ($m_0$ is the free electron mass). In this system the averaged radiative lifetimes are 4 ps and 12 ps for transverse and longitudinal excitons respectively. In order to give a rough estimation of the characteristic times coming into play in the phonon scattering, we calculate the total rate of absorption for the excitons at k=0. We obtain a typical absorption rate $R_{abs} = \gamma T$ with $\gamma = 4\mu eV/K$. This compares well with degenerate four wave mixing and photoluminescence linewidth measurements [Shultheis, 1986], [Kim, 1992], [Gammon, 1995]. Larger absorption rates are found for excitons with $\mathbf{k} \neq 0$ because of additional phonon emission processes and because of a wider scattering phase space. Once all the rates $W_{\mathbf{k}\to\mathbf{k}'}$, $\Gamma_0$, and the initial distribution $n_{\mathbf{k}}(0)$ are known, the rate equations can be numerically integrated to obtain the time dependence of $n_{\mathbf{k}}$. The luminescence signal is easily extracted because it is proportional to the total number of photons emitted in the whole solid angle per unit time

$$I_{PL}(t) \propto \sum_{|\mathbf{k}|\leq k_0} \Gamma_{\mathbf{k}} n_{\mathbf{k}}(t) \; . \tag{2.24}$$

In Fig.2.3 we show the solution $n_{\mathbf{k}}(t)$ of Eq.2.19 at different times after the non resonant excitation as a function of $\mathbf{k}$. The initial exciton population created with an excess energy cools down by emission of phonons. The initial condition correspond to the assumption of exciton formation by emission of acoustic phonons. This corresponds to a particular choice for the excitation energy in the continuum, and we will better investigate this point in Chap.3. In this first part of the evolution, shown in Fig.2.3 (a), the total number of excitons in the radiative zone increases and the PL intensity, shown in Fig.2.4, correspondingly rises. The exciton distribution subsequently tries to thermalize to the lattice temperature but the coupling with photons drains the excitons away from the radiative zone, preventing full thermalization of the excitonic population. We see indeed that the exciton distribution is depleted in the radiative region. Afterwards, the population maintains a stationary shape and rigidly decreases in time as shown in Fig.2.3 (b) so that it may be parametrized as $n_{\mathbf{k}}(t) = f_{\mathbf{k}}^{stat} N_{tot}(t)$. The total population, the radiative population, and the PL intensity therefore decay with the same characteristic time $\tau_D$. This decay time may be calculated by summing Eq.2.19 over $\mathbf{k}$

$$-\frac{\dot{N}_{tot}}{N_{tot}} = \frac{1}{\tau_D} = \frac{\sum_{|\mathbf{k}|\leq k_0} \Gamma_{\mathbf{k}} n_{\mathbf{k}}}{\sum_{\mathbf{k}} n_{\mathbf{k}}} = \sum_{|\mathbf{k}|\leq k_0} f_{\mathbf{k}}^{stat} \Gamma_{\mathbf{k}} \; . \tag{2.25}$$

We observe that $\tau_D$ depends on the fraction of excitons in the radiative region only.

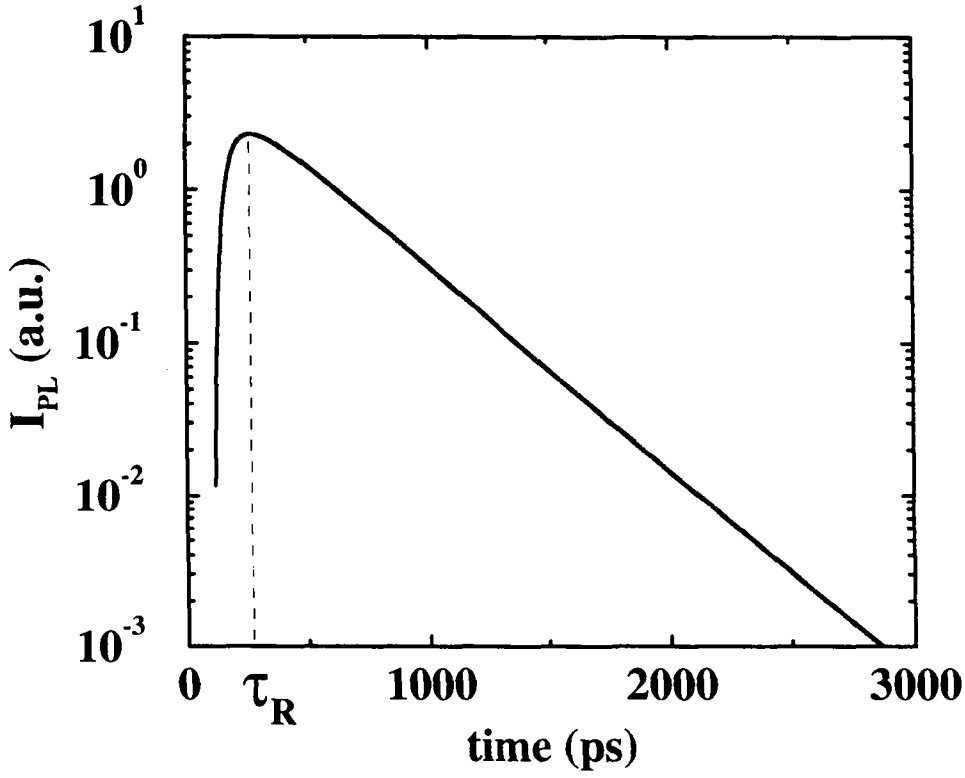


Figure 2.4: Photoluminescence signal as a function of time for non resonant excitation. Same parameters as in Fig.2.3. The rise time of the signal is indicated by $\tau_R$.

## 2.4 Temperature dependence of the decay time

The rise of the calculated photoluminescence signal is affected by the shape of the initial condition for the exciton population. On the other hand, in the experiment the rise of the photoluminescence contains information on the dynamics of exciton formation, and often a single rise time cannot be identified. In fact, a complex structure in the rise of the photoluminescence is observed (see Chap.3). However, we have found that the results on the stationarity of the exciton distribution function still hold independently on the formation mechanism, and the values of the decay times do not change in an appreciable way.

In the literature two major results about the temperature dependence of the decay time exist: in the first one the decay time $\tau_D$ is calculated through an average over the Boltzmann distribution of the radiative recombination time, and can be obtained from the Eq.2.25, using a Boltzmann distribution function for $f_{\mathbf{k}}^{stat}$ [Andreani, 1991]. This result gives a linear dependence on the teperature of the decay time. The second approach [Feldmann, 1987], is based on the idea that the excitons have an *ad hoc* defined Coherence area, proportional to the exciton homogeneous broadening $\Gamma_h$, and predicts a dependence of the decay time proportional to $\Gamma_h$. In the first approach the excitons are considered as particles with delta like spectral functions (see Chap.5) distributed thermally over the $1s$ band. The second approach instead consider the excitons as quasiparticles with a broadening $\Gamma_h$, the occupation of the 1s exciton band is neglected (only $k = 0$ excitons are considered), and the thermal average is done over the exciton spectral function. Citrin [Citrin, 1993] has shown in the framework of a Green's functions formalism that the thermal average has to be done both over the occupation of the $1s$ band and over the exciton spectral function. However, depending on the ratio between the exciton homogeneous broadening and the thermal energy the exact results reduce to the results obtained in the two simplified approaches:

$$\tau_D = \frac{k_B T}{4\Gamma_0 E_1}, \text{for } \Gamma_h \ll k_B T \tag{2.26}$$

$$\tau_D = \frac{\Gamma_h}{4\Gamma_0 E_1 (1 - e^{-\Gamma_h / K_B T})}, \text{for } \Gamma_h \gg k_B T \ , \tag{2.27}$$

where $E_1 = (\hbar k_0)^2/(2M) \sim 0.1 meV$, and only transverse excitons have been considered. In the regime of low excitation density the homogeneous broadening due to phonon scattering is of the order of $\Gamma_h \sim \gamma T$ with $\gamma = 5\mu eV/K$, and is always smaller than the thermal energy $K_B T$ ($k_B = 86\mu eV/K$). The picture of Andreani *et al.* is thus the most appropriate in this case. The picture of Feldmann *et al.* works better in the regime of high density where Coulomb scattering contribute to the homogeneous broadening of the

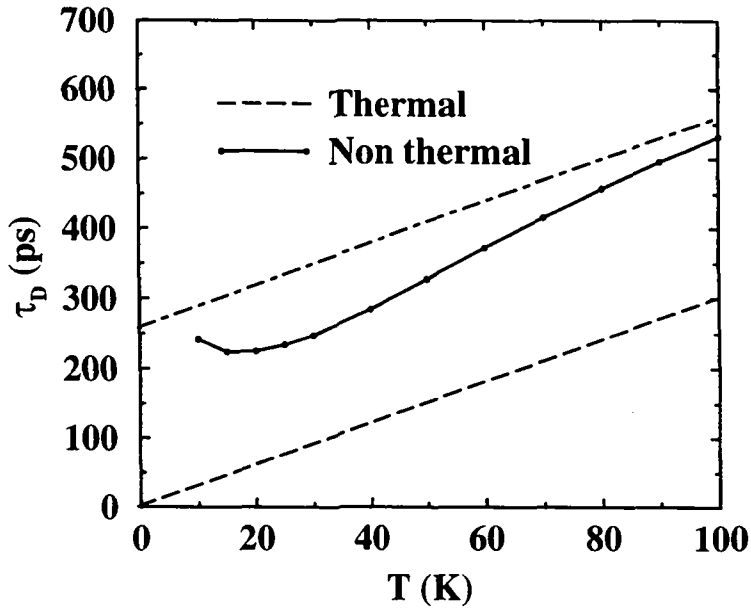


Figure 2.5: Temperature dependence of the photoluminescence decay time $\tau_D$ for a QW of 40 Å. The dashed line represents the full thermalization case. The dot-dashed line is a guideline parallel to the previous one.

exciton spectral function. In fact, the formula 2.27 has been successfully employed in the analysis of the photoluminescence decay in this regime [Eccleston, 1992]. Moreover, we remark that also in this second case for sufficiently high temperature the same behavior of Eq.2.26 is recovered. In our investigation, a delta like exciton spectral function is considered, but the kinetic of the system is numerically investigated without the assumption of the thermal equilibrium. We give in Fig.2.5 the temperature dependence of the decay times for transverse excitons. The corresponding dependence resulting from the assumption of full thermalization (Eq.2.26) is also shown. The decay times are underestimated by the full thermalization picture, but the thermal slope is recovered at high temperatures as indicated by the guideline in Fig.2.5. Furthermore, the linear behavior does not intercept the origin of the axis, but an offset in the linear behavior is observed. This behavior can be explained considering the role of the deviations from the thermal distribution. In fact, we observe that the stationary shape $f_{\mathrm{k}}^{stat}$ differs from the thermal distribution mainly in the radiative region. This means, according

to Eq.2.25, that recombination rates obtained by averaging over the distribution $f_{\mathbf{k}}^{stat}$ become smaller. We show in Fig.2.6 two stationary distribution functions at different temperatures. The deviations are smaller at higher temperature but do not vanish. Let us discuss in detail the role of these deviations. We write the population $n_{\mathbf{k}}$ as

$$n_{\mathbf{k}} = N_{tot}(t) f_{\mathbf{k}}^{stat} = N_{tot} f_{\mathbf{k}}^{0} - \delta n_{\mathbf{k}} \ , \tag{2.28}$$

where $f_{\mathbf{k}}^{0}$ is the Boltzmann distribution and $\delta n_{\mathbf{k}}$ represents the deviations. We have $\sum_{\mathbf{k}} \delta n_{\mathbf{k}} = 0$ because distribution functions are normalized. Using the detailed balance principle

$$W_{\mathbf{k}' \to \mathbf{k}} n_{\mathbf{k}}^{0} - W_{\mathbf{k} \to \mathbf{k}'} n_{\mathbf{k}'}^{0} = 0 \tag{2.29}$$

holding for all $\mathbf{k}$ and $\mathbf{k}'$, and inserting Eq.2.28 into Eq.2.19, we obtain

$$\dot{n}_{\mathbf{k}} = -\sum_{\mathbf{k}'} W_{\mathbf{k}' \to \mathbf{k}} \ \delta n_{\mathbf{k}'} + \sum_{\mathbf{k}'} W_{\mathbf{k} \to \mathbf{k}'} \ \delta n_{\mathbf{k}} - \Gamma_{\mathbf{k}} n_{\mathbf{k}} \ . \tag{2.30}$$

In deducing Eq.2.30 from Eq.2.19 we have assumed $n_{\mathbf{k}} \ll 1$ and we have neglected all the $(n_{\mathbf{k}} + 1)$ terms. We now introduce a simplified model in order to analyse the role of the deviations from the thermal distribution. For this purpose we define two effective levels which represent the totality of radiative and non radiative excitons respectively. We will indicate the quantities related to the radiative and non radiative regions with indexes R and NR respectively. We first consider the behavior of the total non radiative population $N_{NR}(t)$. Summing Eq.2.30 over $|\mathbf{k}_{NR}|$ in the non radiative zone we obtain

$$\dot{N}_{NR}(t) = \sum_{\mathbf{k}_{NR}} \sum_{\mathbf{k}'_{R}} (-W_{\mathbf{k}'_{R} \to \mathbf{k}_{NR}} \ \delta n_{\mathbf{k}'_{R}} + W_{\mathbf{k}_{NR} \to \mathbf{k}'_{R}} \ \delta n_{\mathbf{k}_{NR}}) \ . \tag{2.31}$$

Clearly, the scattering inside the non radiative zone does not modify $N_{NR}(t)$. Therefore in Eq.2.31 we consider only exchanges between non radiative and radiative zones. We define the total exchange rates as

$$W_{R \to NR}(\mathbf{k}'_{R}) = \sum_{\mathbf{k}_{NR}} W_{\mathbf{k}'_{R} \to \mathbf{k}_{NR}} \ , \tag{2.32}$$

$$W_{NR \to R}(\mathbf{k}_{NR}) = \sum_{\mathbf{k}'_{R}} W_{\mathbf{k}_{NR} \to \mathbf{k}'_{R}} \ . \tag{2.33}$$

These rates are flat functions of $\mathbf{k}$ where the deviation $\delta n_{\mathbf{k}}$ are large. We rewrite Eq.2.31 as

$$\dot{N}_{NR}(t) = -W \delta N_{R} \ , \tag{2.34}$$

where we have defined $\delta N_R = \sum_{\mathbf{k}_R} \delta n_{\mathbf{k}_R} = -\delta N_{NR} = -\sum_{\mathbf{k}_{NR}} \delta n_{\mathbf{k}_{NR}}$ and $W = W_{R \to NR} + W_{NR \to R}$. Analogously, by summing Eq.2.19 over the radiative states, we obtain

$$\dot{N}_{R}(t) = W \delta N_{R} - \Gamma N_{R} \ . \tag{2.35}$$

Eq.2.34 shows that a transfer of excitons from the non radiative to the radiative region is proportional to the deviation from the thermal equilibrium $\delta N_R$. Summing Eq.2.28 over the radiative region we write

$$N_R = \sum_{\mathbf{k}_R} n_{\mathbf{k}} = \alpha N_{tot} - \delta N_R \ , \tag{2.36}$$

where $\alpha = \sum_{\mathbf{k}_{Ra}} f^0_{\mathbf{k}} = 1 - e^{-E_1/(k_B T)}$. For $T \gg 1K$ $\alpha \sim E_1/K_B T$. The dynamics of the two effective levels is described by a linear system and can be written in the form:

$$\begin{pmatrix} \dot{N}_{tot} \\ \dot{N}_R \end{pmatrix} = \begin{pmatrix} 0 & -\Gamma \\ W\alpha & -(W+\Gamma) \end{pmatrix} \cdot \begin{pmatrix} N_{tot} \\ N_R \end{pmatrix} \ . \tag{2.37}$$

The eigenvalues of the 2x2 matrix in the equation 2.37 are:

$$\gamma_1 = -\frac{W+\Gamma}{2} + \frac{W+\Gamma}{2}\sqrt{1 - \frac{W\Gamma}{(W+\Gamma)^2}4\alpha} \sim -\frac{W\Gamma}{W+\Gamma}\alpha \tag{2.38}$$

$$\gamma_2 = -\frac{W+\Gamma}{2} - \frac{W+\Gamma}{2}\sqrt{1 - \frac{W\Gamma}{(W+\Gamma)^2}4\alpha} \sim -(W+\Gamma) \ , \tag{2.39}$$

where the approximated expressions holds for $\alpha \ll 1/2$ ($T \gg 2K$). The two modes associated with $\gamma_1$ and $\gamma_2$ describe the decay of the two levels with the same characteristic time. It is clear that the decay time of the photoluminescence is given by the smaller $\gamma_1$ which corresponds to a constant ratio $N_R/N_{tot} = W\alpha/(W+\Gamma)$. We remark that this ratio reduce to the thermal one in the case of $W \gg \Gamma$. The main contribution to $W$ comes from the term $W_{R \to NR}$, as can be deduced form the sum over the final states in Eq.2.33, and can be parametrized as $W(T) = \gamma T$, with $\gamma = 4\mu eV/K$. Using this parametrization we obtain

$$\tau_D(T) = \left(\frac{1}{\Gamma} + \frac{1}{W}\right)\frac{k_B T}{E_1} = \frac{k_B T}{\Gamma E_1} + \frac{k_B}{\gamma E_1} \ . \tag{2.40}$$

$\tau_D(T)$ increases with a slope $(k_B)/(4\Gamma_0 E_1) = 3.0$ ps/K for transverse excitons as predicted in the full thermalization limit. In addition we find an offset $k_B/(\gamma E_1) = 150$ ps. Comparison of this latter result to the calculated $\tau_D(T)$ given in Fig.2.5 shows that our simplified model slightly underestimates this offset, and the slope. This fact may be due to the assumption of a $\mathbf{k}$ independent $W(\mathbf{k})$. The deviations from a thermal distribution are found also in the case of continuous wave (cw) non resonant excitation luminescence. The shape of the distribution function, which is stationary in this case, is very similar to the $f^{stat}_{\mathbf{k}}$ shown in Fig.2.6. Let us finally discuss the role of localized states in the temperature dependence of the decay times. This point has been addressed by Citrin [Citrin, 1993] which has calculated the radiative lifetime for exciton trapped

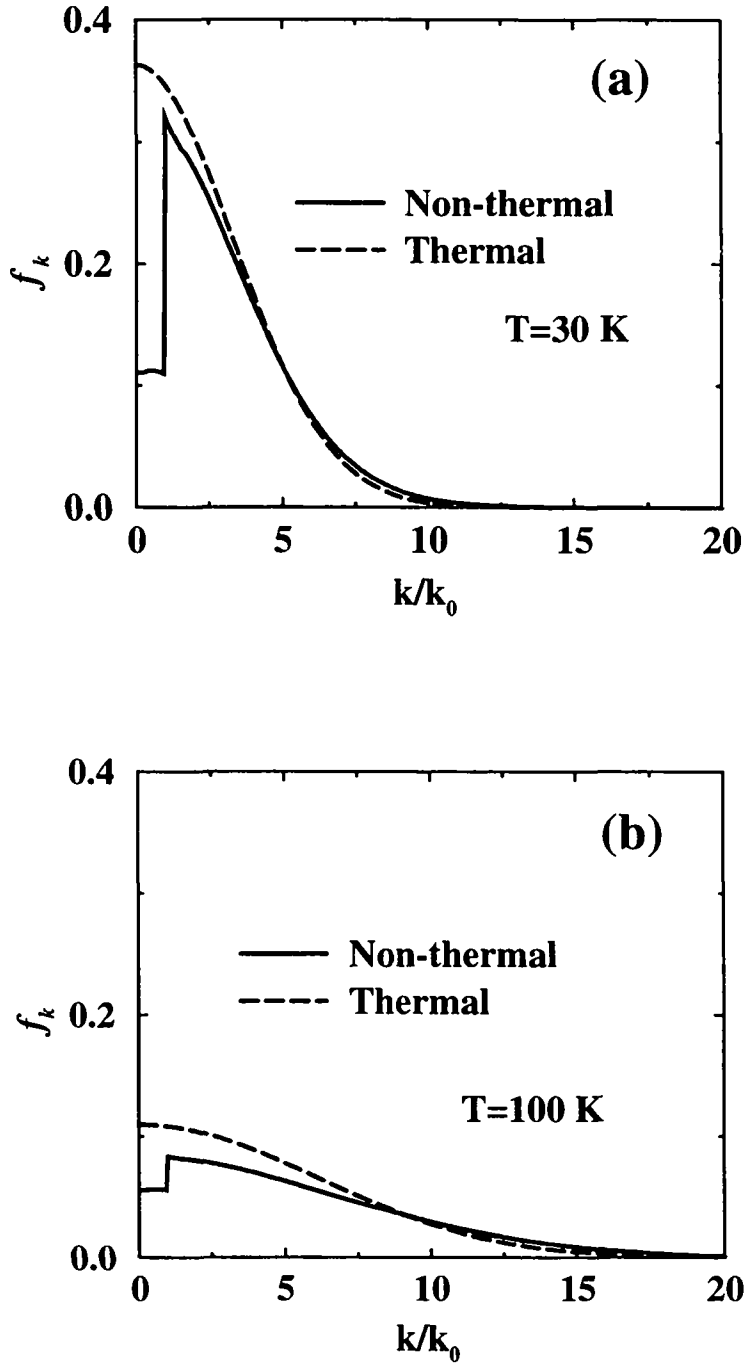


Figure 2.6: Normalized exciton distribution functions $f_k^{stat}$, for two different temperatures, 700 ps after the excitation. The dashed lines show the thermal distributions corresponding to the same temperatures.

by disorder interface. The typical lifetime are of the order of 100 ps. The average over the localized and free exciton states gives for the decay time

$$\frac{1}{\tau_D} = \frac{N_{free}\Gamma_{free} + N_{loc}\Gamma_{loc}}{N_{tot}} \tag{2.41}$$

in the limit of low temperature the exciton population consists mainly of localized excitons and the decay time observed corresponds to $1/\Gamma_{loc}$. However, the effect of the localized states affects the temperature dependence of the decay time also at temperatures larger than the typical energies of localization. The effect on $\tau_D$ of the localization in this regime of high temperature gives

$$\tau_D = \frac{1}{2\Gamma_{free}}(1 + \frac{N_{loc}\Gamma_{loc}}{N_{free}\Gamma_{free}})^{-1} \tag{2.42}$$

In this limit the ratio $\frac{N_{loc}\Gamma_{loc}}{N_{free}\Gamma_{free}}$ is independent on the lattice temperature is typically on the order of unity or 10 depending on the density of interface defects. This theory predicts thus a decrease of the slope of the linear dependence at high temperature due to the interface roughness. We remark that in presence of localized states, a linear behavior that intercept the origin is still predicted, while the presence of a finite intercept can be explained only taking into account the deviation from the thermal equilibrium discussed above. Even introducing a broadened exciton spectral function the intercept of the linear behavior remains the origin. In fact, the offset comes from an exact compensation between the linear dependence in T of $\tau_D$ and the linear dependence of the phonon scattering rate $W = \gamma T$. Obviously this compensation becomes difficult to observe when other mechanisms as exciton exciton scattering and disorder interface contribute to the scattering rate between radiative and non radiative states $W$.

Up to now, we have only considered the dynamics of transverse excitons. Actually, there are four HH exciton levels: one longitudinal, and one transverse which correspond to the $\Gamma_5$ representation of the $T_d$ point group, and two dark excitons, whose states belong to the representation $\Gamma_1$ and $\Gamma_2$. The dark excitons do not couple with the light. We have not extended our model in order to take into account the scattering and the dynamics of thermalization within these four exciton bands. But in order to compare with the experimental results, we make here some qualitative considerations about the role of this scattering in the overall dynamics of excitons. We can make two different assumption on the way the thermalization between the four level is reached:

The first assumption is that the scattering rates between the optically active excitons and the dark excitons are negligible, and the scattering rate between the two optically active states is fast. When this scattering rate is faster than the radiative recombination

rates, the populations of longitudinal and transverse excitons are equal. Therefore the averaged radiative recombination rate is

$$< \Gamma >= \frac{< \Gamma_{\mathbf{k}}^{L} > + < \Gamma_{\mathbf{k}}^{T} >}{2} . \tag{2.43}$$

The second assumption is that a fast scattering involves all the four levels. In this case we need a scattering mechanism between optically active excitons (J=± 1) and dark excitons (J=± 2). Inserting into the rate equation the averaged radiative rate over the four levels

$$< \Gamma >= \frac{< \Gamma_{\mathbf{k}}^{L} > + < \Gamma_{\mathbf{k}}^{T} >}{4} , \tag{2.44}$$

we calculate the corresponding dynamics. We show in Fig.2.7 (b) the decay time $\tau_D(T)$ corresponding to the two assumption of thermalization over the optically active states only and over the four excitonic levels.

The linear dependence of the decay time has a function of the temperature has been experimentally measured [Martinez-Pastor, 1993] and compared with theory. The measured slope of the linear dependence is quite larger (of about a factor 2) with respect to the theoretical prediction from the full thermalized model (notice that in the paper [Martinez-Pastor, 1993] the reported theoretical decay times should be divided by a factor 2 ). The slope that we find in our calculation for a 5 nm QW ranges from 10 ps/K to 12ps/K and is quite smaller than the measured slope of 22 ps/K. We finally remark that a clear evidence of an offset in the linear temperature dependence of the decay time has been recently observed in good quality InGaAs/GaAs samples [Yu, 1995]. This offset is the clear signature of the presence of deviation from the thermal equilibrium in these samples.

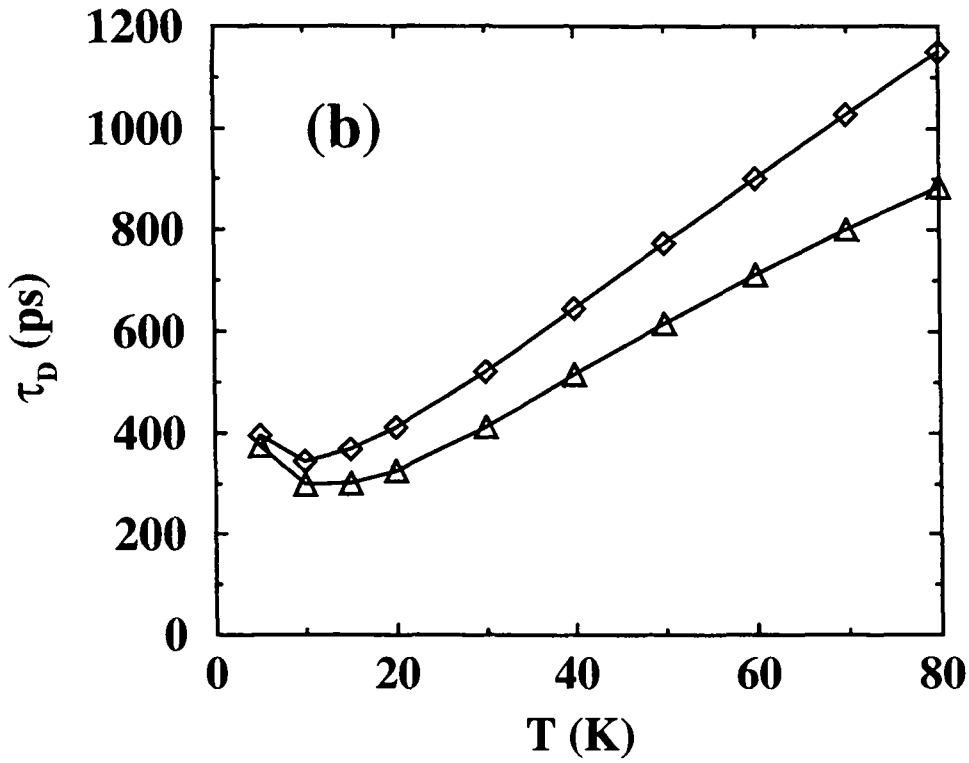


Figure 2.7: Temperature dependence of $\tau_D$ for a QW of 50 Å corresponding to the two hypothesis: fast scattering rate between the two optically active states (triangles), fast scattering rates between all the four exciton spin levels (diamonds).

# Chapter 3

# Exciton formation

We will now focus on the dynamics of the excitons starting from the excitation of electron hole pairs in the continuum. In a non-resonant photoluminescence experiment, the optical pump excites free electron-hole pairs which eventually relax to form bound excitons. In this chapter we will calculate the characteristic times of this relaxation process which we will call exciton *formation* process since it results in the formation of bound excitons. We will analyse the effects of the formation process on the rise of the photoluminescence signal in typical experiments. During the last few years, several experiments have been carried out in order to clarify the exciton formation process both in bulk and QW semiconductor systems. Most experiments are based on time-resolved techniques, which include time resolved photoluminescence of the excitonic resonance [Damen, 1990], [Roussignol, 1992], [Blom, 1993], [Robart, 1995], and of the free carrier continuum [Deveaud, 1993], [Kumar, 1996a], [Kumar, 1996b], time resolved Raman spectroscopy [Prabhu, 1996], and nonlinear cross-correlated photoluminescence [Sasaki, 1989], [Strobel, 1991], [Emiliani, 1997]. However, the results of time resolved experiments do not allow a clear identification of the exciton formation rate, because in the dynamics it is difficult to distinguish between the formation process itself from the exciton relaxation within the excitonic band. When a photon from the pump pulse is absorbed by the sample, an electron hole pair is created. The electron and the hole in this pair have opposite momentum, and are strongly correlated. However, this correlation is rapidly lost through scattering with the other carriers and with phonons. These scattering mechanisms are the same which provide a fast thermalization within the free carriers. Consequently, we distinguish between two different cases: direct formation of the exciton from the initially created electron hole pair before correlation is lost (geminate formation) and indirect formation from thermalized electron-hole pairs (bimolecular formation). The rate of geminate formation is proportional to the created pairs density, and

is therefore linear in the pulse intensity. The bimolecular formation rate is proportional to the probability that the thermalized electrons and holes interact, and is proportional to the product of electron and hole densities. This is valid for a non-degenerate Fermi gas, which corresponds to the excitation densities in most experiments. We will analyse in detail the geminate and bimolecular formation, and the exciton dissociation process, which is the inverse process of formation and is important when the lattice thermal energy is close to the exciton binding energy [Piermarocchi, 1997a]. Using the calculated formation and dissociation rate we reproduce the dynamics of the photoluminescence rise [Piermarocchi, 1997b], [Piermarocchi, 1997c]. The most interesting feature of the photoluminescence rise consists by the presence of two characteristic times in it. The first charateristic time is very rapid (few picoseconds) and related to the emission of optical phonon, while the second time is of the order of several hundreds of picoseconds and is due mainly to the relaxation by acoustic phonons emission. We have checked the thermal equilibrium between free carriers and bound states. As for the case of radiative versus non radiative population discussed in Chap. 2, in the regime of low temperature, strong deviation from the action mass law (thermodynamic equilibrium between exciton and free carrier) exists up to several hundreds of picoseconds. Consequently, during the dynamics of the photoluminescence, an excess of free carriers with respect to the thermal case results.

Recent experiments [Amand] show that the first rapid time appears in the photoluminescence even for excitation of a cold free carrier plasma, which in principle cannot relax by emission of optical phonons. This feature is not explained by the interaction of the carriers and excitons with phonons. A possible explaination of this effect come from the role of Coulomb interaction in these systems. However in order to address this point a more general approach to the exciton problem in the optical spectra is needed. In order to obtain a satisfactory description of the build up of the photoluminescence, the quantum kinetics of relaxation has to include the broadening of the states in a accurate way. The broadening of the states affects the phase space for the scattering since it relax the conservation energy in the transitions. This is particularly inportant for the broadening induced by Coulomb scattering. In fact, in the picture of free carries and bound excitons with no broadening, the formation of excitons may occur through Auger-like processes which gives a formation rate proportional to the square of the total density of carriers. This $n^2$ dependece, which is not observed in the experiment even at very high densities [Strobel, 1991], is probably modified by the density dependence of the collision broadening. In more simple way, the Fermi's golden rule approach does not give the correct rates since the broadening of the states it is not much smaller than

the energy jumps in the relaxation, and introduces an additional dependence on the density. Moreover, in order to distinguish the scattering within the continuum from the scattering toward bound states, the energy and wavevector dependent broadening has to be calculated with a self consistent treatement. The self consistent T matrix approach we will proposed in Chap.5 is probably the best tools for this purpose. In fact the single particle self energy, thus the broadening, calculated in this approximation contains both the contribution from free and bound pairs scattering.

## 3.1 Geminate formation

The geminate formation process consists of three steps: excitation of en electron hole pair by a photon, propagation of the created pair through the crystal with total momentum close to zero, and finally conversion of the correlated pair into an exciton via interaction with phonons. The rate of creation is therefore proportional to the density of pump photons. We stress the fact that the electron-hole pair involved in the formation has total zero momentum. In the geminate process, two interactions are involved: the carrier-phonon interaction $V_p$ and the carrier-photon interaction $V_\gamma$. The formation rate of an exciton with a given center of mass wavevector $\mathbf{q}$, produced by a photon with energy $\hbar\omega$, is calculated by second order perturbation theory. The emission of optical phonons gives the dominant contribution to this formation rate, and has a threshold at $\hbar\omega = E_{gap} + \hbar\omega_{LO} - E_b$. We have checked that the contribution from the acoustic phonons in the geminate formation is four orders of magnitude smaller. The carrier optical phonon interaction considered here is the Frölich interaction, which is due to the polarization field created by the ions oscillating in opposite direction. Confined and localized optical phonon mode has been shown to play a marginal role in the relaxation rate for an electron plasma [Rücker, 1992], and the same should be valid for the exciton formation mechanisms. Therefore we consider in the calculation the interaction of carriers with bulk optical phonons. The formation rate by emission of optical phonons reads

$$R(\hbar\omega \to \mathbf{q}) = \frac{2\pi}{\hbar} \sum_{q_z} \left| \sum_{\mathbf{k_r}} \frac{\langle 0|V_\gamma|\mathbf{k_r}\rangle \sqrt{(n_p+1)} \langle \mathbf{k_r}|V_p|\mathbf{q}\rangle}{\hbar\omega - E_{gap} - \hbar^2|\mathbf{k_r}|^2/2\mu + i\Gamma} \right|^2$$
$$\times \delta\left(\hbar\omega - \hbar\omega_{LO} - E_{gap} + E_b - \frac{\hbar^2|\mathbf{q}|^2}{2M_{exc}}\right) . \tag{3.1}$$

Here $|0\rangle$ is ground state, $|\mathbf{k_r}\rangle$ represents an electron-hole state with relative momentum $\mathbf{k_r}$, $|\mathbf{q}\rangle$ is the exciton state, and $\mu$ is the reduced electron hole mass. All the intermediate states have zero center of mass momentum and we sum only on the relative momentum

$\mathbf{k_r}$ of the electron-hole pair. Furthermore, the in-plane wavevector conservation implies that the created exciton and the emitted optical phonon have opposite momentum. The optical phonons are in thermal equilibrium at the temperature $T_l$, and $n_p$ is therefore negligible in the range of considered temperatures. The sum over $q_z$ of the final phonon is due to the breaking of the translational symmetry in the growth direction. The energy $\Gamma$ gives the broadening of the intermediate states, is assumed to be frequency independent, and is produced by the same process which thermalizes the carriers. We have investigated the effect of this broadening on the total rate of the process, and we have found that for $\Gamma$ larger than $\simeq$ 10 meV, the geminate rate decreases rapidly. This is related to the loss of correlation in the intermediate pair for $\Gamma$ larger than the exciton binding energy $E_b$. In the following, we assume $\Gamma$ to be smaller than 10 meV. We give in Appendix A the explicit calculation of the geminate relaxation rate. The total rate of formation is then obtained from Eq. 3.1 summing over all the final exciton states, and can be written as a function of the pump power $P$ and the pump frequency $\omega$ as (see App.A

$$\left(\frac{dn_{ex}}{dt}\right)_{gem} = \alpha_{gem}(\hbar\omega)P(\hbar\omega). \tag{3.2}$$

We obtain for a QW of 50 Å a coefficient $\alpha = 1.4\ 10^{15}(\mathrm{Ws})^{-1}$, for an excitation energy of 40 meV above the band edge. We have found that $(dn_{ex}/dt)$ is slowly dependent on the excitation energy above the energy threshold. For a 1 ps pump pulse and 1 KW/cm$^2$ power, about $10^6$ cm$^{-2}$ excitons are formed by the geminate process. In order to quantify the importance of the geminate formation process, we compare it with the total formation rate of free carriers for the same excitation conditions, and obtain

$$\frac{\left(\frac{dn_{ex}}{dt}\right)_{gem}}{\left(\frac{dn_e}{dt}\right)_{carr}} = \frac{\alpha_{gem}(\hbar\omega)P(\hbar\omega)}{\alpha_{carr}(\hbar\omega)P(\hbar\omega)} \simeq 0.05 \tag{3.3}$$

Here the total free carrier rate $\alpha_{carr}(\hbar\omega)P$ is related to the free carrier absorption, and is energy independent for excitation above the band edge. The equation 3.3 states that about 5% of the carriers created by the photons flowing into the sample are directly converted in excitons through the geminate process.

## 3.2 Bimolecular formation

The scattering terms in the Boltzmann equation describing the bimolecular formation process read

$$\left(\frac{df_e(\mathbf{k_e})}{dt}\right)_{form} = -\sum_{\mathbf{k_{ex}},\mathbf{k_h}} F_{\mathbf{k_e},\mathbf{k_h}\rightarrow\mathbf{k_{ex}}} n_h(\mathbf{k_h}) n_e(\mathbf{k_e}) \tag{3.4}$$

where the $F_{\mathbf{k_e},\mathbf{k_h}\to\mathbf{k_{ex}}}$ represents the the probability per unit time for a free electron with wavevector $\mathbf{k_e}$ to bind together with a free hole with wavevector $\mathbf{k_h}$ giving rise to an exciton with a wavevector $\mathbf{k_{ex}} = \mathbf{k_e} + \mathbf{k_e}$. The occupation numbers for electrons and holes are denoted by $n_e(\mathbf{k_e})$ and $n_h(\mathbf{k_h})$. An equation analogous to Eq. 3.4 holds also for the hole and exciton distribution functions. The formation rate $F_{\mathbf{k_e},\mathbf{k_h}\to\mathbf{k_{ex}}}$ is evaluated using the Fermi's golden rule. For the exciton we use a two dimensional hydrogenic-like wavefunction as in Chap. 2, and the electron-hole pair wavefunctions in the continuum are approximated by plane waves. We will discuss this latter approximation at the end of this section. We assume that during the evolution of the system, the free electrons and holes are thermalized at the same temperature $T_c$. This thermalization is produced by fast carrier-carrier scattering. Typical thermalization times in GaAs QW are found to be of the order $\sim$ 100 fs for carrier density above $10^{10}$ cm$^{-2}$ [Knox, 1992], which are faster than all the other scattering times, in particular when compared to the exciton formation time. In the scattering term of Eq.3.4, we use for $n_e(\mathbf{k_e})$, and $n_h(\mathbf{k_h})$ equilibrium Boltzmann distribution function at $T_c$. Consequently, by summing Eq.3.4 over $\mathbf{k_e}$, we obtain an adiabatic equation for the evolution of the electronic density $n_e = (\sum_{\mathbf{k_e}} n_e(\mathbf{k_e}))/S$

$$\frac{dn_e}{dt} = -\sum_{\mathbf{k_{ex}}} F(\mathbf{k_{ex}}) n_e n_h \equiv -C n_e n_h \ . \tag{3.5}$$

The coefficient $C$ is the bimolecular formation coefficient, which depends on both $T_c$ and the lattice temperature $T_l$ through the interaction with the phonons, and $F(\mathbf{k_{ex}})$ is defined as

$$F(\mathbf{k_{ex}}) = \left(\frac{2\pi\hbar^2}{k_B T_c}\right)^2 \frac{1}{m_e m_h S} \sum_{\mathbf{k_e},\mathbf{k_h}} F_{\mathbf{k_e},\mathbf{k_h}\to\mathbf{k_{ex}}} e^{-(E_e(\mathbf{k_e})+E_h(\mathbf{k_h})/k_B T_c)} \ . \tag{3.6}$$

The carrier temperature $T_c$ immediatly after the pump pulse depends on the excess energy $\Delta E = E_{pump} - E_{gap}$, and is defined by $k_B T_c = \Delta E/2$. However, in the dynamics, $T_c$ approaches the lattice temperature $T_l$ through emission of phonons showing two characteristic times: a short one, usually few picoseconds, associated to the emission of optical phonons, and a longer one, of the order of several hundreds of picoseconds, associated to acoustic phonons. The optical phonon emission drives the dynamics for $T_c$ above 50 K. We do not consider the evolution of the temperature $T_c$, which may be experimentally measured [Yoon, 1996], and we evaluate the formation coefficient $C$ as a function of $T_c$ and $T_l$. In Fig.3.1 we report $C$ as a function of $1/T_c$ for a fixed lattice temperature $T_l$ =10 K, for a GaAs QW of 50 Å. The two contributions from the acoustic and optical phonons are shown separately. The optical phonon contribution

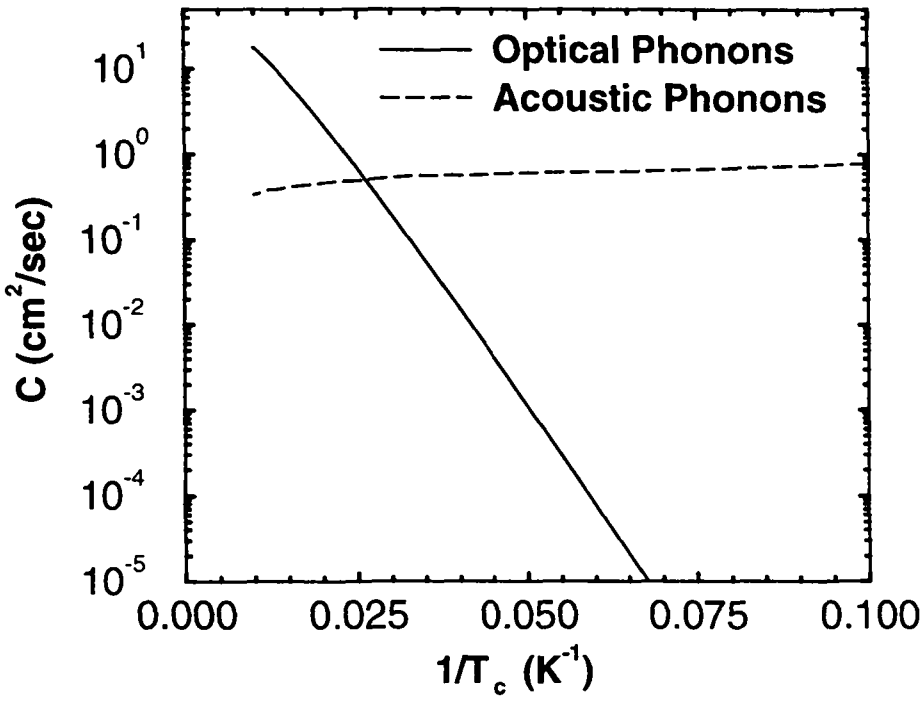


Figure 3.1: The exciton formation coefficient $C$ as a function of the inverse of the carrier temperature $T_c$, at a fixed lattice temperature $T_l$=10 K.

dominates for temperatures larger than 40 K, and in the Arrhenius plot of Fig.3.1 we can define an activation energy of 26 meV for this process. This energy corresponds to the difference between the optical phonon energy ($\hbar\omega_{LO}$ = 36 meV) and the exciton binding energy ($E_b$ = 10 meV). We conclude that the formation process at short times is mainly governed by optical phonon emissions. For the acoustic phonon process, we do not find any activation energy. In fact, both the emission and absorption of acoustic phonons contribute to exciton formation. The difference between the two processes appears clearly in their dependence on the lattice temperature $T_l$. The optical phonon contribution do not depend on $T_l$, whereas the acoustic phonon one increases linearly with $T_l$. The qualitative difference between exciton formation by the optical and by acoustic phonons is also clearly shown in Fig.3.2 (a), where $F(E) = F(k_{ex} = \sqrt{2ME/\hbar^2})$ is plotted as a function of the energy E of the created exciton. Since optical phonons are dispersionless, the energy exchanged in the transition is always the same, and the distribution of the created excitons follows the shape of the thermal tail of the free carrier at $T_c$. The created excitons come from electrons and holes at the tail of the Boltzmann distribution function. Even if the population at the tail is very small, the polar interaction is so strong with respect to the deformation potential interaction, that already for 40 K the contribution form optical phonon emision is overwhelming. The energies exchanged by acoustic phonon emission and absorption are of the order of one meV, and the excitons are created through quasi-elastic transitions. Therefore, excitons from this process are formed close to the band-edge, at an energy $E$ close to $E_b$. Similar remarks can be done for the dissociation process (Fig.3.2 (b)). Dissociation through the emission or absorption of acoustic phonon can occurr only if the dissociating exciton is close to the band edge. The dissociation through absorption of an optical phonon is instead independent on the energy od the exciton.

Several experiments have been done in order to determine directly the value of the bimolecular coefficient $C$. Strobel *et al.* [Strobel, 1991] find $C$ =6 cm$^2/s$, Emiliani [Emiliani, 1996], [Emiliani, 1997] find $C \sim 10 - 20$ cm$^2/s$, Robart *et al.* [Robart, 1995] find $C \sim 14$ cm$^2/s$, Kumar *et al.* [Kumar, 1996a], [Kumar, 1996b] find $C$ =0.5 cm$^2/s$, and Deveaud *et al.*[Deveaud, 1993] find $C$ ~0.5-1 cm$^2/s$. Small changes in the experimental parameters, such as the quantum well width and the lattice temperature, should not significantly modify the value of the bimolecular coefficient. The different values obtained for $C$ in different experiments can be explained taking into account the temporal evolution of free carrier temperature $T_c$, and the different techniques used in the determination of this coefficient. It is clear, for instance, that the values $C$ =10-20 cm$^2/s$ refer to the formation assisted by optical phonons, which corresponds to a carrier

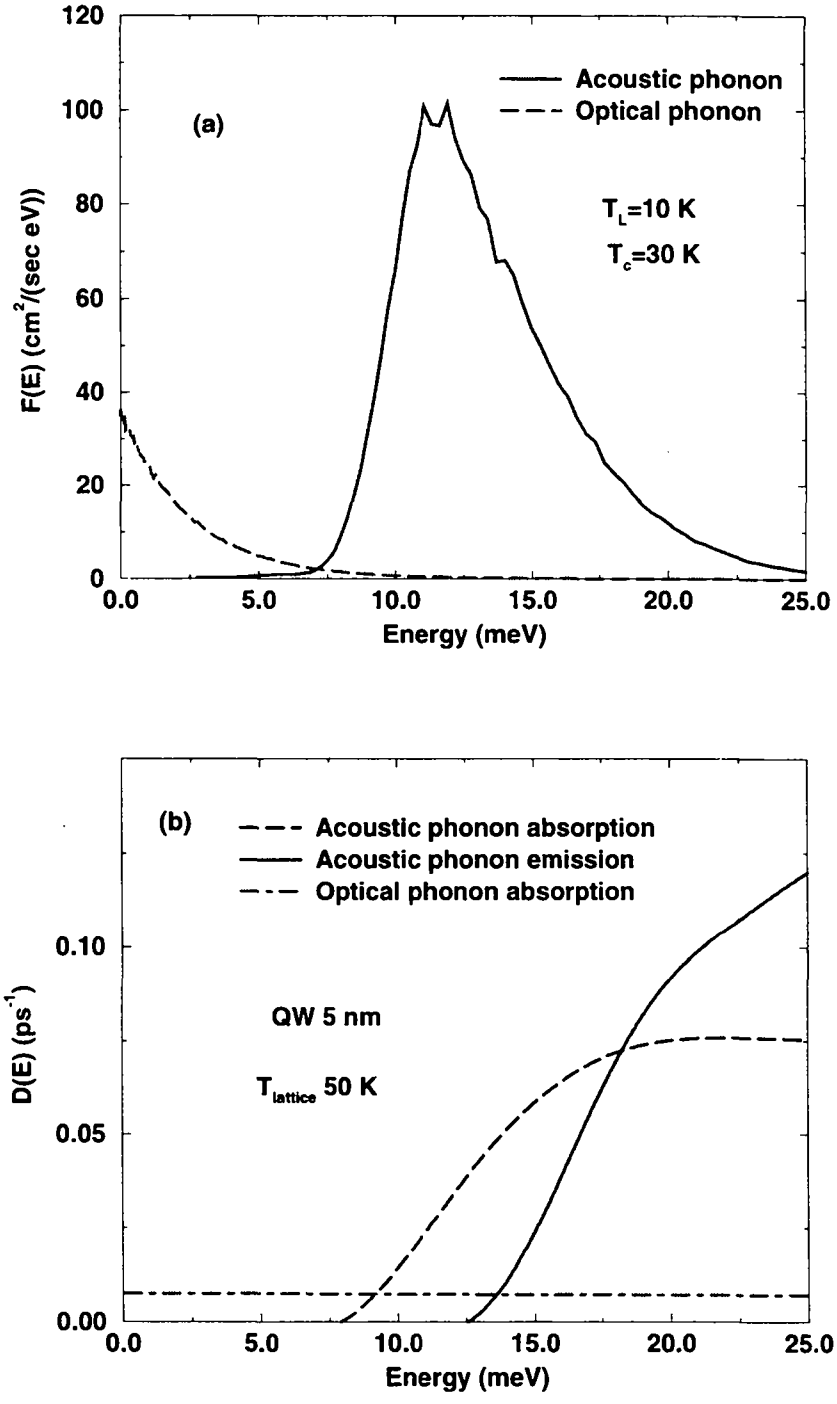


Figure 3.2: (a) Exciton formation rates as a function of the energy of the created exciton. (b) Exciton dissociation rate.

temperature larger than 40 K. These values have been estimated from cross correlated photoluminescence experiments which investigate the dynamics of the system at early times. The value of 14 $cm^2/s$ has been obtained by measuring the time evolution of the homogeneous broadening of the exciton which is assumed to be proportionoal to the free carrier density. In this case too, the determination of the bimolecular coefficient has been carried out looking at the first 10 ps of this evolution. On the other hand the values $C$ = 1-0.5 $cm^2/s$, which has been measured looking to the temporal decay of the photoluminescence in the electron hole continuum, has been extrapolated from the dynamics after about 50 ps, where the carrier temperature is likely below 40 K, and refer to the iormation assisted by acoustic phonons. Using accurate MonteCarlo simulations, it has been shown that the contribution due to the optical phonons can also be sensitive to the laser excess energy. At very short time the formation due to this process shows an oscillatory behavior related to $\hbar\omega_{LO}$ [Gulia, 1997]. This can be understood by a contribution from the carrier population which is not yet thermalized. The contribution from the acoustic phonon scattering is instead constant, and quantitatively not sensitive to the details of the distribution function considered.

The characteristics of the geminate and bimolecular processes are different. The geminate formation exists only during the pump pulse, whereas the bimolecular formation takes place also at later times, and depletes the carrier population during the exciton formation. Due to the quadratic dependence of the rate on the density of free carriers, the temporal evolution of $n_e$ is not given by a simple exponential. However, a characteristic formation time for $n_e = n_h$ may be defined as $(Cn_e)^{-1}$. Typical values for this time are in the range of 1 to 20 ps for $n_c$ of $10^{10}$ $cm^{-2}$. For later times, the dynamics becomes more complex because of exciton and carrier temperature relaxation processes, and of the dissociation of the excitons. In order to compare the geminate and bimolecular exciton formation rates, a given experimental condition of pump power $P$, pump duration $\Delta t$, carrier temperature $T_c$ and lattice temperature $T_l$ has to be considered. As discussed above, the carrier temperature $T_c$ is not simply related to the excess excitation energy $\Delta E$. Here, the excess energy is always above the geminate generation threshold. Therefore, we consider a typical range of possible carrier temperatures $T_c$ from 50 K to 100 K which may result after the excitation [Robart, 1995], [Yoon, 1996]. The geminate formation rate is written in term of the carrier density $n_e$ created by the pulse by approximating $(dn_e/dt) \sim n_e/\Delta t$ and using Eq. 3.3 to obtain

$$\left(\frac{dn_{ex}}{dt}\right)_{gem} \simeq \frac{\alpha_{gem}}{\alpha_{carr}} \frac{n_c}{\Delta t F_S} , \tag{3.7}$$

where $F_S$ is a form factor due to the shape of the laser pulse. We consider a Gaussian pulse of full width at half maximum equal to $\Delta t$, and we average the geminate rate over

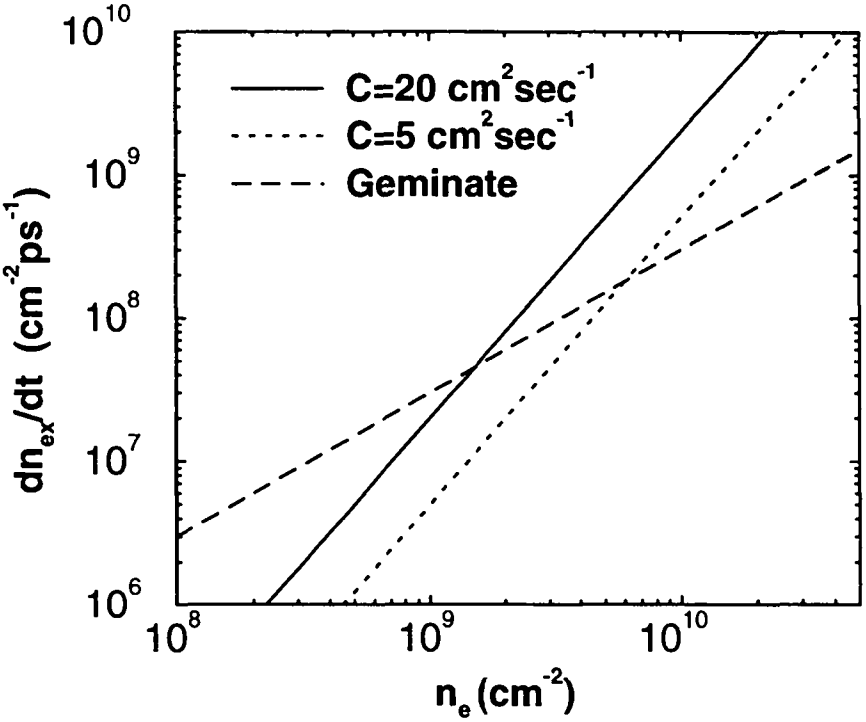


Figure 3.3: Geminate and bimolecular exciton formation rates as functions of the carrier density $n_e$. Other parameters are given in the text.

the temporal width of the pulse. The correspondig $F_S$ is 1.426. In Fig. 3.3 we report both the geminate and bimolecular formation rates at short times as a function of $n_e$, for $\Delta t$=1 ps and $T_c$ = 50 K and 100 K, and $T_l$ =10 K. Clearly, at large carrier density, the bimolecular formation rate dominates over the geminate rate. The crossing of the two rates depends on both $\Delta t$ and the carrier temperature $T_c$. For the chosen parameters, the crossover corresponds to $n_c = 10^9$ cm$^{-2}$. The crossover density decreases with increasing $\Delta t$ as shown in Eq.3.7. Measurements by Amand et al. [Amand, 1994] on the relative weight of the two processes confirm that for carrier density $n_e$ above $10^9$ cm$^{-2}$, the geminate process is negligible.

Other formation processes assisted by carrier-carrier scattering (Auger processes) and scattering by disorder and impurities take place in any available sample. The first process has a cubic dependence on $n_e$, and should have a small influence for densities lower than $10^{11}$cm$^{-2}$, as shown experimentally [Strobel, 1991]. Both a direct contribution and a correction to the calculated phonon assisted rates exists due to the interface disorder and impurities. Clearly, correction to the optical phonon assisted rates is negligible, due to the large energy exchanged in the process compared to the typical broadening due to disorder effects. Acoustic phonon assisted processes may be slightly modified by the presence of disorder, especially when the disorder inhomogeneous broadening are larger than the typical exchanged energies of 1 meV. For large inhomogeneous broadening, we expect also that the disorder-assisted formation process becomes relevant, and comparable to the acoustic phonon-assisted process.

Finally we want to discuss the validity of the approximation of plane waves used for the states in the continuum. In the optical transition the effect of the electron hole Coulomb correlation in the continuum produces in two and three dimensional systems an enhancement of the matrix element whith respect to the calculation done without the Coulomb corrections. This enhancement is described by a factor (Sommefeld factor) which corrects the spectra calculated with free carriers. The matrix element for the radiative transitions has the advantage that it does not depend on the relative and center of mass momentum. On the contrary, in the case of the transition leading to the exciton formation by phonons absorption or emission, the matrix element depends on the relative momentum and on the center of mass wavevector of the initial and final state. As a consequence, the effects of the Coulomb correlation in the continuum cannot simply be described by a Sommerfeld factor. However, taking into account the qualitative behaviour of the matrix elements, we can state that the optical Sommerfeld factor (which in two dimensions is about a factor 2 at the edge of the continuum) gives un upper limit for the Coulomb enhancement. In our approximation, the transition rate

for the formation of a bound 1s exciton by emission of a phonon with wavevector $\mathbf{q}$ reads

$$F_{\mathbf{k_e},\mathbf{k_h}\to\mathbf{K}-\mathbf{q}} = \frac{2\pi}{\hbar}\sum_{q_z}|\langle \mathbf{k_r},\mathbf{K}|V_{ph}(\mathbf{q},q_z)|\mathbf{K}-\mathbf{q},1s\rangle|^2\delta(E_f-E_i) \tag{3.8}$$

where $\mathbf{K}=\mathbf{k_e}+\mathbf{k_h}$, and $\mathbf{k_r}$ indicates the relative electron hole momentum. The envelope functions for the in plane motion of the states in the continuum are then

$$\Phi_{\mathbf{K}}(\mathbf{R})\Psi^f_{\mathbf{k_r}}(\rho) = \frac{e^{i\mathbf{K}\cdot\mathbf{R}}}{\sqrt{S}}\frac{e^{i\mathbf{k_r}\cdot\rho}}{\sqrt{S}}\ . \tag{3.9}$$

Actually, the correct envelope functions for the in plane relative motion with the e-h Coulomb correlation read

$$\begin{aligned}\Psi^c_{\kappa,m}(\rho) &= \frac{1}{\sqrt{\mathcal{R}}}\frac{|\Gamma(m+\frac{1}{2}-\frac{i2}{\kappa a_B})|}{\Gamma(2m+1)}e^{\frac{\pi}{\kappa a_B}} \\ &\quad \sqrt{2\kappa}e^{i\kappa\rho}(2\kappa\rho)^m F(m+\frac{1}{2}-\frac{i2}{\kappa a_B},2m+1,2i\kappa\rho)\frac{e^{\pm im\phi}}{2\pi}\end{aligned} \tag{3.10}$$

where $\kappa=\sqrt{2\mu E_r/\hbar^2}$ ($E_r$ is the energy due to the relative motion), and $m$ is an integer. $F(\alpha,\beta,\gamma)$ is the confluent hypergeometric function and $\mathcal{R}$ is the Radius of the circular quantization surface. The most important deviations in the envelope functions of Eq.3.10 with respect to the free case in Eq.3.9 are in the region $\kappa\sim 0$ and for $m=0$. Let us consider the formation by emission of a phonon $\mathbf{q}$ starting from one of these unbound but strongly correlated electron-hole pair at $\kappa\sim 0$ and $m=0$. The transition rate is

$$\begin{aligned}F_{\kappa\sim 0,m=0,\mathbf{K}\to\mathbf{K}-\mathbf{q},1s} &= \frac{2\pi}{\hbar}\sum_{q_z}|\langle\kappa\sim 0,m=0,\mathbf{K}|V_{ph}(\mathbf{q},q_z)|\mathbf{K}-\mathbf{q},1s\rangle|^2\delta(E_f-E_i) \\ &= \frac{2\pi}{\hbar}|\sum_{\mathbf{k_r}}\langle\kappa\sim 0,m=0|\mathbf{k_r}\rangle\langle\mathbf{k_r},\mathbf{K}|V_{ph}(\mathbf{q},q_z)|\mathbf{K}-\mathbf{q},1s\rangle|^2\delta(E_f-E_i)\end{aligned} \tag{3.11}$$

We know that the matrix element $\langle\mathbf{k_r},\mathbf{K}|V_{ph}(\mathbf{q},q_z)|\mathbf{K}-\mathbf{q},1s\rangle$ (See App.A) decreases as $1/(k_r a_B)^3$ for large $k_r$ and has a maximum in the region $k_r\sim 0$. Then we can write

$$F_{\kappa\sim 0,m=0,\mathbf{K}\to\mathbf{K}-\mathbf{q},1s} \le |\sum_{\mathbf{k_r}}\langle\kappa\sim 0,m=0|\mathbf{k_r}\rangle|^2 F_{\mathbf{k_r}\sim 0,\mathbf{K}\to\mathbf{K}-\mathbf{q},1s} \tag{3.12}$$

where

$$|\sum_{\mathbf{k_r}}\langle\kappa,m|\mathbf{k_r}\rangle|^2 = |\Psi_{\kappa,m}(\rho=0)|^2 \tag{3.13}$$

gives the optical Sommerfeld factor. The inequality 3.12 states that the Coulomb correlation in the continuum cannot strongly affects the formation rates by phonon interaction.

## 3.3 Formation dynamics

Our approach consists in a rate equation model where excitons, electrons and holes are considered as three independent particle species interacting with a thermal bath of acoustic and optical phonons [Piermarocchi, 1997b], [Piermarocchi, 1997c], [Marie, 1998]. Phonons provide the mechanism for the different relaxation processes. Taking into account the whole exciton dispersion, the rate equation reads

$$\begin{aligned} \dot{n_X}(\mathbf{k_X}) &= \sum_{\mathbf{k_X'}} W_{\mathbf{k_X'}\to\mathbf{k_X}}\, n_X(\mathbf{k'_X})(n_X(\mathbf{k_X})+1) - \sum_{\mathbf{k_X'}} W_{\mathbf{k_X}\to\mathbf{k_X'}}\, n_X(\mathbf{k_X})(n_X(\mathbf{k'_X})+1) \\ &\quad -\Gamma_{\mathbf{k_X}} n_X(\mathbf{k_X}) + \sum_{\mathbf{k_e},\mathbf{k_h}} F_{\mathbf{k_e},\mathbf{k_h}\to\mathbf{k_X}} n_e(\mathbf{k_e}) n_h(\mathbf{k_h}) - D_{\mathbf{k_X}} n_X(\mathbf{k_X}). \end{aligned} \tag{3.14}$$

All wavevectors are two dimensional and refer to the in-plane directions. In Eq. (3.14) the occupation numbers for electrons, holes and excitons are denoted by $n_e(\mathbf{k_e})$, $n_h(\mathbf{k_h})$, $n_X(\mathbf{k_X})$ respectively. All the scattering rates have been calculated using the Born approximation, and only $1s$ excitons have been considered. The last two terms in Eq.3.14 represent the formation and dissociation of excitons respectively, while $\Gamma_{\mathbf{k_X}}$ is the radiative recombination rate. By assuming a thermal, time-independent distribution function for the free carriers, we can derive an equation for the total free carrier density $n_e$

$$\frac{dn_e}{dt} = -\sum_{\mathbf{k_X}} F_{\mathbf{k_X}} n_e n_h + \sum_{\mathbf{k_X}} D_{\mathbf{k_X}} n_X(\mathbf{k_X}) \ , \tag{3.15}$$

where the term $F_{\mathbf{k_X}}$ is given in Eq.3.6. The dissociation by optical phonons, on the other hand, is nearly independent on the exciton energy. We remark that already at 50 K the dissociation rates are of the same order of the radiative recombination rates, and consequently it is essential to take into account their role in the photoluminescence dynamics.

By solving the rate equations (3.14) and (3.15), we obtain the evolution of the photoluminescence signal. Only excitons with a negligible center-of-mass in plane momentum are allowed to interact with the radiation field and thus to recombine radiatively. This feature is a consequence of the energy and momentum conservation of the system of excitons and photons. In order to obtain a photoluminescence signal, we need to populate the excitonic states in the region at the bottom of their band. This region in the in plane wave vector space is called radiative region. The analysis of the rise time of the photoluminescence indicates how the excitonic states in the radiative region are populated. There are, indeed, two different ways to produce radiative excitons. The first one consists in a direct radiative exciton formation from the free carrier plasma. This direct formation in the radiative region is provided by the emission of optical phonons, and the

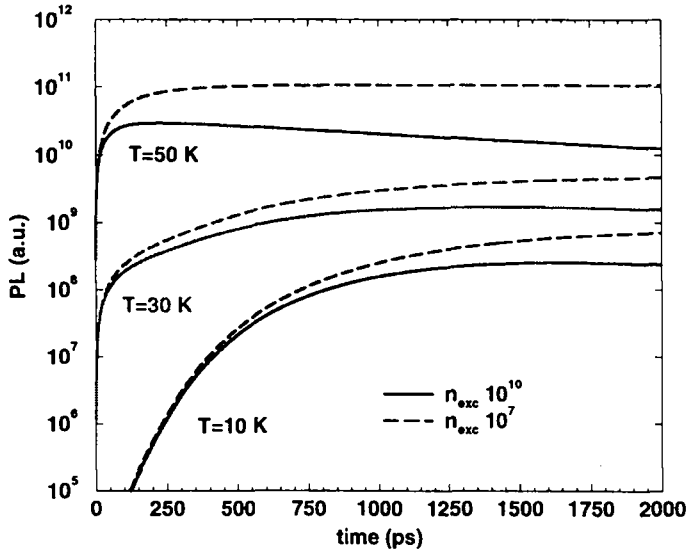


Figure 3.4: Time evolution of the photoluminescence for three different temperature and two excitation densities. The same temperature for the plasma and the lattice is considered. The quantum well width is 12 nm.

created excitons are thermally distributed with the same temperature as the free carrier plasma. The second way to populate the radiative region is provided by non-radiative excitons which are brought by phonons into the radiative region. This second way is related to the cooling of the exciton distribution towards the lattice temperature, and it is generally slower than the direct formation of radiative excitons. We show in Fig.3.4 the time evolution of the photoluminescence for two different initial excitation densities $n_{exc}$. We considered the same temperature for the free carriers and lattice. At 50 K, the initial fast rise corresponds to a direct formation of excitons in the radiative region. At 10 K, instead, the direct formation in the radiative region is strongly inhibited and only excitons near the band edge are created by emission of acoustic phonons. The slow rise in the time evolution of the photoluminescence thus reflects the exciton cooling towards the radiative zone. The case at the intermediate temperature T=30 K reveals a double structure in the time dependence of the signal. This corresponds to the presence of both effects described above. The dependence on the initial excitation density is weak, but we remark that for very low excitation density, our assumption of instantaneous thermalization for the plasma becomes less realistic. A full dynamics of the free carriers should be considered in this last case. The condition $T_c = T_L$ considered in Fig.3.4 can

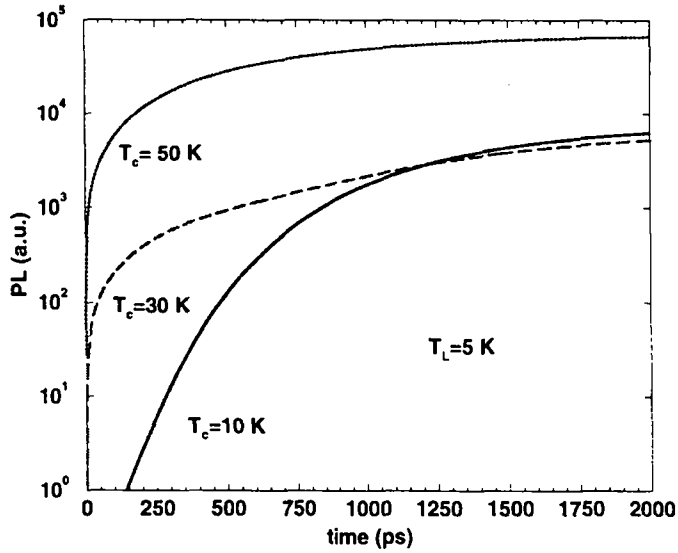


Figure 3.5: Time evolution of the photoluminescence at low lattice temperature for different values of the plasma temperature. The quantum well width is 12 nm and the excitation density $10^7$ cm$^{-2}$.

be experimentally obtained by tuning the laser excess energy. In fact, the initial average kinetic energy of the e-h plasma, which is proportional to the laser excess energy, can be chosen close to $k_B T_L$. This experimental setup allows a clear analysis of the dynamics of exciton formation from a photoluminescence experiment because cooling of the e-h plasma does not take place. However, photoluminescence experiments are usually performed with large excess energy above the e-h continuum and low lattice temperature. We consider this case in Fig.3.5, where we plot the photoluminescence dynamics corresponding to two different values of the free carrier and lattice temperature. The free carrier temperature is initially given by the excitation energy. Then, a fast cooling through optical phonon emission occurs which brings the carrier to a temperature of 40 $\sim$ 50 K, corresponding to the inhibition of the optical phonon emission. Afterwards, the only mechanism allowed to cool down the plasma to lower temperatures is the emission of acoustic phonons which is very slow[Yoon, 1996]. Consequently, in a non resonant experiment, even at low lattice temperature, the carrier temperature is close to the temperature of 50 K during the exciton formation. However, the effect of the e-h plasma cooling should provide a change in the photoluminescence dynamics with respect to what predicted in Fig.3.5. In fact, for short times (less than 10 ps), the carrier temperature

is in general larger than 50 K and we expect a faster formation rate. Furthermore, for very long times (of the order of a few ns) the cooling due to acoustic phonon emission should also be taken into account. The results shown in Fig.3.5 do not include these two effects. We did not investigate the formation in presence of simultaneous cooling of the e-h plasma because we believe that the best experimental setup for the study of the exciton formation process corresponds to the situation discussed in Fig.3.4. The case depicted in Fig.3.5, corresponding to $T_c = 10$ K, can be obtained only by a resonant creation of a cold plasma, and an ad hoc excitation should be made. Moreover, we have remarked that the dynamics of relaxation is strongly affected by the values used for the delectron and hole masses, and for the deformation potential, which are known with low accuracy. We used for masses, Bohr radius, binding energies and oscillator strength the values calculated theoretically [Andreani, 1990]. However, recent calculations have shown that the heavy hole dispersion presents a strong anisotropy [Triques, 1997]. Since the time evolution of the photoluminescence is very sensitive to the HH mass, we believe that the effects of the anisotropy have to be taken into account in order to obtain a better agreement with the experimental results.

The action mass law for the 2D case reads

$$\frac{n_e n_h}{n_X} = \frac{\mu k_B T}{2\pi\hbar^2} e^{-E_b/K_B T} , \tag{3.16}$$

where $n_e$, $n_h$, and $n_X$ indicate the free electron, free carriers, and exciton densities respectively. $E_b$ is the exciton binding energy, and $\mu$ is the reduced electron-hole mass. We analyze now the evolution of the system of excitons and free carriers towards the equilibrium which is described by (3.16). We consider a QW of 120 Å with a binding energy for the 1s exciton of 8.7 meV, and with $m_e$=0.08 and $m_h$=0.17. The initial excitation density is $10^{10}$ cm$^{-2}$. We focus only on the dynamics of thermalization and consequently we consider in the dynamics non radiative excitons. We plot in Fig. 3.6 the time evolution of the ratio $n^* = n_e n_h / n_X$, where the same temperature for the free carriers and for the lattice is assumed. In the thermal equilibrium the action mass law is valid, but the time necessary to reach this regime is strongly dependent on the lattice temperature. The equilibrium occurs on a time scale of the order of 10 ps for a temperature of 100 K, while at 20 K the system, even after 20 ns, is not thermalized. The value approached by $n^*$ for long times corresponds to the one predicted by the action mass law. This obtained dynamics indicates that at low temperature the system strongly deviates from the equilibrium and an excess of free carriers results. For lower excitation density the evolution toward the equilibrium does not differ sensitively. The experimental check of the action mass law has been carried out only for temperature larger than 100 K in the case of continuous wave photoluminescence [Colocci, 1990]. The dynamics of thermal-

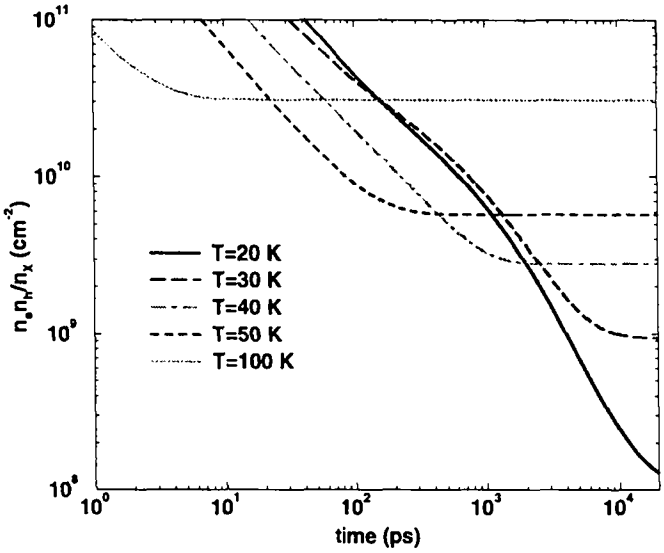


Figure 3.6: Time evolution of the ratio $n_e n_h/n_X$. The constant value for long times corresponds to the value predicted by the action mass law.

ization between free carriers and excitons has not yet been investigated experimentally. We expect that in the time evolution of the photoluminescence spectrum, which can nowadays be obtained with good energy and time resolutions [Yoon, 1996], the equilibrium will take quite long to be achieved for $K_B T \ll E_b$. Finally, we remark that in our analysis we have disregareded the radiative recombination of excitons, nevertheless the calculated times give indications on the characteristic times for the equilibrium between free carriers and excitons.

# Chapter 4

# Exciton-polariton relaxation in microcavities

In an infinite crystal, the interaction between the radiation field and excitons is characterized by translational invariance and thus wave vector conservation. A single exciton mode couples to a single radiation mode, giving rise to coupled radiation-excitation modes, called polaritons [Hopfield, 1958]. Close to the crossing of the dispersion curves of the photon and the exciton, polaritons are a strong mixture of the exciton and photon. Outside this crossing region, the polariton has either larger exciton content, or larger photon content. We refer to exciton-like and photon-like polaritons depending on the contents of exciton and photon in the mixed modes. Polaritons in the infinite crystal are stationary states and no phase space is left for the decay via radiative recombination. Therefore they may radiate only through propagation to the crystal surface [Toyozawa, 1959]. On the contrary, as remarked in Chap. 2, in a quantum well, because of the reduced dimensionality, the translational symmetry of the electronic states is broken along the growth direction, hereafter denoted by **z**. In this case, a 2D exciton can recombine to a continuum of photon modes with all the possible values of $k_z$ and a finite radiative recombination rate results [Agranovich, 1966]. We do not therefore find strong mixture between the exciton and photon as in the bulk case.

In order to realize the two dimensional analogue of the bulk polariton, a planar structure where both the photon and exciton are confined in the growth direction is necessary. Semiconductor microcavities are planar devices in which the electromagnetic field is confined by means of two parallel plane semiconductor mirrors. When a quantum well is placed inside a microcavity, excitons are coupled to the electromagnetic modes of this dielectric structure. Typical microcavities have a thickness of a few integer mul-

tiples of half the photon wavelength at the exciton resonance frequency. Consequently, an exciton is coupled to a *single* cavity mode according to the in-plane wave vector conservation. Thus, this system constitutes the 2D analogous of the bulk polariton [Savona, 1996]. In microcavities the photons have a finite lifetime which originates from the finite transmittivity of the mirrors. This implies a radiative mechanism for microcavity polaritons which, in contrast to bulk polaritons, does not involve propagation and surface recombination.

The photoluminescence process is the result of the interplay between radiative recombination and energy relaxation through the interaction of excitons with phonons. In bulk systems, the relaxation processes and the results of photoluminescence measurements have been successfully understood after detailed theoretical investigations of the dynamics of polaritons [Toyozawa, 1959, Sumi, 1975]. The effective recombination times in these systems vary by orders of magnitude, being very short for photon-like polaritons, and much longer for exciton-like polaritons. When the interaction with phonons is taken into account, the relaxation times due to phonon scattering become much longer for the photon-like polariton than for the exciton-like polariton. This effect is due to the reduced exciton content in the photon-like polariton and to the increased slope of its dispersion. The combination of the increase of radiative rate and decrease of the relaxation rate in passing from the exciton-like to the photon-like modes results in a depletion of polaritons in the photon like region, and in the absence of any further energy relaxation in this region. This overall dynamics of the 3D polariton has thus been called a bottleneck dynamics [Toyozawa, 1959]. This dynamical effect considered above has been observed in the bulk both in continuous wave [Weisbuch, 1979] and time resolved experiments [Askari, 1985].

The small exciton binding energy in bulk GaAs makes the bulk polariton weak to both large temperatures and impurity concentration. Therefore, the bottleneck effects are observed only in very pure samples at low temperature. However, these type of dynamics may be more easily observed in a system of reduced dimensionality, like semiconductor microcavities, where the exciton binding energies are increased and the radiative recombination process becomes allowed. In this chapter, we will study the dynamics of microcavity polaritons, and analyse the fundamental processes underlying the photoluminescence in time resolved experiments. Particular attention will be paid to identify the characteristic features of the microcavity polariton dynamics with respect to the dynamics of bare quantum well excitons. As for the dynamics of bare excitons, strong deviation from the thermal equilibrium are found. In the case of microcavity polaritons, since they are in some extent the two dimensional equivalent of

bulk polariton, these deviation can be referred to as a two dimensional bottleneck effect [Tassone, 1996], [Tassone, 1997]. Moreover, we will show that the modification of the dispersion of the exciton polariton due to the coupling with the cavity mode leads to a strong inhibition of the polariton acoustic phonon scattering. This reduced scattering rate results in a strong suppression of the homogeneous broadening which has been observed experimentally [Stanley, 1998], [Savona, 1997b].

## 4.1 Relaxation and formation rates of microcavity polaritons

As for the bare quantum well dynamics, we identify three steps in the description of photoluminescence from semiconductors microcavities: an excitation provided by an external pump, a relaxation process in which the energy of the excitation is redistributed among the electronic states and released to the lattice, and a radiative recombination process. In general, all these processes are characterized by different time scales. We give in Fig.4.1 a schematic picture of the polariton dispersion and of the possible scattering processes governing its dynamics and photoluminescence that we are going to consider. These include acoustic phonon scattering within the polariton branches, polariton formation from a thermal reservoir of free carriers through acoustic or optical phonon emission, and polariton radiative recombination. Neglect of other processes like exciton-carrier and exciton-exciton scattering is justified by the range of low carrier densities considered. The Boltzmann equation for microcavity polaritons reads

$$\dot{n}_{i,\mathbf{k}} = \sum_{j,\mathbf{k}'} W_{j,\mathbf{k}'\to i,\mathbf{k}}\; n_{j,\mathbf{k}'}(n_{i,\mathbf{k}}+1) - \sum_{j,\mathbf{k}'} W_{i,\mathbf{k}\to j,\mathbf{k}'}\; n_{i,\mathbf{k}}(n_{j,\mathbf{k}'}+1) - \Gamma_{i,\mathbf{k}} n_{\mathbf{k}} + \sum_{\mathbf{k_e},\mathbf{k_h}} F_{\mathbf{k_e},\mathbf{k_h}\to i,\mathbf{k}} n_e(\mathbf{k_e}) n_h(\mathbf{k_h})\;. \tag{4.1}$$

Note that with respect to Eq.3.14 the presence of the two polariton branches (index $i$) has to be considered, and interbranch scattering terms appears. Moreover, dissociation of exciton-polaritons into free carriers by absorption or emission of phonons is negligible at the low lattice temperatures considered, and can be neglected. The terms containing $(n+1)$ correspond to stimulated polariton emission and is hereon approximated by unity because of the low density considered. $W_{i,\mathbf{k}\to j,\mathbf{k}'}$ are the phonon mediated polariton scattering rates, $\Gamma_{i,\mathbf{k}}$ is the radiative recombination rate, and the last term in the right hand side represent the source term due to the injection of polaritons from the free carriers.

The scattering rates of microcavity polaritons by acoustic phonons $W_{i,\mathbf{k}\to j,\mathbf{k}'}$, where

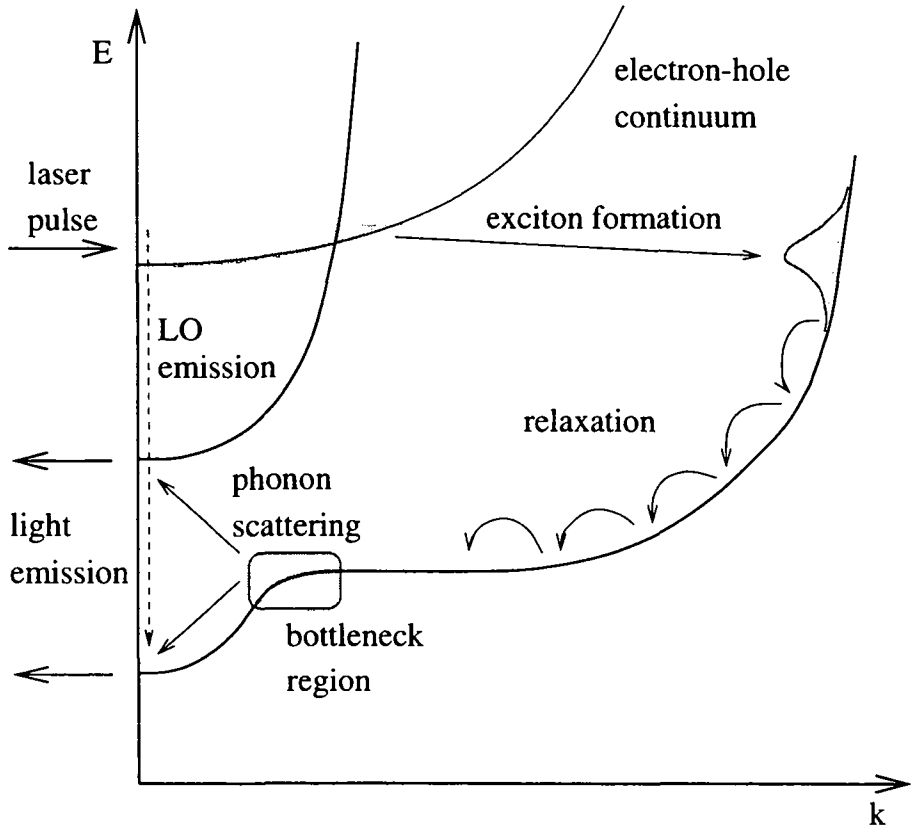


Figure 4.1: Schematic representation of the polariton dispersion, the free carrier thermal reservoir, and the possible polariton formation processes, scattering processes by acoustic phonon emission or absorption, and radiative recombination.

$\mathbf{k}$ and $\mathbf{k}'$ are the in-plane microcavity polariton wave vectors, $i, j$ are the branch indexes, are calculated using the deformation potential interaction and the Born approximation, in the same way as for the bare exciton scattering rates. Emission and absorption of optical phonons within the microcavity polariton bands is impossible, due to the large LO phonon energy. The scattering rate $W_{i,\mathbf{k}\to j,\mathbf{k}'}$ is the sum of two contributions arising from phonon emission and absorption. The Born approximation for the absorption (-) or emission (+) term gives:

$$W^{\pm}_{i,\mathbf{k}\to j,\mathbf{k}'} = \frac{2\pi}{\hbar}\sum_{q_z}\left|X^{\star}_{j,\mathbf{k}'}\langle\mathbf{k}'|\langle 0_{\mathbf{q},q_z}|H_{exc-ph}|1_{\mathbf{q},q_z}\rangle|\mathbf{k}\rangle X_{i,\mathbf{k}}\right|^2 \times$$
$$\delta\left(\hbar\Omega_{j,\mathbf{k}'} - \hbar\Omega_{i,\mathbf{k}} \pm E^{(ph)}_{\mathbf{q},q_z}\right)\left(n_{E^{(ph)}_{\mathbf{q},q_z}} + 1/2 \pm 1/2\right) . \qquad (4.2)$$

Here $\mathbf{q} = \mathbf{k}' - \mathbf{k}$ is the exchanged in plane momentum, $H_{exc-ph}$ is the deformation potential interaction, $|n_{\mathbf{q},q_z}\rangle$ is a phonon number state, $|\mathbf{k}\rangle$ is the exciton state of wave vector $\mathbf{k}$, $\hbar\Omega_{i,\mathbf{k}}$ is the polariton energy, branch $i$, wave vector $\mathbf{k}$, $n(E^{(ph)})$ is the Bose occupation number for phonons, and $E^{(ph)}_{\underline{\mathbf{q}}} = \hbar u\underline{\mathbf{q}}$ is the phonon energy. The $X_{i,\mathbf{k}}$ are the Hopfield coefficients whose square modulus gives the exciton content in the polariton state of branch $i$, wave vector $\mathbf{k}$. With respect to the case of bare quantum wells of expression in Eq.2.14 we have a different dispersion law for the particles involved in the scattering, and the presence of the Hopfield factors.

In order to calculate the scattering rates, we need to specify the exact energy dispersion $\Omega_{i,\mathbf{k}}$ of the polariton modes. We consider a GaAs based realization of a one-wavelength semiconductor microcavity having a single quantum well embedded at its center. High-reflectivity Distributed Bragg reflectors (DBR) consisting of 24 and 20 pairs of quarter-wavelength layers respectively enclose the cavity. The exact mixed exciton-cavity modes are calculated analytically by diagonalizing the exciton-photon interaction, where the free electromagnetic modes of the full DBR structure are considered. We give in Fig.4.2 the polariton dispersion corresponding to the considered structure. Two polariton branches appear denoted by $n = 1$ (lower polariton mode) and $n = 2$ (upper polariton). The modes given here corresponds to the situation when the detunig, defined as $\delta = \hbar\Omega_{cav} - \hbar\omega_{exc}$, with $(\Omega_{cav} = c\pi/L_{cavity})$, is zero. In some microcavities the detuning can be modified since through the sample the cavity length $L_{cavity}$ is not constant, and the $\Omega_{cav}$ can be changed exciting the sample on different spatial regions . A Rabi splitting, defined as the energy difference between the two polariton branches at $\mathbf{k} = 0$, $\hbar\Omega_R = \hbar\Omega_{upper,\mathbf{k}'=0} - \hbar\Omega_{lower,\mathbf{k}=0} = 4$ meV results for the considered microcavity. In Fig. 4.3 we plot the total radiative broadening of the modes $\Gamma_{i,\mathbf{k}}$ for a detuning $\delta = 0$. Radiative lifetimes are in the picosecond range, a value which is also typical of GaAs based quantum well structures, and has been observed experimentally

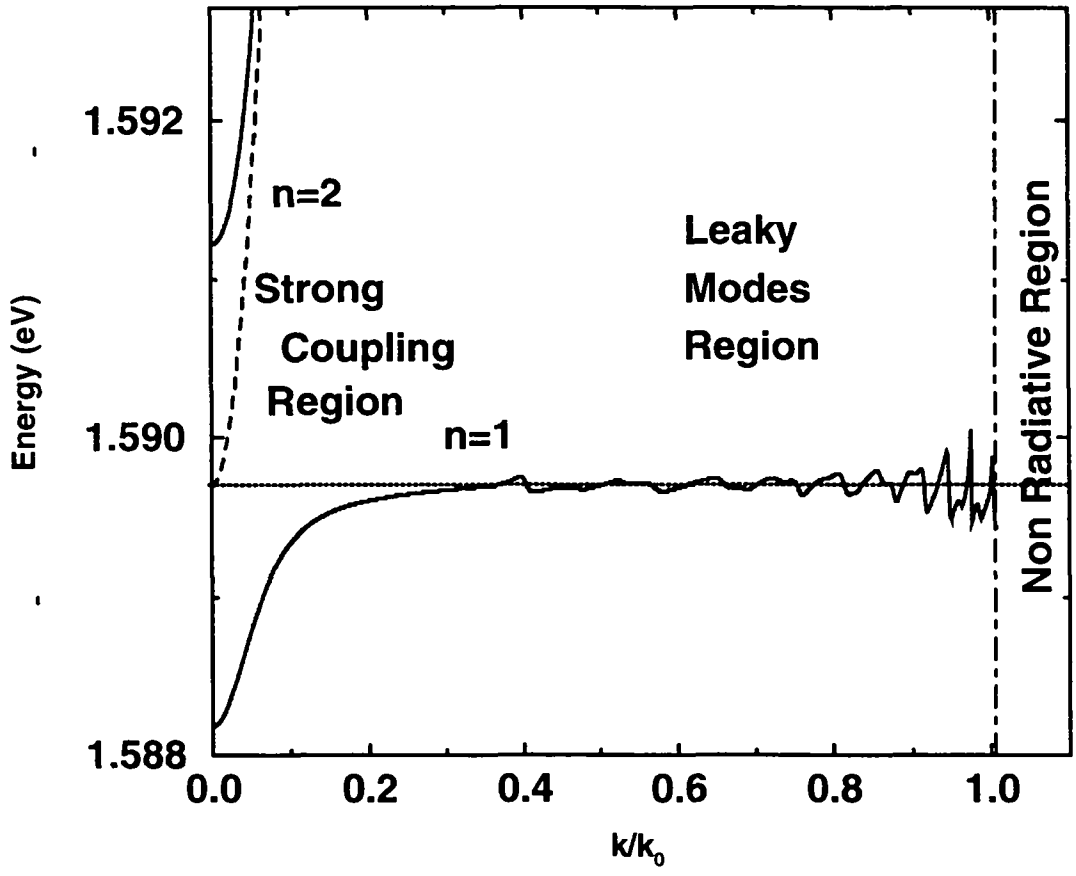


Figure 4.2: Micro-cavity polariton modes for the GaAs sample considered in this work, at $\delta = 0$. The strong coupling region, and leaky modes region are indicated, the non radiative zone corresponds to $k > k_0$

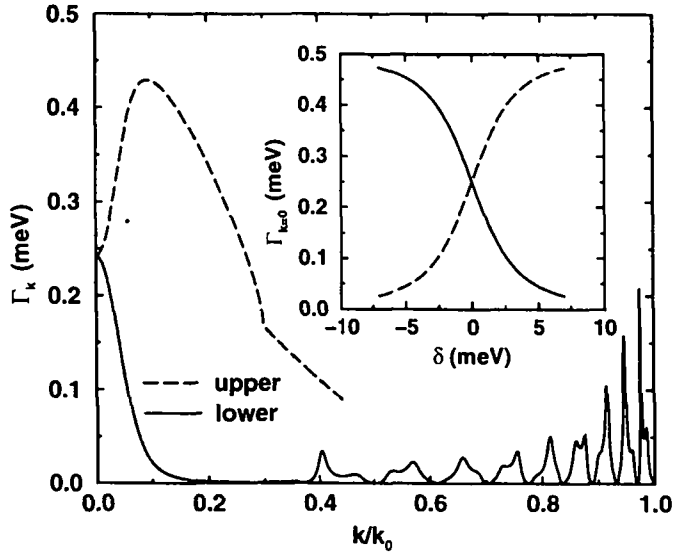


Figure 4.3: Micro-cavity polariton radiative recombination rate $\Gamma_{\mathbf{k}}$ for the GaAs sample considered in this work, at $\delta = 0$. The inset shows the normal direction radiative recombination rate as a function of the detuning $\delta$.

[Sermage, 1996]. As for the bare quantum well, the radiative rate vanishes outside the radiative region $k < k_0 = n_{cav}\Omega_{exc}/c$, where $n_{cav}$ is the cavity index of refraction. In the inset of Fig. 4.2 we plot $\Gamma_{i,0}$ as a function of the detuning $\delta$. We notice that this is rather large, and is proportional to the cavity photon fraction of the polariton mode, exception made for exciton-like modes, when $\delta \gg \hbar\Omega_R$. We remark the presence of several peaks for $k > 0.3k_0$. These structure are due to the coupling of the exciton with the leaky modes of the cavity. Leaky modes are electromagnetic modes propagating at finite angles with respect to the growing direction through the DBE into the substrate. They are due to the peculiar structure of the DBRs, which introduces additional resonances in the electromagnetic field at finite angles [Savona, 1995]. We can therefore distinguish three regions in the lower polariton dispersion which correspond to a different radiative recombination features. The first region is the strong coupling region characterized by a strong radiative emission in the growth direction, in our case corresponds to $k < 0.3k_0$. The second region, with $0.3k_0 < k < k_0$, is dominated by the leaky modes, with emission at large angles. The third region is non radiative and correspond to $k > k_0$. We are going to consider the polariton dynamics for several values of the exciton cavity detuning $\delta = 0$, $\hbar\Omega_R$,-$\hbar\Omega_R$,-2$\hbar\Omega_R$. For practical purposes, we have also used an analytical

approximation to the exact dispersion, which neglects details of the dispersion effects in the leaky modes region [Savona, 1996]. Its form is given by the usual solutions of the polariton dispersion equations [Savona, 1995]

$$(\Omega_{exc,\mathbf{k}} - \Omega_{i,\mathbf{k}})(\Omega_{cav,\mathbf{k}} - \Omega_{i,\mathbf{k}}) = \Omega_R^2/4 \tag{4.3}$$

where $\Omega_{cav,\mathbf{k}} = \sqrt{c^2/\epsilon_{cav}\mathbf{k}^2 + \Omega_{cav}^2}$. For ease of reference, we also report the expression for the square modulii of the Hopfield coefficients:

$$|X_{i,\mathbf{k}}|^2 = \frac{\Omega_R^2/4}{\Omega_R^2/4 + (\Omega_{i,\mathbf{k}} - \Omega_{exc,\mathbf{k}})^2}. \tag{4.4}$$

Let us finally discuss how the photoluminescence is calculated after the populations resulting from the solution of Eq.4.1. The width of this peaks is practically broadened by various effects, but here we are interested in their overall intensity. In the framework of the rate equation model, summarized in Eq.4.1, the photoluminescence at a given angle $\theta$ is proportional to the photon emission rate $\Gamma_{i,\mathbf{k}} n_{i,\mathbf{k}}$ into the corresponding k vector, $k = n_{cav} \sin\theta \Omega_{i,\mathbf{k}}/c$. Here $n_{cav}$ is the cavity index of refraction, and $\theta$ is the propagation angle in the cavity. The propagation angle in air $\theta_{air}$ is easily calculated from the relation $\sin\theta/\sin\theta_{air} = n_{cav}$. Given the large index of refraction of $GaAs$, we find total internal reflection for most leaky modes. The calculation of the population $n_{i,\mathbf{k}}$ therefore allows us to calculate the photoluminescence emission at any given angle $\theta_{air}$ for either the upper or the lower polariton.

Formation of exciton-polaritons may occur through the absorption or emission of acoustic phonons, or through the emission of optical phonons, as schematically shown in Fig.4.1. The expression for the bimolecular formation coefficient $C$ is similar to the one given in Chap.3, provided the appropriate Hopfield factors for exciton content in the final state are included. As for the bare quantum well case, the exchange of acoustic phonons involves energies of the order of less than a meV, and polaritons are created with large in plane momentum $\mathbf{k}$ in the exciton like region of the lower polariton. Since the final states are exciton like the distribution in energy of the created exciton is the same of Fig. 3.2. Concerning optical phonon emission, it is clearly not quasi-elastic due to the large, dispersionless energy of the optical phonon. Thus, both lower and upper branch polaritons are formed by this process. We notice the fact that the LO phonon is dispersion-less, therefore the distribution in energy of the injected polaritons mirrors that of the free carriers, times the Hopfield factor. We remark that the formation by optical phonon can be very efficient in order to directly populate the region of the lower polariton close to $k = 0$ [Pau, 1997]. This region cannot be reached by emission of acoustic phonons due to the presence of the bottleneck region where the polaritons are stopped.

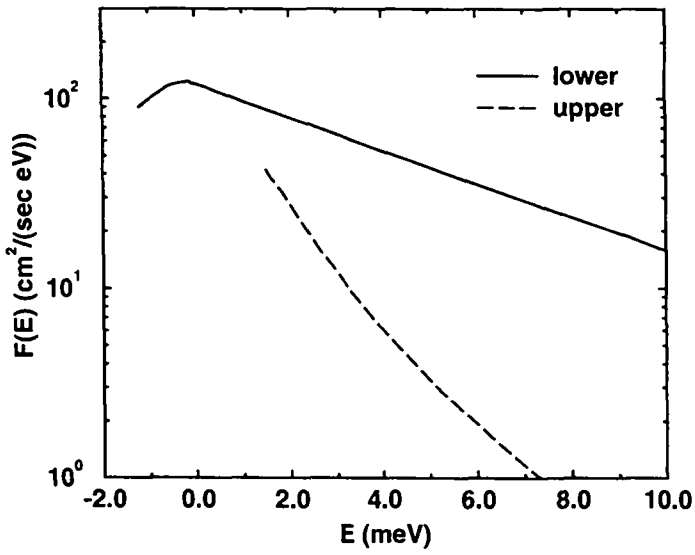


Figure 4.4: The lower branch (solid line) and upper branch (dashed line) polariton LO phonon formation rates as a function of the polariton energy (the origin is fixed at the exciton energy), at a carrier temperature $T_C$=60 K.

We present in Fig. 4.4 the polariton formation coefficient $F_{LO,j}(E)$ as a function of the energy of the created polariton for $T_C$=60 K. We notice that in the region close to $k = 0$ the coefficient follows the variation of the Hopfield coefficient. Therefore the upper polariton formation coefficient is rapidly cut-off at high energies. On the exciton-like lower branch the formation coefficient simply shows the Boltzmann tail at the free-carrier temperature $T_C$ (a temperature of 60 K is equivalent to an energy of about 6 meV). This calculation also shows that although the formation rate is reduced in the strong-coupling region by the presence of the Hopfield factor, it still remains sizeable. Thus lower-branch polaritons in the strong coupling region are likely to be directly injected by LO phonon emission, while it is unlikely for them to be injected by intrabranch acoustic phonon scattering. Qualitative changes in the dynamics and in the photoluminescence are thus expected for large $T_C$.

## 4.2 Polariton dynamics

The Boltzmann equation 4.1 has been numerically integrated choosing a sharply peaked distribution for the lower branch at the energy of the exciton continuum ($\sim$ 10 $meV$)

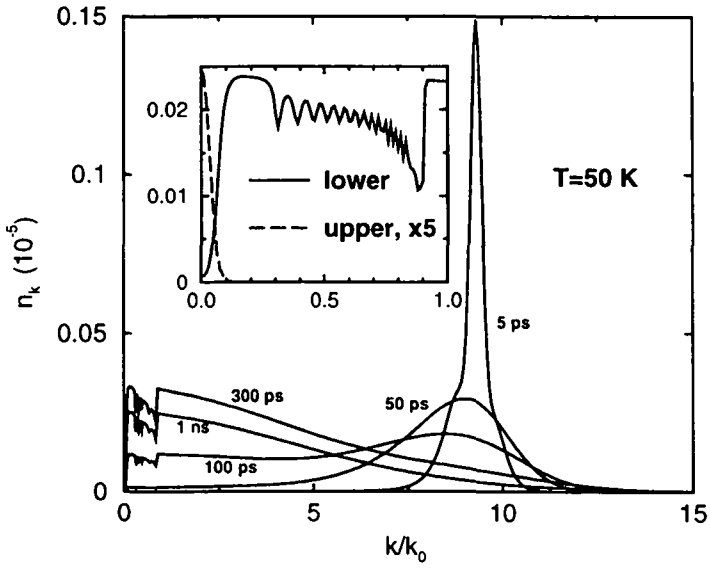


Figure 4.5: The population of the lower polaritons at different time delays after the initial excitation, at zero detunig and $T = 50K$. The inset shows a detail of the radiative region and includes also the upper branch population at a time delay of 1 ns.

as the initial condition. This initial condition correspond to formation assisted by emission of acoustic phonons. In the first part of the evolution, up to a few hundreds of picoseconds, both lower and upper branch polaritons at small $k$ are created after several steps of phonon emission, as shown in Fig. 4.5, for $T = 50$ K and $\delta = 0$. The photoluminescence signal correspondingly rises. For longer times, the polariton distribution reaches a quasi-stationary shape which rigidly decreases in time (Fig. 4.5, inset). The photoluminescence signal therefore follows this decay time.

The photoluminescence decay and rise times as functions of the temperature and detuning are shown in Fig. 4.6. The photoluminescence decay time $\tau_D$ is found to be linearly increasing with temperature. This behavior of $\tau_D$ is the same one found for the bare quantum well exciton. It is remarkable that both $\tau_D$ and $\tau_R$ are not much influenced by the cavity detuning $\delta$. This fact is surprising when considering that both radiative rates and phonon scattering rates region indeed are strongly affected in the small $k$ region. We notice from Fig. 4.5 that, apart from small deviations in the radiative region, and close to $\mathbf{k} = 0$, the lower branch distribution is Boltzmann like. In particular, among the radiative states, the leaky modes region is mostly populated, while the strong coupling region, close to $\mathbf{k} = 0$ is strongly depleted. Therefore, it is

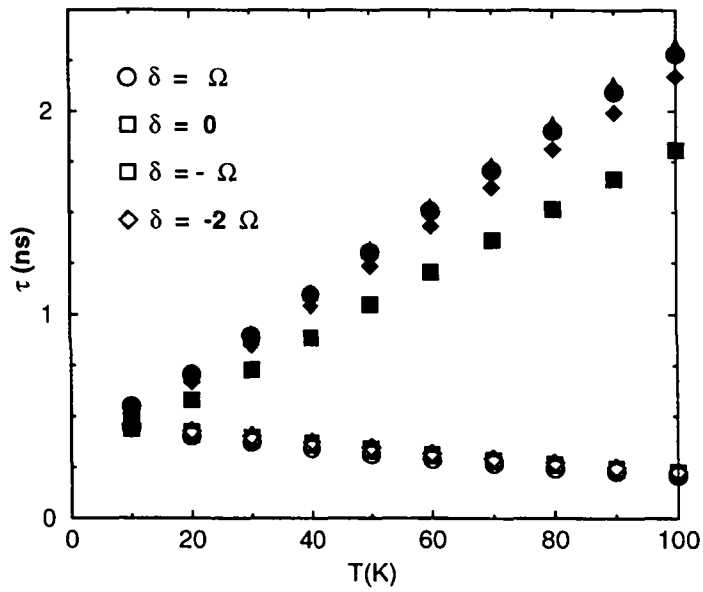


Figure 4.6: The rise times (empty symbols) and the decay times (filled symbols) of the photoluminescence, for different detunings.

only the leaky modes which play the fundamental role in the overall photoluminescence dynamics. In the region of the leaky modes, the radiative recombination rates and the phonon scattering rates are *not* significantly influenced by the cavity detuning $\delta$. This justifies the result found in Fig. 4.6, where little influence on the cavity detuning, and in fact on the presence of the cavity itself, of the characteristic rise and decay times is found. We remark that, as for bare quantum wells (Chap 2), the fact that the finite intercept in linear behavior in the temperature of $\tau_D$ is a signature of the deviation from the thermal equilibrium for the polariton distribution function.

We now discuss in detail the dynamics of the lower and upper branch PL rise-times. The rise time $\tau_R$ has been defined as the time necessary for the photoluminescence signal to reach its maximum. We first notice that in a first step of the relaxation, the excitons cool down to the bottom of the exciton-like branch (bottleneck region) by phonon emission. At this point a bottleneck in further relaxation into the strong coupling region is produced, like for the bulk. It is caused by a the slow down of the phonon emission rates due to the steep polariton dispersion, together with the increased radiative recombination rates. After the polaritons have reached the bottleneck region, relaxation involves a single jump with a single phonon emission toward the $k = 0$, as shown in Fig.4.1. The photoluminescence emission is thus related to this single jump,

which is immediately followed by the radiative recombination. A rather large amount of energy is released during this last step of relaxation, which is assisted by emission of a single acoustic phonon. This is only in apparent contrast to the claimed quasi-elasticity in the scattering of polaritons with phonons. In fact, it results from the calculations that the rate of scattering as a function of energy exchanged is peaked at about one meV, but still displays long tails around this value. The broadening of this energy distribution is both determined by the cutoffs in the superposition integrals and by the shape of the phonon population factor $n(E)$, which enters in the temperature dependence. As a consequence, the rate for scattering from the bottleneck region to the $k = 0$ region, even if very small, is finite. Finally, since the the emission occur after the single jump from the bottleneck region, the build up of the photoluminescence adiabatically follows the buld up of population at the bottom of the exciton-like branch. We conclude that the rise time of the photoluminescence at $\mathbf{k} = 0$ is only determined by the relaxation time in the non radiative and leaky modes regions of the lower polariton branch. Therefore, it is detuning independent. The importance of the bottleneck effects in the interpretation of the experimental results has recently been proved through an angle resolved analysis [Wainstain, 1998].

The upper branch photoluminescence dynamics differs considerably from the lower branch one. In fact for the rise time there is a marked dependence on the detuning. In particular, in Fig.4.7, we see that the rise time decreases with increasing positive detuning. To explain this behaviour we remark that the only mechanism for the population of the upper branch is interbranch scattering from excitons in the lower branch. In fact, we already noticed that upper branch polaritons at the electron-hole continuum energy are unlikely to be formed because of their small exciton content. The interbranch scattering is quasielastic, always in the sense explained in detail above. Then, mostly excitons in a portion of the lower branch having the same energy as the bottom of the upper branch are involved in this interbranch scattering process. These "horizontal" scattering processes are evidenced in Fig. 4.1, and are allowed by the degeneracy in energy of the upper branch and the exciton-like branch. It also happens that even in this case $\Gamma_{up,\mathbf{k}=0}$ is larger than this populating rate. We conclude that the population $n_{up,\mathbf{k}=0}$ adiabatically follows the population of the exciton-like branch at the same energy. The first remark, that the upper branch rise time is usually shorter than the lower branch one, thus finds an obvious explanantion. In fact, cooling excitons reach these higher energies well before reaching the bottom of the exciton-like band. The other remark, that this rise time depends markedly on the detuning, as is shown in Fig. 4.7, is also clearly explained, as for larger positive detunings the energy of the $\mathbf{k}$=0 upper branch

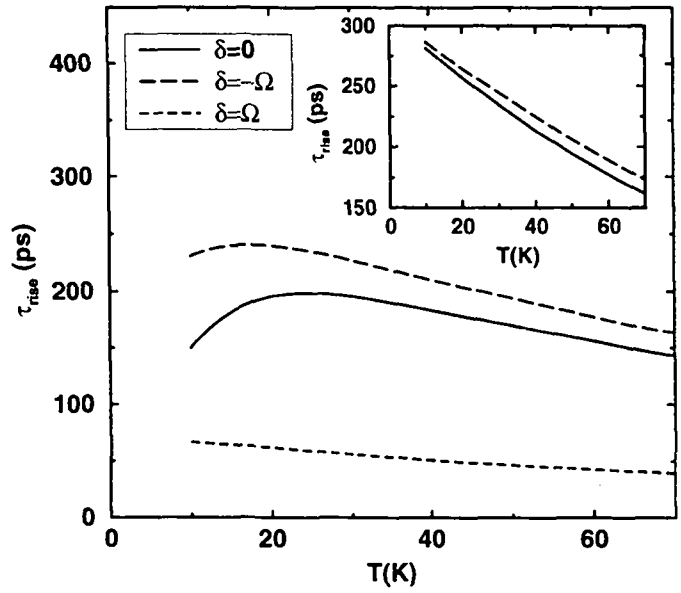


Figure 4.7: Rise-time $\tau_R$ as a function of the lattice temperature for the upper branch PL. Three different detunings are considered considered. The inset show the rise time for the lower polariton branch. Here the $\delta = -\Omega$ case coincide practically whith the $\delta = \Omega$ case, and it is not reported in the figure.

polariton is also higher. On the opposite side of detunings, the upper branch becomes exciton like, thus the photoluminescence rise time approaches the value found for the lower branch, as appears in Fig. 4.7.

## 4.3 Polariton thermal broadening

In the following we will consider the broadening of excitons and polaritons in their fundamental state $1s$ at $k = 0$. We have seen that in typical III-V materials the optical phonon energy is quite large and in experiments at $K_BT \gg \hbar\omega_{LO}$ the main contribution to the thermal broadening comes from the acoustic phonon scattering. In the calculations of the scattering, and thus of the thermal broadening, the dispersion law of the particles involved determines the phase space for the scattering. This phase space is strongly different for the bare quantum well exciton and for the microcavity polaritons. Therefore, we expect some modification in the thermal broadening for the two different systems. Let us consider the case of bare quantum well exciton: The broadening of the

$k = 0$ exciton is given by the sum of the scattering rate to all possible final states

$$\Gamma_{exc} = \sum_k W_{0\to k} \tag{4.5}$$

Assuming the same mass for the electron and the hole, the scattering rates given in formula 2.15 simplify, and the thermal broadening can be written as

$$\Gamma_{exc} = a \int \frac{E(k')}{|\hbar u q_z^0|} |I_{||}(k')|^2 |I_\perp(q_z^0)|^2 \frac{k' dk'}{e^{\beta E(k')} - 1} \tag{4.6}$$

whith $a = |a_c - a_v|^2/2\pi\rho\hbar u^3$. $E(k')$ is the exciton dispersion and the $q_z^0$ is given by energy conservation through $\hbar u\sqrt{(q_z^0)^2 + k^2} = E(k')$. The two superposition integrals $I_{||}(k')$, $I_\perp(q_z^0)$ introduce cut-off in wavevector space. For the materials considered here the important cut-off is the one in $z$ direction. For $q_z^0 \sim 3\pi/L - QW$, $|I_\perp(q_z^0)|^2$ give a reduction of one order of magnitude. Neglecting the in-plane phonon dispersion with respect to the exciton dispersion, $\hbar u q_z^0 \sim E(k')$, and the cut off in $q_z^0$ becomes a cut off in the energy exchanged in the scattering. Therefore we approximate the superposition integral $|I_\perp(q_z^0)|^2 \sim \theta(E_{cut} - E)$, with the cut off energy defined by $E_{cut} = \hbar u 3\pi/L_{QW}$. Using this approximation the bare exciton thermal broadening becomes

$$\Gamma_{exc}(T) = a\frac{M_{ex}}{\hbar^2} E_{cut}^2 Y^2 \int_0^{1/Y} \frac{x}{e^x - 1} dx \tag{4.7}$$

where $Y = k_B T/E_{cut}$. In the limit $k_B T \gg E_{cut}$ we obtain the linear dependence

$$\Gamma_{exc}(T) \sim bT \tag{4.8}$$

Using un $E_{cut}$ =3 meV corresponding to a quantum well of 10 nm, we obtain for the slope $b = 4.7\mu eV/K$ which is in good agreement with the experimental measurements [Shultheis, 1986], and attests the validity of the approximations made.

When the quantum well is embedded in a microcavity structure the polariton at $k = 0$ is a mixture of photon and exciton wheighted by the Hopfield factors given in Eq.4.4. Let's start with the case of lower polariton. We have to considere two different situations. In the first one, the energy separation from the polariton at $k = 0$ (at the energy $E_{pol}$), and the bottleneck region, which is approximatively at the bare exciton energy $E_{exc}$, is larger than the cut off energy $E_{cut}$. In this case the polariton dispersion can be approximated by a parabolic dispersion with a mass $M_{pol}$, and the thermal broadening becomes

$$\Gamma_{pol}(T) = |X_{low,0}|^2 a\frac{M_{pol}}{\hbar^2} E_{cut}^2 Y^2 \int_0^{1/Y} \frac{x}{e^x - 1} dx\ . \tag{4.9}$$

Thus

$$\Gamma_{pol}(T) = |X_{low,0}|^2 \frac{M_{pol}}{M_{exc}} \Gamma_{exc}(T) \ , \tag{4.10}$$

and the polariton broadening is reduced of about four order of magnitude due to the small polariton mass ($M_{pol} \sim 10^{-4} M_{exc}$). For $E_{exc} - E_{pol} < E_{cut}$ the scattering in the bottleneck and above is allowed. In this region the density of states for the scattering is again determined by the bare excitonic mass, therefore the thermal broadening increases. We define a parameter

$$\alpha = \begin{cases} E_{exc} - E_{pol}/E_{cut} & \text{if } E_{exc} - E_{pol}/E_{cut} < 1 \\ 1 & \text{if } E_{exc} - E_{pol}/E_{cut} > 1 \ . \end{cases} \tag{4.11}$$

We then get

$$\Gamma_{pol}(T) = |X_{low,0}|^2 a \frac{M_{exc}}{\hbar^2} E_{cut}^2 Y^2 \int_{\alpha/Y}^{1/Y} \frac{x}{e^x - 1} dx \ . \tag{4.12}$$

As before we can look at the limit $K_B T \gg E_{cut}$ and obtain the simple expression

$$\Gamma_{exc}(T) \sim |X_{low,0}|^2 bT(1 - \alpha) \ . \tag{4.13}$$

For the upper polariton both phonon emission and phonon absorption are allowed. Using the parameter $\alpha$ defined above we obtain

$$\Gamma_{pol}^{up}(T) = |X_{up,0}|^2 a \frac{M_{ex}}{\hbar^2} E_{cut}^2 Y^2 \left( \int_0^{1/Y} \frac{x}{e^x - 1} dx + \int_{\alpha/Y}^{1/Y} \frac{x}{e^x - 1} dx + \alpha^2/Y^2 \right) \ . \tag{4.14}$$

The first term in bracket is due to phonon absorption while the second and the third term are due to the phonon emission. The third term indicate that even at $T = 0$ the emission of acoustic phonon, and transition to the lower polariton branch is always possible. This thermal broadening at $T = 0$ is however very small ($50 \mu eV$) and difficult to observe experimentally. In the limit $K_B T \gg E_{cut}$ we obtain again the linear behavior

$$\Gamma_{exc}(T) \sim |X_{upper,0}|^2 bT(1 + \alpha) \ . \tag{4.15}$$

For $\alpha$ close to 1 and detuning $\delta = 0$, the upper polariton slope in the temperature dependence is the same as the bare quantum well. This slope can never be reduced for the upper polariton, except in the case of strong positive detuning when $X_{upper,0}$ goes to zero.

The parameter $\alpha$ can be changed by detuning the cavity resonance with respect to the exciton level

$$\alpha = \frac{\sqrt{(\hbar\Omega_R)^2 + \delta^2} - \delta}{2E_{cut}} \ . \tag{4.16}$$

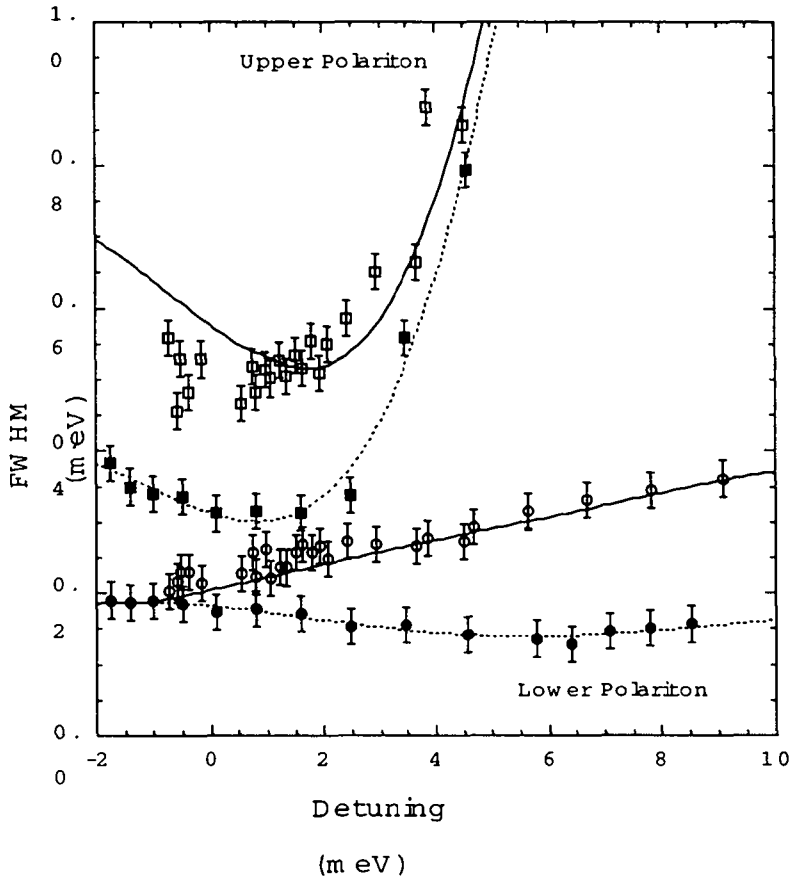


Figure 4.8: Experimental linewidth of upper (squares) and lower (circles) polariton as a function of the cavity exciton detuning. Solid symbols are at 4.2 K and open symbols are at 60 K. The dashed lines are the result of a polynomial interpolation to the low temperature data. The solid lines are the sum of the temperature dependent acoustic phonon scattering at 60 K calculated through the expresions 4.13 and 4.15 and the 4 K linewidth. (Courtesy of R. P. Stanley)

We have compared this theory with recent measurements done in very good quality semiconductor microcavities [Stanley, 1998]. We show in Fig.4.8 the linewidth of the upper (squares) and lower (circles) polariton at 4.2 K (filled symbols) and 60 K. It is clear that for detuning such that $\frac{\sqrt{(\hbar\Omega_R)^2+\delta^2}-\delta}{2E_{cut}} > 1$ the lower polariton thermal broadening is is given by the expression 4.10 and is thus negligible. The only contribution to the observed broadening comes from the inhomogeneous contribution due to the interface roughness. We remark that these samples have the smallest inhomogeneous broadening (200 $\mu$ e V) ever observed up to now in III-V microcavities. This inhomogeneous broadening does not dependent on the temperature. When the detuning is larger, then $\alpha < 1$ and the broadening follows the relation 4.12, and becomes sensitive to the rise of temperature from 4 to 60 K. We remark that for positive detuning a contribution from the exciton free carrier scattering broadens significantly the line of the upper polariton. In order to compare the theory with the experiment the detunig dependence of the broadening at low temperature (T=4K) has been fitted by a polynomial law. Then the density dependent contribution due to the acoustic phonon scattering at 60 K (expressions 4.13, and 4.15) has been added to the polinomial law. The sum of the polinomial law at 4 K with and the thermal broadening contribution is indicated in the figure by continuous lines. The accord is very good, and no adjustable parameters are used in the comparison of the theory with the experiment. The only fitting parameter comes from the estimation of the cut off energy. We have considered the case of an infinite well of 10 nm and set the cut off when the superposition integral has dropped of one order of magnitude. We remark also that the approximation of equal masses for the electron and the hole results to be a good approximation. In fact, the difference between the masses, present only in the superposition integrals of Eq.2.15, is inessential when the exchange phonon momentum is small.

# Chapter 5

# Electron hole correlation in 1D systems

Up to now, the dynamics of the carriers and the optical properties have been investigated in the limit of low densities. We want now rise the total density of carriers in the crystal and investigate the density dependent effects in the optical spectra. We focus on one dimensional systems, and the results are compared with measurements on semiconductor quantum wires. We use a Green's function technique, wich is one of the most powerful tools used in many body problems. The advantage of such an approach consists in the possibility of summing an infinite series of selected contributions (Feynmann diagrams) in the perturbative expansion. In particular, a simple approximation which contains an infinite sum of terms and gives rise to bound states is provided by the ladder approximation (or T matrix approximation). Using this approximation the population of both strong correlated bound electron hole states and weakly correlated "free" carriers are considered on the same footing in the density dependent effects [Piermarocchi, 1998a], [Pereira, 1998] . We will introduce the concept of one particle spectral function and explain how it is affected by the presence of bound states. The one particle spectral function is characterized by a main quasi particle peak and by a satellite structure [Zimmermann, 1988]. This structure accounts for all the excitons that can be formed by the electron. The presence of both bound and free carrier population allows the correct investigation of the spectra in the temperature regime where the thermal energy is lower than the exciton binding energy. We will show that a spectral region with negative absorption can coexist with excitonic features. The negative absorption is the basic ingredient for the optical gain, and thus necessary for the onset of a laser behaviour. The electron hole Coulomb correlation affects also the observation of the renormalization of

the single particle energy (band gap renormalization) in the optical spectra. Using a self consistent T matrix approach [Tassone, 1998], [Schepe, 1998], a frequency dependent broadening of the states is calculated and a non shifting peak in the density dependence of the photoluminescence is obtained, in accord with the experimental observation. The observation of a non shifting peak is explained as a consequence of the persistence of a strong electron hole Coulomb correlation even in the regime of degenerate plasma [Piermarocchi, 1998b].

## 5.1 Excitons as composite fermions

The system of interacting electrons and holes coupled to the electromagnetic field is described by an Hamiltonian of the form

$$H = H_0 + H_C + H_P \ . \tag{5.1}$$

The three terms describe the free electrons, holes and photons ($H_0$), the Coulomb correlation between electrons and holes ($H_C$), and the coupling of electrons and holes with photons in the dipole approximation ($H_P$). The one dimensional electrons and holes are considered as two independent species of particles, thus the effects due to the interband exchange of carriers are neglected. A parabolic dispersion with the same mass is assumed for the electron and hole bands. In the $H_C$ we consider an effective contact potential of the form

$$V_{eff} = a\delta(z) \ , \tag{5.2}$$

where the $z$ is the direction along the quantum wire. An attractive delta-like potential between the electrons and the holes gives one bound state only, and the constant $a$ can be chosen such to reproduce the exciton binding energy in the limit of low density. This simplified potential reproduces the main features of the Coulomb correlation at low densities, as the presence of bound states and the correct Sommerfeld factor above the band edge. In the real systems 2s, 2p, ... bound levels are close to the continuum of states, and practically indistinguishable from the continmuum due to a finite broadening. Therefore, the delta like model gives a good approximation to the optical spectra. Furthermore, we expect that the density dependence of the calculated spectra is mainly affected by the order at which the different many body effects are calculated, and the use of a contact potential allows to go beyond the approximations usually made with more realistic potentials. With the effective potential of Eq.5.2 the interaction Hamiltonian is

$$H_C = -a \sum_{q,k,k',\sigma,\sigma'} c^\dagger(k+q,\sigma) d^\dagger(k'-q,\sigma') c(k,\sigma) d(k',\sigma')$$

$$+\frac{a}{2}\sum_{q,k,k',\sigma} c^\dagger(k+q,\sigma)c^\dagger(k'-q,-\sigma)c(k,-\sigma)c(k',\sigma)$$
$$+\frac{a}{2}\sum_{q,k,k',\sigma} d^\dagger(k+q,\sigma)d^\dagger(k'-q,-\sigma)d(k,-\sigma)d(k',\sigma) \qquad (5.3)$$

where $c$, $d$ ($c^\dagger$, $d^\dagger$), are the electron and hole annihilation (creation) operators respectively. Due to the fermionic nature of the carriers, in the intraband term only the interaction with opposite spin is allowed. In fact, two identical fermions can not interact with a contact interaction due to the Pauli exclusion principle.[1] The use of this manageable potential in the case of electrons and hole in semiconductors allows the investigation of the transition of the system from a regime where only bound states (excitons) are present, to a regime where they ionize and an electron hole plasma results.

In the non equilibrium Green's function formalism [Danielewicz, 1984] we deal with four one particle Green's Functions. The retarded and anticipated Green's functions for the electron are defined as

$$G_e^+(\sigma,k,t,t') = -i\langle T[c(\sigma,k,t)c^\dagger(\sigma,k,t')]_+\rangle\ \theta(t-t'). \qquad (5.4)$$

$$G_e^-(\sigma,k,t,t') = i\langle T[c(\sigma,k,t')c^\dagger(\sigma,k,t)]_+\rangle\ \theta(t'-t). \qquad (5.5)$$

where $T$ is the time ordering operator, and the statistical averages are done with respect to an arbitrary statistical operator $\langle\ldots\rangle = Tr\rho\ldots$. In particular, this statistical operator can be a simple projector and describe pure quantum state. The $[\ ]_+$ represents the anticommutator. The lesser and greater correlation Green's functions read

$$G_e^<(\sigma,k,t,t') = i\langle c^\dagger(\sigma,k,t)c(\sigma,k,t')\rangle\ . \qquad (5.6)$$

$$G_e^>(\sigma,k,t,t') = -i\langle c^\dagger(\sigma,k,t')c(\sigma,k,t)\rangle\ . \qquad (5.7)$$

Similar expressions for the holes Green's functions hold. The four functions of equations 5.4-5.7 can be reduced to a single Green's function $G_e(\tau,\tau')$, with $\tau$ and $\tau'$ defined on the Keldysh contour. The time defined on the Keldysh contour extends from $-\infty$ to $\infty$, and then back to $t_0$. Further details about the Keldysh contour are given in Appendix B. We prefer to use here a formulation with real times and frequencies on the Keldysh contour instead of the formulation with imaginary times and Matzubara poles available for systems at finite temperatures [Mahan, 1981]. In fact, the solution of the self consistent problem is by necessity numerical. Then, the analytical extension

[1] The contact potential interaction we consider here is equivalent to a two components Hubbard model in the limit of infinite width of the band. Recently the Hubbard model treated within the T matrix approximation has been proposed as a powerful tool for the investigation of correlated electronic systems [Kagan, 1998, Kyun, 1998].

to real frequencies, which has to be done for functions defined on the Matzubara poles, is numerically difficult, due to the complex structure of the resulting Green's functions. Moreover, we are interested in extending these calculations to non equilibrium systems. This non equilibrium analysis will help us to understand the dynamics just after excitation, and when strong radiative recombination combines with slow relaxation. In view of developments in this direction we use the non-equilibrium Green's function technique in the real frequencies and time domain, even if we restrict to the quasi-equilibrium, stationary situation.

The Dyson equation for the single particle (electron or hole) $G_e(\tau,\tau')$ Green's function reads [2]

$$G_e(k,\tau,\tau') = G_e^0(k,\tau,\tau') + \oint d\tau'' d\tau''' G_e^0(k,\tau,\tau'')\Sigma_e(k,\tau'',\tau''')G_e(k,\tau''',\tau') \ . \quad (5.8)$$

The time integrations are over the Keldysh contour. The functional dependence of the self energy on the single particle Green's functions determines the degree of approximation. In the T matrix approximation the functional dependence of the self energy is given by the relation

$$\Sigma_e(k,\tau,\tau') = \sum_\alpha g_e(\alpha) \int \frac{dq}{2\pi} i T_{e,\alpha}(k+q,\tau,\tau')G_\alpha(-q,\tau',\tau) \quad (5.9)$$

where $\alpha = \{e,h\}$, and the $T_{e,h}$, and $T_{e,e}$ are solution of the Bethe Salpeter equations in the ladder approximation

$$\begin{aligned} T_{e,h}(q,\tau,\tau') &= -a\delta(\tau,\tau') + \\ &\quad a\oint d\tau'' \int \frac{dk}{2\pi} G_e(k,\tau,\tau'')G_h(q-k,\tau,\tau'')T_{e,h}(q,\tau'',\tau') \quad (5.10) \\ T_{e,e}(q,\tau,\tau') &= a\delta(\tau,\tau') - \\ &\quad a\oint d\tau'' \int \frac{dk}{2\pi} G_e(k,\tau,\tau'')G_e(q-k,\tau,\tau'')T_{e,e}(q,\tau'',\tau'). \quad (5.11) \end{aligned}$$

$g_e(h) = 2$, and $g_e(e) = 1$ are spin factors. We remark that the form of the Bethe Salpeter equation given above is valid only when a contact potential, which corresponds to a constant in the k-space, is used. For a generic instantaneous potential, in fact, taking into account the total momentum dependence, the $T$ matrix has three wavevector index $T(k,q,k')$. We need to solve self consistently the equations 5.8, 5.10, and 5.11 connected through the expression of the self energy in Eq.5.9. The self consistent T matrix approximation for the calculation of the $G_e$ and $G_h$, is a conserving approximation: the total density, total momentum, total energy and total angular momentum of the system

[2]Since the Green's functions are diagonal in the spin index, hereafter we will drop it.

are conserved [Baym, 1961]. We remark that a self consistent treatment is essential for the extension of the ladder approximation to the high density regime. This point has been checked through comparisons of results in self consistent ladder approximation and exact solutions in Hubbard models [Buzatu, 1995].

We want to analyze density dependent effects for systems in quasi-thermal equilibrium, and we consider the statistical operator

$$\rho = e^{-\beta(H-\mu N)}/Tre^{-\beta(H-\mu N)} \ , \tag{5.12}$$

where $\beta = 1/k_B T$. In the case of absorption measurements, the interaction with the electromagnetic field is considered as a probe on the system. Moreover, in the photoluminescence modelization it provides the mechanism for the spontaneous emission. In both cases, the electromagnetic interaction does not strongly affect the statistical properties of the crystal. Therefore, in the Hamiltonian $H$ of Eq.5.12 the term $H_P$ of Eq.5.1 is neglected.

In this stationary and thermal regime the function defined above are related by the Kubo Martin Schwinger relations [Kadanoff, 1962]

$$G_e^<(k,\omega) = -2iImG_e^+(k,\omega)f(\omega-\mu_e) \tag{5.13}$$

$$G_e^>(k,\omega) = 2iImG_e^+(k,\omega)(1-f(\omega-\mu_e)) \ , \tag{5.14}$$

where the Fourier transformation with respect to the quantity $t-t'$ has been done and $f(\omega-\mu_e)$ is the Fermi function. The retarded and anticipated Green's functions, related in the stationary case by the simple relation

$$G_e^+(k,\omega) = G^{-*}{}_e(k,\omega) \ , \tag{5.15}$$

contain the information on the spectral properties of the quasiparticles, and are related to the one particle spectral function $A_e(k,\omega)$:

$$A_e(k,\omega) = -2iImG_e^+(k,\omega) \ . \tag{5.16}$$

The correlation functions, instead contain information on the quasi particle occupation number

$$G_e^<(k,t,t) = f_e(k,t) \tag{5.17}$$

$$G_e^>(k,t,t) = 1-f_e(k,t). \tag{5.18}$$

We plot in Fig. 5.1 the electron spectral function at $k_e = 0$, at different densities. For densities below 2 $10^4$ cm$^-$1 the electron spectral function has a Lorentzian shape due to the small constant homogeneous broadening that we have considered for the bare

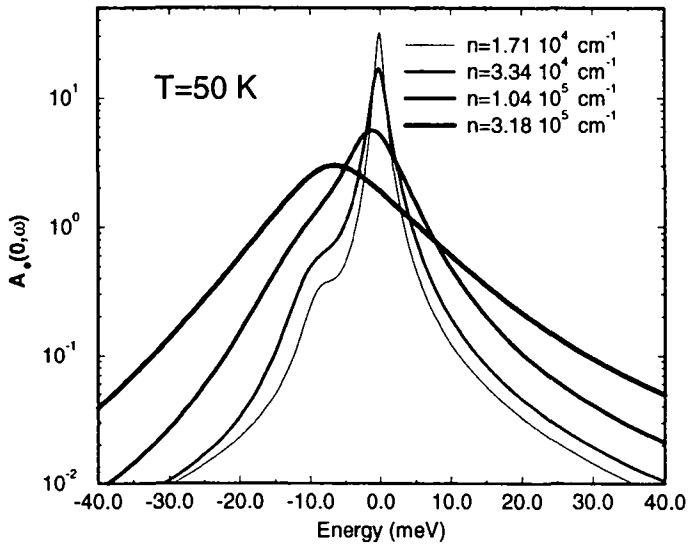


Figure 5.1: Electron spectral function at 50 K. The densities correspond to $\mu_e = \mu_h = -20, -16, -12, -8$ meV respectively.

Green's function. With growing the density, a satellite structure appears in the low energy side of the spectral function. This structure is located at the exciton binding energy, below the main peak, and accounts for the correlation of the electron at $k_e = 0$ with the holes in all populated $k_h$ states. In some way the satellite structure describes excitons with all values for the wavevectors of the center of mass. When this satellite structure grows, it affects the shape of the overall spectral function. For densities above $10^5$, it is difficult to distinguish between the excitonic part and the free part, and a single red shifted quasipaticle structure appears. This red shift is one half of the band gap renormalization. We will discuss the role of band gap renormalization in the last section of this Chapter.

## 5.2 Optical properties

In the dipole and rotating wave approximations, the coupling of the system of interacting electrons and holes with the electromagnetic field is of the form:

$$H_P = \sum_{\mathbf{q},q} C(\mathbf{q},q)(a_{\mathbf{q},q} J^\dagger(q) + a^\dagger_{\mathbf{q},q} J(q)) \ . \tag{5.19}$$

Here, $\mathbf{q}$ represents 2D wavevectors, while $q$ are wavevectors along the wire. The $C(\mathbf{q}, q)$ is the dipole matrix element, and $a$ is the photon annihilation operator. The quantities $J(q)$ are defined as

$$J(q) = \sum_k d(q-k)c(k) \ . \tag{5.20}$$

The interaction has the form of an electron hole current interacting with the photon field. It has been shown [Haug, 1984], that in the regime of linear response the absorption spectrum in the normal direction is given by :

$$\alpha(\omega) \propto ImP^+(\omega) \tag{5.21}$$

where the $P^+$is the retarded part of the current current correlation function

$$P^+(q,t,t') = -i\langle T[J^\dagger(q,t)J(q,t')]_-\rangle\theta(t'-t) \ . \tag{5.22}$$

Here the $[\ ]_-$ represents the commutator. The temporal evolution of the operator $J$ is in principle determined by the complete Hamiltonian of the Eq.5.1. However, we want to address here the optical properties in the limit of weak coupling of the light matter interaction. Therefore, the induced polarization due to the driving external field is completely neglected. This means that the time evolution of the operator $J$ and the statistical averages are calculated without the inclusion of the photon degrees of freedom. Hence, polaritonic effect are not included in our discussion. This approximation is consistent with hypothesis of thermal equilibrium for the excited carriers, because this latter assumption imposes an isolated system to be considered. Our model is appropriate for continuous wave photoluminescence experiments, where the carriers excited in high energy states relax to a quasi-thermal equilibrium, and emit light by spontaneous emission. The calculated absorption spectra refers to a situation where the carriers, created in the system by an non resonant pump, first relax to a quasi equilibrium, and are eventually probed by a weak probe. Assuming the thermal equilibrium, the spontaneous emission spectrum, i.e. the photoluminescence, is related to the absorption spectrum by the relation [Haug, 1984, Zimmermann, 1988]

$$PL(\omega) \propto \alpha(\omega)g(\omega - 2\mu) \ , \tag{5.23}$$

which correspond to

$$P^<(\omega) = -ImP^+(\omega)g(\omega - 2\mu) \ , \tag{5.24}$$

where $g(\omega - 2\mu)$[3], and the $P^<(\omega)$ is the Fourier transform of

$$P^<(q,0,t) = -i\langle J^\dagger(q,0)J(q,t)\rangle. \tag{5.25}$$

[3]Actually, the $2\mu$ should be replaced by $\mu_e + \mu_h + E_g$. The use of the same mass for electrons the holes and charge neutrality imply $\mu_e = \mu_h = \mu$. Moreover, frequencies are redefined $\omega \to \omega - E_g$ in order to simplify the notation.

Eq.5.24 can be easily obtained the from Kubo-Martin-Schwinger relations (Eq.5.14). The $P^<$ and $P^+$ functions look like the correlation and retareded Green's function of a bosonic particle. Going back to the excitonic picture, this corresponds to the boson character of the excitonic operator built from the products of two fermion operators, and the hydrogen-like wave functions. In the excitonic picture, however, when the density grows the exciton operators loose their boson character, while the relation 5.24 is valid at all densities, provided that the system is at thermal equilibrium. The relation between the rate of spontaneous emission and the current-current correlation function in Eq.5.25 can also be obtained in a simple way from a Fermi's golden rule approach [Zimmermann, 1988]. In fact, the total rate of photon emission $W$ in the Fermi's golden rule reads

$$W = \frac{2\pi}{\hbar}\sum_f |\langle i|H_P|f\rangle|^2\delta(E_f - E_i) = \frac{1}{\hbar}\int dt\langle i|H_P(0)H_P(t)|i\rangle \tag{5.26}$$

By inserting the full expression of the $H_P$ in the expectation value of Eq.5.26, we obtain products of photon and current operators. The photonic and fermionic operator are assumed to act on decoupled Fock spaces, this is consistent with the fact that polaritonic effects are neglected. The initial state is thus described by a statistical operator of the form $\rho = |0\rangle_{PP}\langle 0|\otimes\rho_{carriers}$ , where $|0\rangle_P$ represents the photon vacuum. Then, products of photon and current operators can be decoupled in the following way:

$$\begin{aligned}&\langle a(q,\mathbf{q},0)J^\dagger(q,0)a^\dagger(q,\mathbf{q}',t)J(q,t)\rangle \\ &\sim \langle a(q,\mathbf{q},0)a^\dagger(q,\mathbf{q}',t)\rangle\langle J^\dagger(q,0)J(k',t)\rangle\ .\end{aligned} \tag{5.27}$$

In Eq.5.27 we have taken into account the conservation of the electron-hole center of mass momentum in the wire direction. The expectation value for photons is done with respect to the photon vacuum $|0\rangle_P$ (spontaneous emission), and thus only the terms $\langle a(q,\mathbf{q},0)a^\dagger(q,\mathbf{q},0)\rangle \sim 1$ contributes. The rate of total spontaneous emission becomes

$$\begin{aligned}W &= \int\frac{dt}{\hbar^2}\sum_{\mathbf{q},q}|C(\mathbf{q},q)|^2e^{i\omega_{\mathbf{q},q}t}\langle J^\dagger(q,0)J(k',t)\rangle \\ &= \sum_{\mathbf{q},q}|C(\mathbf{q},q)|^2P^<(q,\omega_{\mathbf{q},q})\end{aligned} \tag{5.28}$$

where $\omega_{\mathbf{q},q}$ is the energy of the emitted photon. Using the expression for the dipole matrix element

$$C(\mathbf{q},q) = \frac{I_{\|}(\mathbf{q})\mu_{cv}}{\sqrt{(|\mathbf{q}|^2+q^2)^{1/2}}}\ , \tag{5.29}$$

the sum on the photon modes can be rewritten in the form

$$W = \sum_q 2\pi\mu_{cv}\int d|\mathbf{q}|\frac{|\mathbf{q}|}{\sqrt{|\mathbf{q}|^2+q^2}}|I_{\|}(\mathbf{q})|^2P^<(q,\omega_{\mathbf{q},q}) \tag{5.30}$$

The overlap integral $I_{||}(\mathbf{q})$ is due to the confinement of carriers in the wire. We can now assume that the light is detected in the direction perpendicular to the wire. This correspond to fix $q = 0$. The photoluminescence intensity in normal direction to the wire is thus

$$I_{PL}(q=0) = \mu_{cv} \int d\omega_{\mathbf{q},0} |I_{||}(\omega_{\mathbf{q},0}/c)|^2 P^<(0, \omega_{\mathbf{q},q}) \ . \tag{5.31}$$

For quantum wires much smaller than the optical wavelength $|I_{||}(\omega_{\mathbf{q},0}/c)|^2 \sim 1$, and the spectrum of the photoluminescence at normal emission is given by $P^<(0,\omega)$.

The current-current correlation function can be extended on the Keldysh contour and can be related to the $T$ matrix through the relation[4]

$$\begin{aligned} P(k,\tau,\tau') \ \sim \ & \sum_q G(k/2-q,\tau,\tau')G(k/2+q,\tau,\tau') \\ + \ & \sum_{q,p} \oint_K d\tau'' d\tau''' G(k/2-q,\tau,\tau'')G(k/2+q,\tau,\tau'')T(k,\tau'',\tau''') \times \\ & G(k/2-p,\tau''',\tau')G(k/2+p,\tau''',\tau') \ . \end{aligned} \tag{5.32}$$

We show in Fig.5.2, and 5.3 the absorption and photoluminescence spectra in the normal direction ($q = 0$) at 50 K, for different densities. In the absorption spectrum, the excitonic peak is already bleached for a density of about 3 $10^5$ cm$^{-1}$. However, in the photoluminescence a well defined peak is still there at this density. The binding energy of the exciton in the limit of low density is 10 meV. When the chemical potential rise a region of optical gain appear for $\omega < 2\mu$. This gain regime correspond to a negative absorption coefficient, and in the photoluminescence the peak of the emission corresponds to the minimum of the absorption in the gain region. The thermal tail at high energies, and a non Lorentzian behavior in the low energy side are observed. A blue shift in the regime where excitons are already ionized occurs. This blue shift is due to the rise of the chemical potential of the electron hole plasma. When the electron and hole band are filled up the emission of photons from the electron hole pair shifts the center of the photoluminescence emission toward the blue. The change of sign in the absorption is at $\omega = 2\mu$ and corresponds to the change of sign in the Bose factor, so to assure a well defined, always positive photoluminescence through the relation 5.24. In the same

[4]We remark that using the expression 5.32, we are not calculating the linear response to the external field at the same level of approximation used for the self energy. The response of the system in the T-matrix approximation has a different expression as pointed out by Baym and Kadanoff [Baym, 1961], and contains effects of dynamic excitonic screening on the Coulomb potential. This imply that in the expression 5.32 f-sum rules are not automatically satisfied. However we may expect that the discrepancies are negligeable, since in has been show that the self consistent ladder approximation is a good approximation when compared with available exact solutions in Hubbard models [Buzatu, 1995].

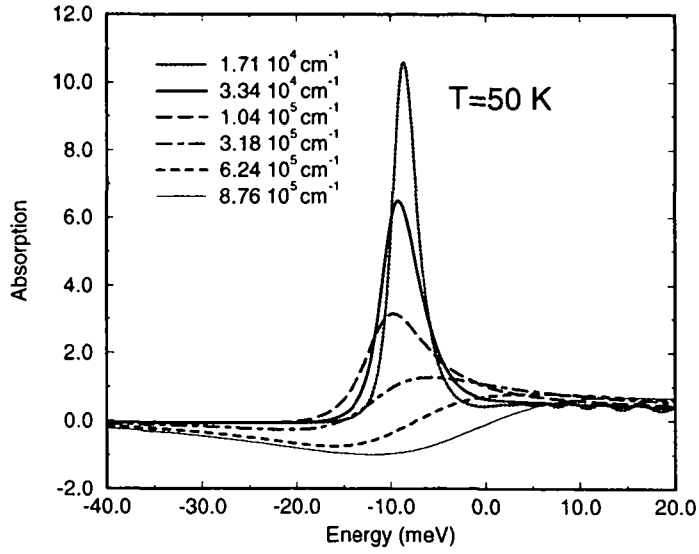


Figure 5.2: Absorption spectra at 50 K. The densities correspond to $\mu_e = \mu_h = -20, -16, -12, -8, -4, 0$ meV respectively.

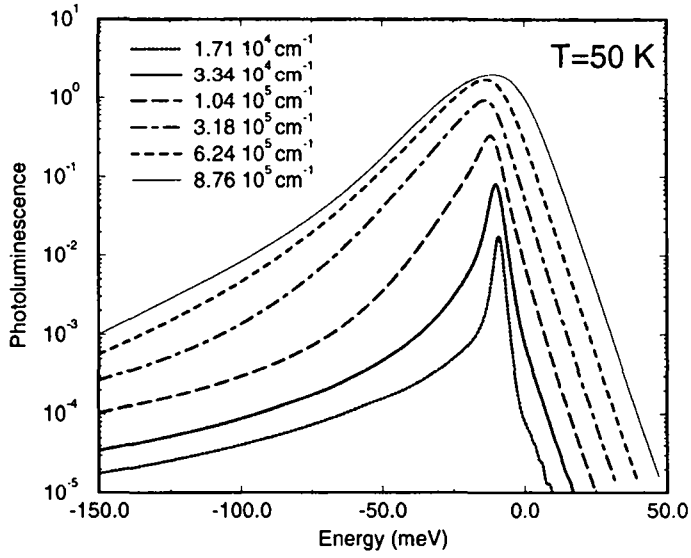


Figure 5.3: Photoluminescence spectra. Same parameters of Fig.5.2.

regime of electron hole plasma we observe a saturation of the photoluminescence peak and of the broadening in the low energy side. This can be understood in terms of the fermionic nature of the carriers: when the electron-hole plasma becomes degenerate the scattering is inhibited and the broadening saturates.

## 5.3 Excitonic gain

In the case of thermal equilibrium, with a contact potential interaction, the absorption coefficient in the direction perpendicular to the wire, can be rewritten in the form

$$\alpha(0,\omega) \propto |T^{+}_{eh}(\omega)|^2 \int \frac{dk}{2\pi}\frac{d\omega'}{2\pi}(1-f(\omega-\omega'-\mu)-f(\omega'-\mu))A_e(k,\omega-\omega')A_h(k,\omega') \ , \quad (5.33)$$

The term $1-f(\omega-\omega'-\mu)-f(\omega'-\mu)$ is the generalization of the Pauli blocking factor for a system where the quasiparticles are described by arbitrary spectral functions. It is useful the equivalence

$$1-f(\omega-\omega'-\mu)-f(\omega'-\mu) = f(\omega-\omega'-\mu)f(\omega'-\mu)/g(\omega-2\mu) \quad (5.34)$$

in order to express the absorption coefficient in the form

$$\alpha(0,\omega) = \frac{|T^{+}_{eh}(\omega)|^2}{g(\omega-\mu)} \int \frac{dk}{2\pi}\frac{d\omega'}{2\pi} f(\omega-\omega'-\mu)f(\omega'-\mu)A_e(k,\omega-\omega')A_h(k,\omega') \ , \quad (5.35)$$

which also allows to give a simple expression for the photoluminescence using the relation in Eq.5.24

$$PL(0,\omega) \propto |T^{+}_{eh}(\omega)|^2 \int \frac{dk}{2\pi}\frac{d\omega'}{2\pi} f(\omega-\omega'-\mu)f(\omega'-\mu)A_e(k,\omega-\omega')A_h(k,\omega') \ . \quad (5.36)$$

The optical gain is usually measured in the regime of degenerate electron-hole plasma. density and in this regime several approximations are usually introduced: spectral functions are approximated by Lorentians, Fermi function are evaluated at the peak of these Lorentians (quasi particle approximation), and the term $|T^{+}_{eh}(\omega)|^2$ in the Eq.5.33 is neglected. The results is that the absorption for normal incidence takes the form ($m_e = m_h$)

$$\alpha(q=0,\omega) \propto \int \frac{dk}{2\pi}\frac{1-2f(\hbar^2k^2/2m-\mu)}{(\omega-\hbar^2k^2/m)^2+\gamma^2} \ . \quad (5.37)$$

A region of negative absorption occurrs when the Pauli blocking factor $(1-2f(\hbar^2k^2/2m-\mu))$ becomes negative, which necessarily requires a chemical potential above the band gap, and an electron hole plasma in the degenerate regime. However, using the more general expression of equation 5.35, we can identify the inversion of the sign in the

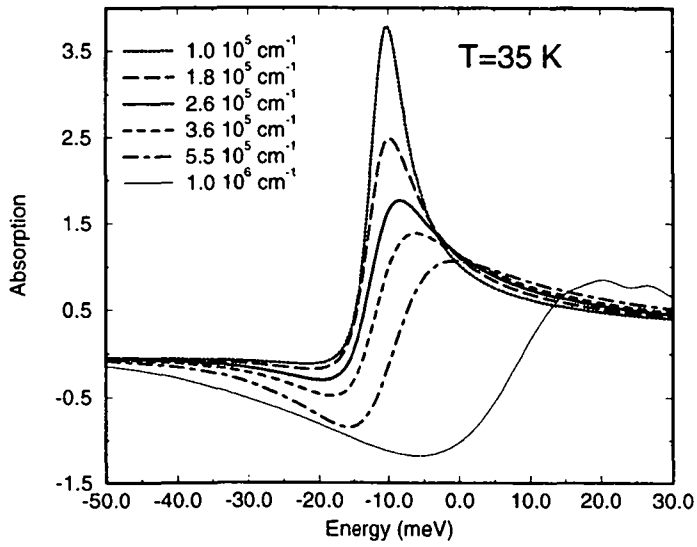


Figure 5.4: Absorption spectra at 35 K. The densities correspond to $\mu_e = \mu_h = -10, -9, -8, -7, -5, 4$ meV respectively.

absorption with the position of the pair chemical potential $2\mu$. Therefore, the inversion of sign does not require the condition that the chemical potential is above the band gap, but may occur in any region of the spectra below the energy corresponding to $2\mu$, in particular, close to the excitonic resonance. In this case we talk of *excitonic gain.* We notice that the spectral functions $A_{e,h}(k,\omega)$ is not vanishing in the energy region below the gap corresponding to the exciton resonance, as can be seen in the satellite structure in Fig.5.1. This characteristic allows the excitonic gain to appear. In Fig.5.4 the absorption spectra at T=35 K are shown. At this temperature, $k_BT \ll E_b$ and the effects of the presence of bound states on the optical properties are more striking. In particular we observe a regime of densities ( $\sim 2\ 10^5$ cm$^{-1}$) where a region of optical gain exists togheter with an excitonic resonance. For growing density a broadening and a bleaching of the exciton resonance occur. For densities above $5.5\ 10^5$ cm$^{-1}$ the system behaves as a degenerate electron-hole plasma and the gain characteristic of this regime appear. We remark that the amplitude in the excitonic gain is smaller than electron-hole plasma gain, but well pronounced. Moreover, the spectral shape of the two gain regions is considerably different. In fact, the excitonic gain is spectrally confined at the exciton resonance, while the gain in the electron hole plasma phase is broadened, and follows the density of state of the continuum. The two gain regimes are well distinct and should

be better experimentally observed in the case of large binding energy and small Bohr radius.

## 5.4 Coulomb correlation and band gap renormalization

We have observed in Fig.5.1 that when the density of excited carrier rises, the main peak of the one particle spectral shifts at lower energies. This effects is a consequence of the Coulomb correlation and exchange effects which reduces the average energy of the carriers, and is called band gap renormalization. The estimation of band gap renormalization from optical measurements has been the subject of several investigations in quantum wires [Cingolani, 1993], [Gréus, 1996], [Ambigapathy, 1997], and quantum wells [Trankle, 1987], [Bongiovanni, 1992], [Kulakovskii, 1989], [Deveaud, 1991b], [Kalt, 1996]. In the case of bulk systems the band gap renormalization is observed as a shift of the photoluminescence spectrum [Kalt, 1996]. As the dimensionality of the system is lowered this direct observation is not so obvious. In quantum wells, at high enough densities, the band gap renormalization may be observed as a shift of the band edge [Trankle, 1987], [Kulakovskii, 1989], [Bongiovanni, 1992], [Deveaud]. The main difficulty of this observation arises as a result of the broadening which may mask the edge. Thus, in the analysis of experimental data this broadening has to be taken into account in order to accurately determine the value of the band gap renormalization. In the one dimensional case even at very high densities there have been no observations of a shifting edge [Ambigapathy, 1997], [Gréus, 1996], [Cingolani, 1993]. In one dimensional systems the observation of band gap renormalization is difficult because, besides the effects of broadening, the e-h Coulomb correlations masks the observation of an edge in the optical spectra. By comparing the experimental results with our theoretical calculation we have evidence that although band gap renormalization does occur in a one dimensional system, it can not be directly observed in the luminescence spectrum. In fact the electron hole Coulomb correlation results in an inhibition of the recombination rate (Sommerfeld factor) at the renormalized band edge which persists even in the regime of a degenerate e-h plasma. This is in strong constrast to the two and three dimensional cases where the Sommerfeld factor causes an enhancement of the optical spectra at the band edge. In the photoluminescence, correlation effects which strongly affect the shape of the spectra, are contained in the term $|T^{+}_{eh}(\omega)|^2$ of the Eq.5.36. We show in Fig. 5.5 a plot of $|T^{+}_{eh}(\omega)|^2$ for different values of the chemical potential $\mu$. In the low density limit ($\mu \leq$ -10 meV) a resonance corresponding to the exciton level is dominant, and at the band edge the T matrix vanishes for $E \rightarrow E^{+}_{g}$. This behavior near the band edge corresponds to a Sommerfeld factor which compensates the singularity $(E - E_g)^{-1/2}$

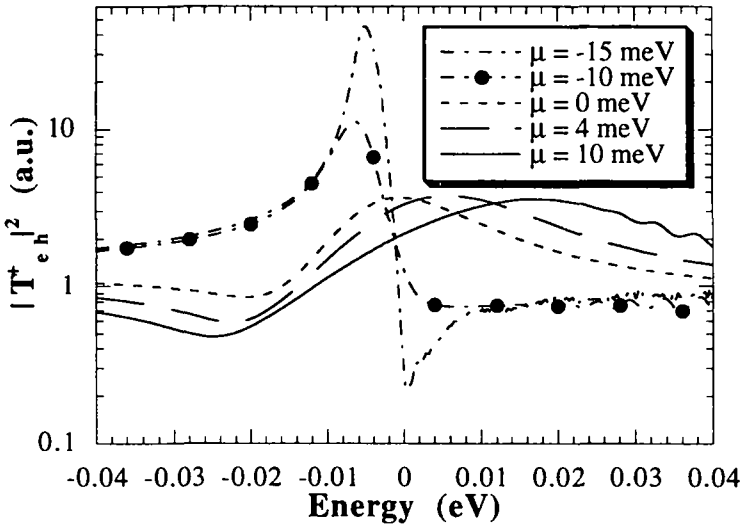


Figure 5.5: T matrix

of the one dimensional joint density of states. Our potential reproduces qualitatively the shape of the spectra obtained from a detailed calculation with a more realistic approximation for Coulomb potential [Ogawa, 1991], [Glutsch, 1993], [Rossi, 1996]. As the chemical potential increases both the excitonic resonance and the Sommerfeld factor are smoothed. However, for chemical potentials above the bare band edge, a maximum at roughly $2\mu$ is still present in the electron hole correlation. This maximum results in a peak of the photoluminescence even in the high degenerate plasma regime. Moreover, a minimum in $|T^{+}_{eh}(\omega)|^2$ occurs at the renormalized band edge. This minimum is similar in nature to the Sommerfeld factor, but due to a finite broadening of the states does not vanish completely. It is the persistence of this Sommerfeld factor which prevents the observation of a shifting peak in the low energy side of the photoluminescence spectra similar to the one present in quantum wells and bulk systems.

In Figs.5.7 and 5.8 we show the calculated and the experimental photoluminescence spectra; we used a value of $a = 10^7 meV cm^{-1}$ for the effective contact interaction. The experiment [Ambigapathy, 1997] has been done on a V-grooved GaAs quantum wires with a nominal thickness of 2.5 nm. The measurement of the spectra has been performed by a time resolved photoluminescence technique, which enables to probe the density dependence of the optical spectra with good experimental resolution. In the theoretical calculation, densities can be rescaled in terms of the Bohr radius, which here is assumed to be 10 nm. The position of the peak at high energy is not considerably shifted with respect to the position of the excitonic resonance at low densities. There is no signature of a shifting peak at low energy, even for high density, either the experimental nor in the

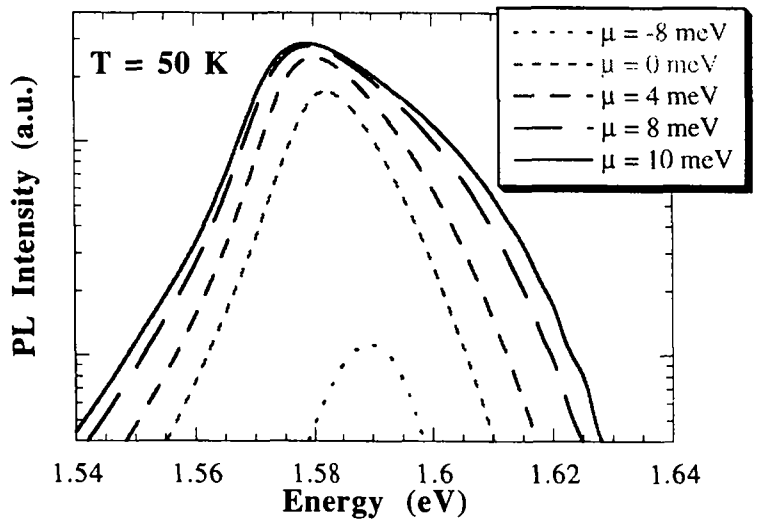


Figure 5.6: Theoretical PL spectra, without the T matrix correction

theoretical spectra. However, we can see from the spectral functions in Fig.5.1 that for the chemical potential $\mu = 0$ a band gap renormalization of about 20 meV is present. We also note that the low energy tail is well reproduced by the theory. In particular it is evident for the spectra at larger densities a change in the curvature of the tail from a Gaussian-like to a Lorentzian like shape, as a function of energy. This change can not be explained in term of disorder effects since it occurs at high densities, with a broadening which is much grater than the one observed at low density. In our treatment the frequency dependence of the broadening results from the calculation of the real and imaginary part of the one particle self energy on the same footing. We observe in both the experiment and the theoretical calculation a saturation of the photoluminescence peak for $2\mu \sim 30meV$. The high energy tail is thermal at about $50K$ and follows the filling of the band. In the experiment, however, for $2\mu > 30meV$ the presence of a second subband is evident. Therefore the theoretical treatment of intersubband interaction should be taken into account for a better comparison with the experiment. In order to stress the importance of the term $T^2$ on the shape of the photoluminescence emission, we give in Fig. 5.6 the spectra calculated without taking into account this term. It evident a strong red shift of the edge at low energy which follows the band gap renormalization.

The main discrepancy in the comparison of theory with the experiment is the theo-

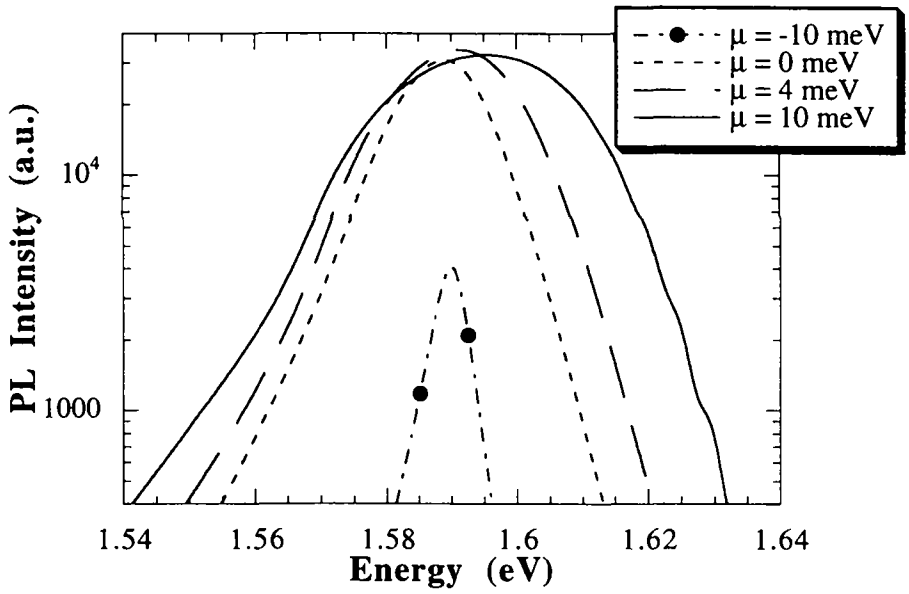


Figure 5.7: Theoretical PL spectra

retically predicted blue shift of the photoluminescence peak after the saturation regime has been reached. To be more precise, this peak follows the filling of the bands, and thus the chemical potential. This discrepancy may be due to the approximation $\mu_e = \mu_h$. In fact, if the two bands have a different band structure (which is actually the case in real structures), the charge neutrality of the system necessarily implies $\mu_e \neq \mu_h$ and the filling of the bands would occur in a different way for electrons and holes. Then, in the Eq.5.36, where a product of two Fermi function with two different chemical potentials would be included, this would result in a PL which follows the more stable chemical potential, thus considerably reducing the blue shift due to the band filling. Finally, we want to compare our approach to previous theory-experiment comparison in the literature done at the Hartree-Fock level [Gréus, 1996]. In the approach by Gréus *et al.* [Gréus, 1996], the excitonic effects on the optical spectra are taken into account within the Hartree-Fock approximation for the one particle self energy. This forced the authors to assume a phenomenological constant broadening, and the total density and plasma temperature are adjusted in order to best fit the shapes and the relative intensities of the measured spectra. This procedure leads to the observation of a red shift of the peak as the density increases, contrary to the experiment. In our approach the temperature of the plasma is fixed, which is well verified experimentally in our case, the chemical potential (thus the density) is changed, and a density dependent self consistent $\gamma(k, \omega)$ is calculated. Using this procedure the shift of the photoluminescence peak is not present.

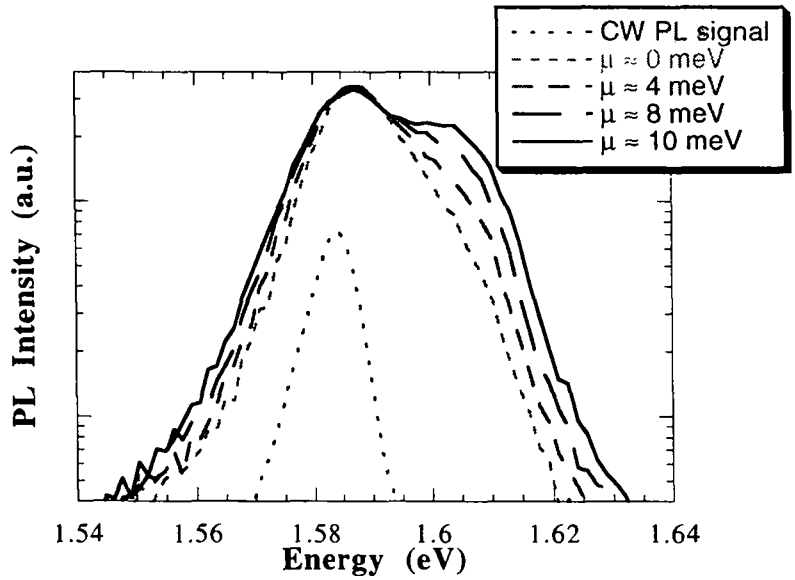


Figure 5.8: Experimental PL spectra (Courtesy of R. Ambigapathy)

We remark that the persistence of the Sommerfeld factor at high densities can already be obtained at the Hartree-Fock level [Rossi, 1996], and is thus contained in the Greus approach. However, a self consistent calculation of both real and imaginary part of the density dependent one particle self energy has to be done for a reliable prediction of the density dependence of the optical spectra. In fact, the position of the peak in the optical spectra cannot be related simply to the one particle shift, but depends on both the real and imaginary parts of the self energies.

# Outlook

The largest part of this thesis has been devoted to the analysis of the interaction of excitons, free carriers and polaritons with acoustic and optical phonons. From this analysis, we have given an interpretation of some features in the optical measurements. In this framework we can include the long decay times observed in the exciton-polariton photoluminescence, the inhibition of acoustic phonon scattering of microcavity polaritons, the extremely long rise time of the photoluminescence due to the slow formation by acoustic phonons. However, the interaction with phonons can explain only partially the complex phenomenology resulting from the optical measurements. A typical example of these limitations is just provided by the interpretation of the rise time in non resonant photoluminescence experiments in quantum wells, which is related to the model of the exciton formation.

Recent experiments in good quality quantum well samples [Amand] show clearly that, when the pump is well below the threshold for the formation assisted by emission of optical phonons, the excitonic luminescence presents an initial very rapid rise time which cannot be explained by the interaction with acoustic phonons. The explanation of this initial, nearly instantaneous, build up of the photoluminescence is likely to be searched in the effects of Coulomb scattering. The build up of the photoluminescence at the energy corresponding to the excitonic resonance has been shown theoretically to have a contribution due only to the Coulomb interaction at early times after excitation in the continuum [Kira, 1998]. However, this result has been obtained in the Hartree-Fock approximation, and the information on the distinction between the populations of bound and free electron-hole pairs is ruled out. Therefore no statements about the exciton formation can be done.

The importance of the broadening of the states is not only essential for the understanding of the dynamics of relaxation but also in the density dependence of the optical spectra. We have already discussed in Chap.5 how the inclusion of single particle broadening can affect the shape of the optical response. In order to be more reliable, the self consistent T matrix approach must be extended to a more realistic potential. One of the

limitations of the delta like potential in our treatment in Chap.5 is that the range of the potential is zero and the effects of the screening are not taken into account. However, the many body diagrams which in the case of Coulomb scattering give rise to the screening effects (RPA sum) can be included in a delta like potential. In this case the screening is represented in the potential as a renormalization of the constant in the delta function, thus of the total strength of the potential, without regarding to the spatial dependence of the corrections. The effects of the RPA corrections can be checked in the case of a delta like potential through the comparison with the exact solution obtained using the Bethe ansatz [Schlottmann, 1994]. Moreover, the effects of screening in the dynamics of carriers and in the formation of the excitons represents an interesting topics for the investigation of the quantum kinetics in systems with strong Coulomb correlations. Some interesting results about the build up of the screening in high excited semiconductors have been already obtained using the technique of non equilibrium Green's functions introduced in this thesis [Bányai, 1998].

A different direction for the improvement in the understanding of the optical properties is represented by the effects related to the interaction of the carriers with a strong external electromagnetic field. The interaction with a strong external field renormalizes the electron and hole spectral functions. One of the most striking effects is represented by the onset of a light induced gap in the quasi particle dispersion at the pump energy. This mechanism is related to new and interesting phenomena, as the observation of a Mollow triplet for excitation resonant with the exciton in semiconductor microcavities [Quochi, 1998]. The possibility of investigation of these effects is strongly stimulated by the availability of microcavity samples where the photon density of states is modified, so to obtain an enhancement in the exciton-photon interaction (filter effect). The interplay of these light induced effects with the Coulomb interaction is a subject deserving further investigation, and a self consistent treatment of the one particle spectral functions is necessary. The light induced gap can be included in the class of the polaritonic effects, and the representation of the excitation of the crystal as polaritons leads also to the investigation of the statistical properties of these excited states. The bosonic nature of the polaritons has been experimentally and theoretically investigated [Tassone, 1998b], and further investigations about the possibility of observation of Bose condensation of these quasiparticles, which should be helped by the small mass of the lower polariton states, are in progress [Fernández, 1998].

In most of the analysis on the exciton dynamics, the spatial homogeneity of the excitation has been assumed. However, the experimental investigation of the spatial dynamics of the excitons is nowadays possible with a very high spatial resolution. From

the theoretical point of view this technical possibility stimulates the investigation of the dynamics in real space, and some description of the interplay of the exciton propagation with the lattice vibrations at short time after the excitation has been already obtained [Knorr, 1998]. Amongst the effects in real space, a special role is played by the effects to the disorder on the optical properties. In the case of microcavity polaritons the the disorder affects the broadening of the polariton and a narrower peak for the lower polariton with respect to the upper polariton results. This point has been well investigated theoretically and experimentally [Savona, 1997], [Whittaker, 1998], [Ell, 1998]. In the scattering of light on a quantum system with disorder, the wavevector conservation in the in plane direction is broken and the scattering of light in directions different from the reflected one can be detected (resonant Rayleigh scattering). The investigation of resonant Rayleigh scattering in these systems can be a very efficient tool for the investigation of the statistics of the quantum excitonic levels in presence of a disordered potential, and it is of great interest from the point of view of fundamental physics.

# Appendix A

# Geminate formation rate

The geminate exciton formation rate is calculated taking into account the interaction of the carriers with both the external electromagnetic field and the thermal bath of phonons. The scattering amplitude is schematically depicted in Fig.A.1. The expression of the formation rate for a given final two dimensional 1s exciton with a fixed in plane center of mass momentum $\mathbf{q}$ is given by

$$R(\hbar\omega \to \mathbf{q}) = \frac{2\pi}{\hbar}\sum_{q_z}\left|\sum_{\mathbf{k_r}}\frac{\langle 0|V_\gamma|\mathbf{k_r}\rangle\sqrt{(n_p+1)}\langle \mathbf{k_r}|V_p|\mathbf{q}\rangle}{\hbar\omega - E_{gap} - \hbar^2|\mathbf{k_r}|^2/2\mu + i\Gamma}\right|^2 \times\delta\left(\hbar\omega - \hbar\omega_{LO} - E_{gap} + E_b - \frac{\hbar^2|\mathbf{q}|^2}{2M}\right) \quad \text{(A.1)}$$

where $\hbar\omega$ is the energy of the pump photon. In the Eq.A.1 $|0\rangle$ is ground state, $|\mathbf{k_r}\rangle$ represents an electron-hole state with relative momentum $\mathbf{k_r}$, $|\mathbf{q}\rangle$ is the created exciton state. $\mu$ and $M$ are the the reduced and total electron hole mass. Due to the small photon wavevector, all the intermediate states have zero center of mass momentum and we sum only on the relative momentum $\mathbf{k_r}$ of the electron-hole pair. Furthermore, the in-plane wavevector conservation implies that the created exciton and the emitted

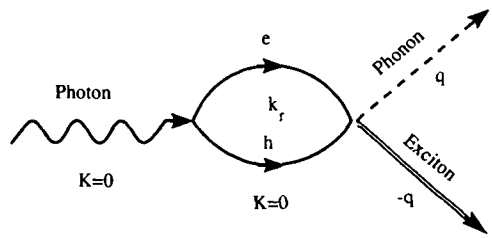


Figure A.1: Scattering amplitude for the geminate formation

optical phonon have opposite momentum. The energy $\Gamma$ gives the broadening of the intermediate states, is assumed to be energy independent, and is produced by the same process which thermalizes the carriers. The exciton phonon vertex is calculated using the Frölich Hamiltonian for bulk LO phonon interacting with electrons and holes which reads

$$\begin{aligned} V_p = H_{e-LO} + H_{h-LO} &= \sum_{\mathbf{q},\mathbf{k},\mathbf{k}',q_z} \left( \frac{2\pi\hbar\omega_{LO}e^2(1/\epsilon_\infty - 1/\epsilon_0)}{V(|\mathbf{q}|^2 + q_z^2)} \right)^{1/2} \\ &\quad (a_{\mathbf{q},q_z} + a^\dagger_{-\mathbf{q},q_z})(c^\dagger_{\mathbf{k}'}c_{\mathbf{k}} - d^\dagger_{\mathbf{k}'}d_{\mathbf{k}})\delta_{\mathbf{k}'+\mathbf{q},\mathbf{k}} \ , \end{aligned} \tag{A.2}$$

where $a_{\mathbf{q},q_z}$, $c_{\mathbf{q}}$, and $d_{\mathbf{q}}$ are the optical phonon, electron and hole operators respectively. In the calculation of the matrix element $\langle \mathbf{k_r}|V_p|\mathbf{q}\rangle$ the pair state in the continuum is described by the envelope function

$$\langle R,\rho,z_e,z_h|\mathbf{k_r},\mathbf{K}\rangle = \frac{e^{i\mathbf{k_r}\rho}}{\sqrt{S}}\frac{e^{i\mathbf{K}\mathbf{R}}}{\sqrt{S}}f_e(z_e)f_h(z_h) = \frac{e^{i\mathbf{k_e}\cdot\mathbf{r_e}}}{\sqrt{S}}\frac{e^{i\mathbf{k_h}\cdot\mathbf{r_h}}}{\sqrt{S}}f_e(z_e)f_h(z_h) \tag{A.3}$$

where $\mathbf{R} = (\mathbf{r_e} + \mathbf{r_h})/\mathbf{2}$ and $\rho = \mathbf{r_e} - \mathbf{r_h}$, and $f_{e\ (h)}(z)$ give the electron-hole confinement in the well. Since the electron hole pairs are created by optical pump, we consider only the case $\mathbf{K} = \mathbf{0}$. For the final exciton we use the 1s hydrogenic envelope function

$$\langle R,\rho,z_e,z_h|1s,\mathbf{q}\rangle = \sqrt{\frac{2}{\pi a_B^2}}\frac{1}{\sqrt{S}}e^{i\mathbf{q}\mathbf{R}}e^{-|\rho|/a_B}f_e(z_e)f_h(z_h) \tag{A.4}$$

where $a_B$ is the exciton Bohr radius. We obtain then for the matrix element

$$\begin{aligned} \langle \mathbf{k_r}|V_p|\mathbf{q}\rangle &= i\sum_{q_z} \left( \frac{2\pi\hbar\omega_{LO}e^2(1/\epsilon_\infty - 1/\epsilon_0)}{V(|\mathbf{q}|^2 + q_z^2)} \right)^{1/2} \\ &\quad \left( I_e^{\parallel}(\mathbf{q},\mathbf{k_r})I_e^{\perp}(q_z) - I_h^{\parallel}(\mathbf{q},\mathbf{k_r})I_h^{\perp}(q_z) \right) \ , \end{aligned} \tag{A.5}$$

The superposition integrals in the parallel direction $I_e^{\parallel}(|\mathbf{q},\mathbf{k_r}|)$ are calculated using the envelope functions in Eqs.A.3-A.4.

$$\begin{aligned} I_e^{\parallel}(\mathbf{q},\mathbf{k_r}) &= \left(\frac{2}{S\pi a_B^2}\right)^{1/2} \int d\theta\ \rho d\rho\ e^{-i|\mathbf{k_r} - m_h\mathbf{q}/M|\rho cos\theta}\ e^{-\rho/a_B} \\ &= 2\pi \left(\frac{2}{S\pi a_B^2}\right)^{1/2} \frac{(-i)(a_B)^2}{(1 + |\mathbf{k_r} - m_h\mathbf{q}/M|^2(a_B)^2)^{3/2}} \ , \end{aligned} \tag{A.6}$$

where we have used

$$\int_0^{2\pi} d\theta e^{i\alpha cos\theta} = i2\pi J_0(\alpha) \tag{A.7}$$

and

$$\int_0^\infty dx x J_0(bx) e^{-ax} = \frac{a}{(a^2+b^2)^{3/2}} \,. \tag{A.8}$$

The expression for $I_h^{\parallel}(\mathbf{q}, \mathbf{k_r})$ is obtained by changing $m_h$ with $-m_e$ in Eq.A.6. The center of mass dependence of the envelope functions gives a Kronecker delta indicating the total center of mass wavevector conservation. The perpendicular superposition integrals are calculated numerically as

$$I_{e\,(h)}^{\perp}(q_z) = \int dz |f_{e\,(h)}(z)|^2 e^{iq_z z} \,, \tag{A.9}$$

taking for the functions $f_{e\,(h)}(z)$ the solution of a particle in a finite square well representing the band profile in the growth direction.

The matrix element for the interaction of the electron hole pair with the external photon field is given by

$$\langle 0|V_\gamma|\mathbf{k_r}\rangle = \left(\frac{eA}{mc}\right) \underline{\epsilon} \cdot \underline{\mu_{cv}} \,, \tag{A.10}$$

where $A$ is the amplitude of the external electromagnetic field, $\underline{\epsilon}$ gives the polarization, and $\underline{\mu_{cv}}$ is the dipole momentum for Bloch functions at the point $\Gamma$ of the Brillouin zone.

We are interested in the quantity

$$\left(\frac{dn_{ex}}{dt}\right)_{gem} = \frac{1}{S}\sum_{\mathbf{q}} R(\hbar\omega \to \mathbf{q}) \tag{A.11}$$

which, using the properties of the delta functions in order to eliminate the integral in the $|\mathbf{q}|$ can be rewritten in the form

$$\left(\frac{dn_{ex}}{dt}\right)_{gem} = \int dq_z C \frac{|K(\tilde{q}, q_z)|^2}{\tilde{q}^2 + q_z^2} 2\theta(\tilde{q}^2) \tag{A.12}$$

where $\theta(x)$ in the step function , and $\tilde{q}$ is given by the zero of the delta function in Eq.A.1

$$\tilde{q} = \left(\frac{2M(\hbar\omega - E_g - \hbar\omega_{LO} + E_b)}{\hbar^2}\right)^{1/2} \,. \tag{A.13}$$

The function $K(q, q_z)$ is defined as

$$\int_{-\pi}^{\pi} d\phi \int_0^\infty k_r dk_r \left( \frac{I_e^{\perp}(q_z)}{(1 + |\mathbf{k_r} - m_h \mathbf{q}/M|^2 (a_B)^2)^{3/2}} - \frac{I_h^{\perp}(q_z)}{(1 + |\mathbf{k_r} + m_e \mathbf{q}/M|^2 (a_B)^2)^{3/2}} \right) \,, \tag{A.14}$$

where $\phi$ is the angle between $\mathbf{k_r}$ and $\mathbf{q}$, and the constant C is

$$C = \frac{M}{(2\pi)^2 \hbar^2} \left(\frac{eA}{mc}\right)^2 |\underline{\epsilon} \cdot \underline{\mu_{cv}}|^2 \omega_{LO} e^2 (1/\epsilon_\infty - 1/\epsilon_0) \frac{2a_B^2}{\pi} (n(\omega_{LO}) + 1) \,. \tag{A.15}$$

We can use the expression for the flux of electromagnetic energy incident on the sample (summed over the photon polarizations)

$$P(\hbar\omega) = N_{ph}\frac{c}{n}\hbar\omega = \frac{A^2\omega^2 n^2}{2\pi c^2}\frac{c}{n}\hbar\omega \tag{A.16}$$

where $N_{ph}$ is the density of photons in the laser beam, and obtain the form given in Eq.3.2

$$\left(\frac{dn_{ex}}{dt}\right)_{gem} = \alpha_{gem}(\hbar\omega)P(\hbar\omega)\ . \tag{A.17}$$

In order to compare the exciton formation with the free carrier formation we consider the following definition for the absorption coefficient for a quantum well

$$w = \frac{absorbed\ energy/(dS\ dt)}{incident\ energy/(dS\ dt)}. \tag{A.18}$$

For energy above the threshold $w$ and is nearly constant, and for a QW of 80 Å$w = 0.007$ [Andreani, 1991]. Then we can write

$$\left(\frac{dn_e}{dt}\right)_{carr} = \frac{w}{\hbar\omega}P = \alpha_{carr}P \tag{A.19}$$

which, togheter with the definition of $\alpha_{gem}$ in Eq.A.17 gives the result of the Eq.3.3. In the case of a pulsed laser we have that the total density created after the pulse is

$$n_c = \frac{dn_c}{dt}\Delta t F_S \tag{A.20}$$

where $F_S$ is a form factor depending on the shape of the pulse which is characterised by a FWHM of $\Delta t$. Then

$$\left(\frac{dn_{ex}}{dt}\right)_{gem} = \frac{\alpha_{gem}}{\alpha_{carr}}\left(\frac{dn_e}{dt}\right)_{carr} = \frac{\alpha_{gem}}{\alpha_{carr}}\frac{n_c}{\Delta t F_S} \tag{A.21}$$

which is useful in order to compare the bimolecular and the geminate formation for a fixed total density of carriers in the system.

# Appendix B

# Non equilibrium diagrammatic expansion

The purpose of this Appendix is to give details about the differences in the diagrammatic technique between the equilibrium and the non equilibrium Green's functions. In the non equilibrium case, the concept of Keldish contour allows to use the same diagrammatic expansion as in the equilibrium case. The physical nature of the Keldish contour is explained and we give some useful rules (Langreth and Wilkins theorem), which allows to relate functions defined on the Keldish contour to functions defined on the ordinary real time axis.

The causal and anticausal one particle Green's functions are defined as

$$G^C(t,t') = -i\langle Tc(t)c^\dagger(t')\rangle \tag{B.1}$$

$$G^A(t,t') = -i\langle \tilde{T}c(t)c^\dagger(t')\rangle \tag{B.2}$$

The operators $c$ and $c^\dagger$ are in the Heisenberg representation, and their evolution is due to the full Hamiltonian of the crystal 5.1. $T$ and $\tilde{T}$ are the causal and anticausal time ordering operators.

$$TA(t)B(t') = \theta(t-t')A(t)B(t') - \theta(t'-t)B(t')A(t) \tag{B.3}$$

$$\tilde{T}A(t)B(t') = \theta(t'-t)A(t)B(t') - \theta(t-t')B(t')A(t) \tag{B.4}$$

$$\tag{B.5}$$

Since the total Hamiltonian of the Eq.5.1 is invariant under spatial translation and do not explicitly depend on the spin of the carriers, the Green's functions are diagonal on the spin and wavevector indexes. In the following we will drop out these wavevector and

spin indexes which do not play an essential role in the discussion of the equilibrium-non equilibrium comparison.[1] The characteristic of non equilibrium systems is that the average $\langle \ldots \rangle$ is taken with respect to an arbitrary statistical operator $\rho$

$$\langle \ldots \rangle = Tr\rho \ldots . \tag{B.6}$$

As explained in Chap.5, the interaction with the electromagnetic field is considered in our approach as a probe on the system and in a first approximation do not affect the evolution of the fermionic operators. Therefore we can introduce a perturbative expansion with respect to carrier carrier Coulomb interaction $H_C$. The interaction representation for the fermionic operators is related to the Heisenberg representation by

$$c(t) = S^{\dagger}(t, t_0)\hat{c}(t)S(t, t_0) \tag{B.7}$$

with

$$S(t, t_0) = Te^{-i\int_{t_0}^{t} \hat{H}_C(t')dt'} , \tag{B.8}$$

the hat identifies operators in interaction representation. The operator $S(t, t_0)$ is the temporal evolution operator from the initial time $t_0$ to the time $t$. Using the interaction representation, the causal Green's function in eq. B.1 becomes

$$G^C(t, t') = -i\langle S^{\dagger}(\infty, t_0)T\hat{c}(t)\hat{c}^{\dagger}(t')S(\infty, t_0)\rangle . \tag{B.9}$$

Let us briefly remind the simplifictions that can be introduced in the eq. B.9 when the system is in equilibrium at zero temperature, and the average is taken over the vacuum state. We refer to [Mahan, 1981] for more details. The simplification in the zero temperature case is carried on in two steps. First, an adiabatic switch on of the interaction $H_C$ is considered, and for $t_0 \to -\infty$ the vacuum state $|0\rangle$ of the crystal coincide with the non interacting vacuum state $|0\rangle_0$. Second, the Gell-Mann Low theorem is used

$$S(\infty, -\infty)|0\rangle_0 = e^{i\phi}|0\rangle_0 , \tag{B.10}$$

which indicated that the state at $t = \infty$ differ from the non interacting initial vacuum state only by a phase. In other words it means that the vacuum still be the vacuum when the time goes on. Moreover, the linked cluster theorem assures that this phase is automatically taken into account when only connected diagrams in the diagrammatic expansion are considered.

$$G^C(t, t') = -ie^{i\phi}{}_0\langle 0|T\hat{c}(t)\hat{c}^{\dagger}(t')S(\infty, -\infty)|0\rangle_0 = -i\,{}_0\langle 0|T\hat{c}(t)\hat{c}^{\dagger}(t')S(\infty, -\infty)|0\rangle_0^{\substack{connected \\ diagrams}} \tag{B.11}$$

[1] We use in this Appendix the causal and anticausal Green's function instead of the retarded and anticipated Green's functions defined in Chap.5 where the anticommutator between the two fermion operator is considered. This choice is more convenient for the aim of this Appendix.

At this point the perturbative expansion can be obtained by developing the operator $S(\infty, -\infty)$ in power of $\hat{H_C}$. At the order N the problem is reduced to the evaluation of the expectation value of $4N+2$ fermionic operators in interaction representation, which can be done diagrammatically using the Wick theorem.

However the simplifications due to the Gell-Mann-Low theorem cannot be introduced when the average is taken with respect to an excited state of the system described by an arbitrary statistical operator $\rho$ at $t = t_0$. Thus the full expression B.9 must be used in the perturbation expansion. An excited state is not transformed into itself by the operator $S(\infty, t_0)$, but into a superposition of other excited states, which may be intuitively regarded as the result of all possible process of mutual scattering of the particles. The causal Green's function using

$$S^\dagger(\infty, t_0) = S(t_0, \infty) = S(-\infty, \infty)S(t_0, -\infty) \tag{B.12}$$

becomes

$$G^C(t,t') = -i\langle S(-\infty,\infty)T\hat{c}(t)\hat{c}^\dagger(t')S(\infty,-\infty)\rangle \ . \tag{B.13}$$

Here both the $S(\infty, -\infty)$, and $S(-\infty, \infty)$ operators has to be expanded in the perturbation theory. However, when the expansion of the term $S(-\infty, \infty)$ is done we remark that the the time ordering operator acts on an integrals going backward in time, and correspond to an anticausal ordering and to an interaction with the reversed sign

$$S(-\infty,\infty) = Te^{-i\int_\infty^{-\infty}\hat{H}_C(t')dt'} = \tilde{T}e^{i\int_{-\infty}^{\infty}\hat{H}_C(t')dt'} \ . \tag{B.14}$$

The Wick theorem is thus applied on averages where products of fermions operator are both in causal and anticausal order. Therefore the causal Green's function in Eq. B.1 is not only expressed as a function of products of bare causal Green's functions $G_0^C(t,t') = -i\langle T\hat{c}(t)\hat{c}^\dagger(t')\rangle$, but also anticausal Green's functions $G_0^A(t,t') = -i\langle \tilde{T}\hat{c}(t)\hat{c}^\dagger(t')\rangle$, and correlation functions $G_0^<(t,t') = i\langle \hat{c}(t)\hat{c}^\dagger(t')\rangle$ and $G_0^>(t,t') = -i\langle \hat{c}(t)\hat{c}^\dagger(t')\rangle$ appear.

The presence of the four different Green's function in the perturbation theory can be handled introducing the concept of Keldish contour [Schwinger, 1961, Keldysh, 1965], depicted in Fig. B.1. The time on the contour goes from $-\infty$ to $\infty$ then back to $-\infty$. A time ordering operator $T_\mathcal{K}$, following a clockwise orientation on the contour, and a Green's $G^\mathcal{K}(\tau,\tau')$ function can be defined

$$G^\mathcal{K}(\tau,\tau') = -i\langle T_\mathcal{K}\hat{c}(\tau)\hat{c}^\dagger(\tau')S_\mathcal{K}\rangle \tag{B.15}$$

where the operator $S_\mathcal{K}$ is defined as

$$S_\mathcal{K} = T_\mathcal{K}e^{-i\oint_\mathcal{K}\hat{H}_C(\tau')d\tau'} \tag{B.16}$$

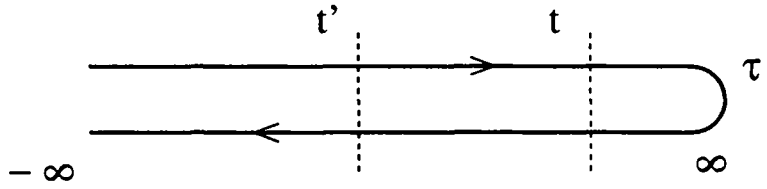


Figure B.1: Keldish contour

When $\tau$ and $\tau'$ are taken on the first upper branch of the Keldish contour the causal Green's function is obtained. The anticausal Green's function corresponds to $\tau$ and $\tau'$ on the lower branch, while in the correlation functions $\tau$ and $\tau'$ are on opposite branches, and thus automatically ordered in the contour. The Eq. B.15 has the same structure of the Eq. B.11, thus the same diagrammatic rules used in the case of $T = 0$ can be applied. In particular, integral equations describing the sum of infinite series of diagrams, as in the ladder approximation or random phase approximation (RPA), and the Dyson equation have the same form as in the zero temperature case. These equations defined on the Keldish contour can be rewritten back in a new set of equation defined on the ordinary time axis using the Langreth and Wilkins theorem [Langreth, 1968]. This theorem allows to express products and time integrals of two functions defined on a contour, as a function of their retarded, anticipated, and correlation part. The theorem can be used in an iterative way so that products and integrals in time of N functions can be easily obtained. We refer to [Haug, 1996] for details about this theorem. The Langreth and Wilkins relations are given in Tab.B.1. We give here some exemples about the use of this therorem. Consider, for instance product of two functions defined on the countour

$$C(\tau, \tau') = A(\tau, \tau')B(\tau', \tau) \tag{B.17}$$

then the Langreth and Wilkins theorem states that the retarded part of the function C (which is defined in term of ordinary times $t$ and $t'$) reads

$$C^{+}(t, t') = A^{+}(t, t')B^{<}(t', t) + A^{<}(t, t')B^{+}(t', t) \tag{B.18}$$

while for the correlation part of C we have

$$C^{<}(t, t') = A^{<}(t, t')B^{<}(t', t) \ . \tag{B.19}$$

This result can be used for instance in the expression 5.9

$$\Sigma_e(k, \tau, \tau') = \sum_{\alpha} g_e(\alpha) \int \frac{dq}{2\pi} i T_{e,\alpha}(k + q, \tau, \tau') G_{\alpha}(-q, \tau', \tau) \tag{B.20}$$

to obtain the expression for the retarded part of the self energy

$$\Sigma_e^+(k,t,t') = \sum_\alpha g_e(\alpha) \int \frac{dq}{2\pi} i T_{e,\alpha}^+(k+q,t,t') G_\alpha^<(-q,t',t) + T_{e,\alpha}^<(k+q,t,t') G_\alpha^+(-q,t',t) \quad \text{(B.21)}$$

and for the correlation part

$$\Sigma_e^<(k,t,t') = \sum_\alpha g_e(\alpha) \int \frac{dq}{2\pi} i T_{e,\alpha}^<(k+q,t,t') G_\alpha^>(-q,t',t) \ . \quad \text{(B.22)}$$

For integration on the contour we have different rules. For

$$C(\tau,\tau') = \oint_\mathcal{K} d\tau'' A(\tau,\tau'') B(\tau'',\tau') \quad \text{(B.23)}$$

the retarded and correlation part of $C$ can be expressed in term of intergrals on the ordinary time axis

$$C^+(t,t') = \int dt'' A^+(t,t'') B^+(t'',t') \quad \text{(B.24)}$$

$$C^<(t,t') = \int dt'' A^+(t,t'') B^<(t'',t') + A^<(t,t'') B^-(t'',t') \quad \text{(B.25)}$$

These last expressions are used in the Dyson , and Bethe Salpeter integral equations (Eqs.5.8, 5.11, 5.10). In fact, we can define the function describing all the e-h pairs with a given center of mass $q$

$$H_{eh}(q,\tau,\tau') = \int \frac{dk}{2\pi} i G_e(q-k,\tau,\tau') G_h(k,\tau,\tau') \quad \text{(B.26)}$$

then the Bethe Salpeter in Eq.5.10 become equivalent to the two equations:

$$T_{e,h}^+(q,t,t') = -a\delta(t-t'') + a \int dt'' H_{eh}^+(q,t,t'') T_{e,h}^+(q,t'',t') \quad \text{(B.27)}$$

$$T_{e,h}^<(q,t,t') = a \int dt'' H_{eh}^+(q,t,t'') T_{e,h}^<(q,t'',t') + H_{eh}^<(q,t,t'') T_{e,h}^+(q,t'',t') \quad \text{(B.28)}$$

| Contour | Real axis |
|---|---|
| $C = \oint AB$ | $C^< = \int A^+B^< + A^<B^-$<br>$C^+ = \int A^+B^+$ |
| $D = \oint ABC$ | $D^< = \int A^+B^+C^< + A^+B^<C^- + A^<B^-C^-$<br>$D^+ = \int A^+B^+C^+$ |
| $C(\tau,\tau') = A(\tau,\tau')B(\tau,\tau')$ | $C^+(t,t') = A^+(t,t')B^<(t,t') + A^<(t,t')B^+(t,t') + A^+(t,t')B^+(t,t')$<br>$C^<(t,t') = A^<(t,t')B^<(t,t')$ |
| $C(\tau,\tau') = A(\tau,\tau')B(\tau',\tau)$ | $C^+(t,t') = A^<(t,t')B^-(t',t) + A^+(t,t')B^<(t',t)$<br>$C^<(t,t') = A^<(t,t')B^>(t',t)$ |
| | |

Table B.1: Langreth and Wilkins relations

# Acknowledgments

I would like to thank all may collaborators: Vincenzo Savona, Cristiano Ciuti, Paolo Schwendimann, Antonio Quattropani, and Francesco Tassone. This thesis is the result of many ideas discussed fruitfully within this group. I'm particularly grateful to Antonio Quattropani and Paolo Schwendimann for having offered to me the possibility of a Ph.D at the EPFL, and for having transmitted part of their experience both in scientific and non scientific subjects. A special thank to Francesco Tassone who gave me precious hints in the initial stages of the thesis, and has been able to keep the collaboration active even at very large distance.

I acknowledge for encouragements and constructive discussions T. Amand, R. Ambigapathy, L. C. Andreani, G. Bastard, G. Bongiovanni, M. Colocci, A. D'Andrea, M. Di Ventra, B. Deveaud, V. Emiliani, R. Girlanda, G. Grosso, M. Gulia, S. Haacke, G. R. Hayes, M. Hartig, O. Heller, R. Houdré, M. Ilegems, S. W. Koch, X. Marie, P. Nozières, D. Oberli, G. Pastori-Parravicini, S. Pau, M. F. Pereira, C. A. Piguet, F. Quochi, F. Rossi, S. Savasta, P. E. Selbmann, L. J. Sham, J. L. Staehli, R. Stanley, B. Velický, Y. Yamamoto, and in particular R. Zimmermann for his contributions to the results presented in the last chapter of this thesis.

Finally, I whish to thank all my friends in Lausanne, my family, and in particular Carmen for her support and her infinite patience.

# Bibliography


[Agranovich, 1966] V. M. Agranovich, and A. O. Dubowskii, *Effect of retarded interaction on the exciton spectrum in one dymansional and two dimensional crystals*, Pis'ma Zh. Eksp. Teor. Fiz. **3** , 345 (1966) [JETP Lett. **3**, 233 (1996)].

[Ambigapathy, 1997] R. Ambigapathy, I. Bar-Joseph, D. Y. Oberli, S. Haacke, M. J. Brasil, F. Reinhardt, E. Kapon, and B. Deveaud, *Coulomb correlation and band gap renormalization at high carrier densities in quantum wires*, Phys. Rev. Lett. **78**, 3579 (1997).

[Amand, 1994] T. Amand, B. Dareys, B. Baylac, X. Marie, J. Barrau, M. Brousseau, D. J. Dunstan, and R. Planel, *Exciton formation and hole spin relaxation in intrinsic quantum wells*, Phys. Rev. B, **50**, 11624, (1994).

[Amand] T. Amand, Private Communication.

[Andreani, 1989] L. C. Andreani, *Ph. D. Thesis : Theory of excitons and polaritons in semiconductor quantum wells*, Scuola Normale Superiore, Pisa (1989).

[Andreani, 1990] L. C. Andreani and A. Pasquarello, *Accurate theory of excitons in $GaAs$-$Al_xGa_{1-x}As$ quantum wells.*, Phys. Rev. B **42**, 8928 (1990).

[Andreani, 1991] L. C. Andreani, F. Tassone, and F. Bassani, *Radiative lifetime of free excitons in quantum wells*, Solid State Commun. **77**, 641 (1991).

[Askari, 1985] F. Askari and P.Y. Yu, *Exciton-polariton bottleneck and the thermalization of polariton luminescence in CdS and CdSe*, Phys. Rev. B **31**, 6643 (1985).

[Bassani, 1975] F. Bassani and G. Pastori Parravicini, *Electronic states amd optical transitions in solids*, Pergamon Press, London (1975).

[Baym, 1961] G. Baym and L. P. Kadanoff, *Conservation laws and correlation functions*, Phys. Rev. **124**, 287 (1961).

[Bányai, 1998] L. Bányai, Q. T. Vu, B. Mieck, and H. Haug, *Ultrafast Quantum kinetics of time dependent RPA-screened Coulomb scattering*, Phys. Rev. Lett. **81**, 882 (1998).

[Blom, 1993] P. W. Blom, P. J. van Hall, C. Smit, L. P. Cuypers, and H. Wolter, *Selective exciton formation in thin GaAs-$Al_xGa_{1-x}As$ quantum wells*, Phys. Rev. Lett. **71**, 3878 (1993).

[Bobrysheva, 1980] A. I. Bobrisheva, V. T. Zukov, and S. I. Beryl, *The interaction of surface excitons*, phys. stat. solidi (b) **101**, 69 (1980).

[Bongiovanni, 1992] G. Bongiovanni and J. L. Staehli,*Electron hole plasma decay time in GaAs/AlGaAs quantum wells*, phys. stat. solidi (b) **173**, 365 (1992).

[Braun, 1998] W. Braun, M. Bayer, A. Forchel, O. M. Schmitt, L. Bányai, H. Haug, and A. I. Filin, *Size dependence of exciton exciton scattering in semiconductor quantum wires*, Phys. Rev. B **57**, 12 364 (1998).

[Buzatu, 1995] F. D. Buzatu, *Ground-state energy of the one dimensional Hubbard model in a simple self consistent version of the ladder approximation*, Mod. Phys. Lett. B **9**, 1149 (1995).

[Chang, 1984] K. J. Chang, S. Froyen, and M. L. Cohen, *Pressure coefficients of band gaps in semiconductors*, Solid State Commun. **50** 105 (1984).

[Cingolani, 1993] R. Cingolani, R. Rinaldi, M. Ferrara, G. C. La Rocca, H. Lage, D. Heitmann, K. Ploog, and H. Kalt, *Band gap renormalization in quantum wires*, Phys. Rev. B **48**, 14331 (1993).

[Citrin, 1993] D. S. Citrin, *Radiative lifetime of excitons in quantum wells: localization and phase-coherence effects*, Phys. Rev. B **47** 3832 (1993).

[Ciuti, 1998] C. Ciuti, V. Savona, C. Piermarocchi, A. Quattropani, and P. Schwendimann, *Role of the exchange of carriers in elastic exciton-exciton scattering in quantum wells*, Phys. Rev. B **58** 7926 (1998).

[Colocci, 1990] M. Colocci, M. Gurioli, and A. Vinattieri, *Thermal ionization of excitons in GaAs-AlGaAs quantum well structures*, J. Appl. Phys. **68**, 2809 (1990).

[Combescot, 1989] M. Combescot and R. Combescot, *Optical Stark effect of the exciton: biexcitonic origin of the shift*, Phys. Rev. B **40** , 3788 (1989).

[Danielewicz, 1984] P. Danielewicz, *Quantum theory of nonequilibrium processes*, Ann. of Phys. (USA) **152**, 239 (1984).

[Damen, 1990] T. C. Damen, Jagdeep Shah, D. Y. Oberli, D. S. Chemla, J. E. Cunningham, and J. M. Kuo, *Dynamics of exciton formation and relaxation in GaAs quantum wells*, Phys. Rev. B **42**, 7434 (1990).

[Deveaud, 1991a] B. Deveaud, F. Clérot, N. Roy, K. Satzke, B. Sermage, and D. S. Katzer,*Enhanced radiative recombination of free excitons in GaAs quantum wells* Phys. Rev. Lett. **67**, 2355 (1991).

[Deveaud, 1991b] B. Deveaud F. Clérot, K. Fujiwara, and K. Mitsunaga, *Raddiative properties of highly excited quantum wells*, Appl. Phys. Lett. **58**, 1485 (1991).

[Deveaud, 1993] B. Deveaud, B. Sermage, and D. S. Katzer, *Free exciton versus free carrier luminescence in a quantum well*, Journal de Physique IV Coll. C5, Supp. Journal de Physique II **3**, 11 (1993).

[Deveaud] B. Deveaud, Private Communication.

[Eccleston, 1992] R. Eccleston, B. F. Feuerbacher, J. Kuhl, W. W. Rüle, and K. Ploog, *Density dependent exciton radiative lifetimes in GaAs quantum wells*, Phys. Rev. B **45**, 11 403 (1992).

[Ell, 1998] C. Ell, J. Prineas, T. R. Nelson Jr., S. Park, H. M. Gibbs, G. Khitrova, S. W. Koch, and R. Houdré, *Influence of structural disorder and light coupling on the excitonic response of semiconductor microcavities*, Phys. Rev. Lett. **80**, 4795 (1998).

[Elliott, 1957] R. J. Elliott, *Intensity of optical absorption by excitons*, Phys. Rev. **108**, 1384 (1957).

[Emiliani, 1996] V. Emiliani, *Ph. D. Thesis: Dinamiche di tunneling in eterostrutture a pozzi quantici di semiconduttore II-V*, Universitá degli Studi di Roma, Roma (1996).

[Emiliani, 1997] V. Emiliani, S. Ceccherini, F. Bogani, M. Colocci, A. Frova, S. S. Shi, *Optical investigation of carrier tunneling in semiconductor nanostructures*, Phys. Rev. B **56**, 4807 (1997).

[Feldmann, 1987] J. Feldmann, G. Peter, E. O. Göbel, P. Dawson, K. Moore, C. Foxon, and R. J. Elliott, *Linewidth dependence of radiative exciton lifetimes in quantum wells*, Phys. Rev. Lett. **59**, 2337 (1987).

[Fernández, 1998] J. Fernández-Rossier, C. Tejedor, and R. Merlin, *Exciton condensates in semiconductor quantum wells emit coherent light*, Cond-mat/9806123.

[Gammon, 1995] D. Gammon, S. Roudin, T. L. D. S. Katzer, and C. S. Kyono, *Phonon broadening of excitons in $GaAs/Al_xGa_{1-x}As$ quantum wells*, Phys. Rev. B **51**, 16 785 (1995).

[Glutsch, 1993] S. Glutsch, and F. Bechstedt, *Effects of the Coulomb interaction on the optical spectra of quantum wires*, Phys. Rev. B **47**, 4315 (1993).

[Gréus, 1996] C. Gréus, A. Forchel, R. Spiegel, F. Faller, S. Benner, and H. Haug, *Phase space filling and band gap renormalization in the luminescence of highly excited InGaAs/GaAs quantum wires.*, Euro Phys. Lett. **34**, 213 (1996).

[Gulia, 1997] M. Gulia, F. Rossi, E. Molinari, P. E. Selbmann, and P. Lugli, *Phonon-assisted exciton formation and relaxation in*

*$GaAs/Al_xGa_{1-x}As$ quantum wells*, Phys. Rev. B **55**, R16 049 (1997).

[Imamoglu, 1996] A. Imamoglu, R. J. Ram, *Quantum dynamics of excitonic laser*, Physics Lett. A **214**, 193 (1996).

[Hanamura, 1972] E. Hanamura, *Optical response of many exciton system*, Solid. State. Commun. **11**, 485 (1972).

[Hanamura, 1977] E. Hanamura, and H. Haug, *Condensation effects of excitons*, Phys. Rep. **33**, 209 (1977).

[Haug, 1984] H. Haug, and S. Schmitt-Rink, *Electron theory of the optical properties of laser excited semiconductors*, Progr. Quantum Electronics **9** 3 (1984).

[Haug, 1996] H. Haug, and A. P. Jauho, *Quantum kinetics in transport and optical properties of semiconductors*, Springer, Berlin (1996).

[Hiroshima, 1989] T. Hiroshima, *Nonresonant excitonic optical nonlinearities in semiconductors*, Phys. Rev. B **40**, 3862 (1989).

[Hopfield, 1958] J. J. Hopfield, *Theory of the contribution of excitons to the complex dielectic constant of crystals*, Phys. Rev. **112**, 1555 (1958).

[Kadanoff, 1962] L. P. Kadanoff, and G. Baym, *Quantum statistical mechanics*, W. A. Benjamin, Reading (1962).

[Kagan, 1998] M. Y. Kagan, R. Frésard, M. Capezzali, and H. Beck, *One-electron spectral function of the attractive Hubbard model for intermediate coupling.*, Phys. Rev. B **57**, 5995 (1998)

[Kalt, 1996] H. Kalt, *Optical Properties of III-V Semiconductors* (Springer-Verlag, Berlin, 1996)

[Keldysh, 1965] L. V. Keldysh, *Diagram technique for nonequilibrium processes*, Sov. Phys. JETP, **20**, 1018 (1965).

[Kim, 1992] Dai-Sik Kim, J. Shah, J. E. Cunningham, T. C. Damen, W. Shäfer, M. Hartmann, and S. Schmitt-Rink, *Giant excitonic resonance in time-resolved four-wave mixing in quantum wells*, Phys. Rev. Lett. **68**, 1006 (1992).

[Kira, 1998] M. Kira, F. Jahnke, and S. W. Koch, *Microscopic theory of excitonic signatures in semiconductor photoluminescence*, Phys. Rev. Lett. **81** 3263 (1998).

[Knox, 1963] R. S. Knox, *Theory of excitons* , Solid State Phys., Supp. 5, Academic Press, New York (1963).

[Knox, 1992] W. H. Knox, in *Hot carriers in Semiconductor Nanostructures*, ed. by J. Shah, Academic Press, San Diego (1992).

[Knorr, 1998] A. Knorr, F. Steininger, B. Hanewinkel, S. Kuckenburg, P. Thomas, and S. W. Koch, *Thory of ultrafast spatio-temporal dynamics in semiconductor quantum wells: electronic wavepackets and near-field optics*, phys. stat. solidi (b) **206**, 139 (1998).

[Kozlov, 1996] V. Kozlov, P. Kelkar, A. Vertikov, A. Nurmikko, C. C. Chu, J. Han, C. G. Hua, and R. L. Gunshor, *Gain spectroscopy of excitonic molecules and its dynamics in a ZnSe single quantum well*, Phys. Rev. B **54**, 13 932 (1996).

[Kulakovskii, 1989] V.D. Kulakovskii, E. Lach, A. Forchel, and D. Grützmacher, *Band gap renormalization and band filling effects in a homogeneous electron hole plasma in InGaAs/InP single quantum wells*, Phys. Rev. B **40**, 8087 (1989).

[Kumar, 1996a] R. Kumar, A. S. Vengurlekar, S. S. Prabhu, J. Shah, and L. N. Pfeiffer, *Picosecond time evolution of free electron-hole pairs into excitons in quantum wells*, Phys. Rev. B **54**, 4891 (1996).

[Kumar, 1996b] R. Kumar, A. S. Vengurlekar, S. S. Prabhu, J. Shah, and L. N. Pfeiffer, *Measurements of frequency upconversion and picosecond excitation correlation luminescence spectra in GaAs quantum wells and determination of time constants describing exciton dynamics*, J. Appl. Phys. **80**, 5921 (1996).

[Kyun, 1998] B. Kyung, E. G. Klepfish, and P. E. Kornilovitch, *Density-induced breaking of pairs in the attractive Hubbard model*, Phys. Rev. Lett. **80** , 3109 (1998).

[Langreth, 1968] D. C. Langreth, and J. W. Wilkins, *Theory of spin resonance in diluite magnetic alloys*, Phys. Rev. B **6**, 3189 (1972).

[Landolt, 1982] *Physics of Group IV Elements and III-V Compounds* , edited by A. M. Hellwege and O. Madelung, Landolt-Börnstein, New Series, Group III, Vol. 17 , Pt. a (Springer-Verlag, Berlin, 1982).

[Lindberg, 1988] M. Lindberg, and S. W. Koch, *Effective Bloch equation for semiconductors*, Phys. Rev. B **38** , 3342 (1988).

[Mahan, 1981] D. G. Mahan, *Many particle physics*, Plenum Press (1981).

[Manzke, 1984] G. Manzke, V. May, and K. Henneberger, *Excited states and colective excitations in a dense gas of excitons*, phys. stat. solidi (b) **125** 693 (1984).

[Marie, 1998] X. Marie, J. Barrau, P. Le Jeune, T. Amand, and M. Brosseau, *Exciton formation in quantum wells*, phys. stat. solidi. (a) **10**, 359 (1998).

[Martinez-Pastor, 1993] J. Martinez-Pastor, A. Vinattieri, L. Carraresi, M. Colocci, Ph. Roussignol, and G. Weimann, *Temperature dependence of exciton lifetimes in* $GaAs/Al_xGa_{1-x}As$ *single quantum wells*, Phys. Rev. B **47**, 10456 (1993).

[Ogawa, 1991] T.Ogawa and T. Tagakahara, *Optical absorption and Sommerfels factors of one dimensional semiconductors: an exact treatment of excitonic effects*, Phys. Rev. B **44**, 8138 (1991).

[Östreich, 1998] T. Östreich, K. Schönhammer, and L. J. Sham, *Theory of exciton-exciton correlation in nonlinear optical response*, cond-mat/9807135 (1998); *Exciton-exciton correlation in nonlinear optical regime*, Phys. Rev. Lett. **74**, 4698 (1995).

[Pau, 1997] S. Pau, G. Björk, H. Cao, F. Tassone, R. Huang, Y. Yamamoto, and R. P. Stanley, *LO-phonon-enhanced microcavity polariton emission* , Phys. Rev. B **55**, R1942 (1997).

[Pereira, 1998] M. Pereira, and K. Henneberger *Microscopic theory of the influence of coulomb correlations in the light emission properties of semiconductor quantum wells*, Phys. Rev. B **58**, 1064 (1998).

[Pfeffer, 1984] P. Pfeffer, I. Gorczyca, and W. Zawadzki, *Theory of free electron optical absorption in n-GaAs*, Solid State Commun. **51**, 179 (1984).

[Piermarocchi, 1995] C. Piermarocchi, F. Tassone, V. Savona, A. Quattropani, and P. Schwendimann, *Effect of the scattering by phonons on the temperature dependence of the free QW excitons radiative lifetimes*, Il Nuovo Cimento **17** D, 1663 (1995).

[Piermarocchi, 1996] C. Piermarocchi, F. Tassone, V. Savona, A. Quattropani, and P. Schwendimann, *Nonequilibrium dynamics of free quantum well excitons in time resolved photoluminescence*, Phys. Rev B **53**, 15 834 (1996).

[Piermarocchi, 1997a] C. Piermarocchi, F. Tassone, V. Savona, A. Quattropani, and P. Schwendimann, *Exciton formation rates in GaAs quantum wells* Phys. Rev B **55**, 1333 (1997).

[Piermarocchi, 1997b] C. Piermarocchi, V. Savona, A. Quattropani, P. Schwendimann, and F. Tassone, *Photoluminescence and carrier dynamics in GaAs quantum wells*, phys. stat. solidi (a) **164**, 221 (1997).

[Piermarocchi, 1997c] C. Piermarocchi, V. Savona, A. Quattropani, P. Schwendimann,and F. Tassone, *Role of carrier phonon interaction on the exciton formation in quantum wells*, phys. stat. solidi (b) **204**, 191 (1997).

[Piermarocchi, 1998a] C. Piermarocchi, V. Savona, A. Quattropani, P. E. Selbmann, P. Schwendimann, and F. Tassone, *Photoluminescence spectra in semiconductor confined systems: effects of Coulomb correlation*, phys. stat. solidi (b) **206**, 455 (1998).

[Piermarocchi, 1998b] C. Piermarocchi, R. Ambigapathy, D. Oberli, E. Kapon, B. Deveaud, and F. Tassone, *Unpublished.*

[Prabhu, 1996] S. S. Prabhu, A. S. Vengurlekar, and J. Shah, *Picosecond luminescence study of exciton formation dynamics in CdSe*, Phys. Rev. B **53**, R 10465 (1996).

[Quochi, 1998] F. Quochi, G. Bongiovanni, A. Mura, J. L. Staehli, B. Deveaud, R. P. Stanley, U. Osterle, and R. Houdré, *Strong driven semiconductor microcavities: from the polariton doublet to an ac Stark triplet*, Phys. Rev. Lett. **80** , 4733 (1998).

[Robart, 1995] D. Robart, X. Marie, B. Baylac, T. Amand, M. Brousseau, G. Bacquet, G. Debart, R. Planel, and J. M. Gerard, *Dynamical equilibrium between excitons and free carriers in quantum wells*, Solid State Commun. **95**, 287 (1995).

[Rossi, 1996] F. Rossi, and E. Molinari,*Coulomb induced suppression of band edge singularities in the optical spectra of realistic quantum wire structures*, Phys. Rev. Lett. **76**, 3642 (1996).

[Roussignol, 1992] Ph. Roussignol, C. Delalande, A. Vinattieri, L. Carraresi, and M. Colocci, *Dynamics of exciton relaxation in* $GaAs/Al_xGa_{1-x}As$ *quantum wells* , Phys. Rev. B **45**, 6965 (1992).

[Rücker, 1992] H. Rücker, E. Molinari, and P. Lugli, *Microscopic calculation of the electron-phonon interaction in quantum wells*, Phys. Rev. B **45**, 6747 (1992).

[Sasaki, 1989] F. Sasaki and Y. Masumoto,*Tunneling and relaxation of photogenerated carriers in semiconductor quantum wells*, Phys. Rev. B **40**, 3996 (1989).

[Savasta, 1996] S. Savasta, and R. Girlanda, *Quantum optical effects and nonlinear dynamics in interacting electron systems*, Phys. Rev. Lett. **77**, 4736 (1996).

[Savona, 1995] V. Savona, L. C. Andreani, A. Quattropani, and P. Schwendimann, *Quantum well excitons in semiconductor microcavities: unified treatment of weak and strong coupling regimes*, Solid State Commun. **93** , 733 (1995).

[Savona, 1996] V. Savona, F. Tassone, C. Piermarocchi, A. Quattropani and P. Schwendimann, *Theory of polariton photoluminescence in arbitrary semiconductor microcavity structures*,Phys. Rev. B **53**, 13 051 (1996).

[Savona, 1997] V. Savona, C. Piermarocchi, A. Quattropani, F. Tassone, and P. Schwendimann, *Microscopic theory of motional narrowing of microcavity polaritons in a disordered potential*, Phys. Rev. Lett. **78**, 4470 (1997).

[Savona, 1997b] V. Savona, and C. Piermarocchi *Microcavity polaritons: Homogeneous and Inhomogeneous broadening in the strong coupling regime*, phys. stat. solidi (a) **164**, 45 (1997).

[Savona, 1998] V. Savona, C. Piermarocchi, A. Quattropani, P. Schwendimann, and F. Tassone, *Optical properties of microcavity polaritons*, Phase Transitions (1998).

[Schepe, 1998] R. Schepe, T. Schmielau, D. Tamme, and K. Henneberger, *Damping and T-Matrix in dense e-h plasmas*, phys. stat. solidi (b) **206**, 273 (1998).

[Schlottmann, 1994] P. Schlottmann, *A soluble model for the formation of exciton bands and electron-hole droplets in one dimension* , J. Phys. Condens. Matter **6**, 3719 (1994).

[Schwinger, 1961] J. Schwinger, *Brownian motion of a quantum oscillator*, Journ. Math. Phys. **2**, 407 (1961).

[Sermage, 1996] B. Sermage, S. Long, I. Abram, J. Y. Marzin, J. Bloch, R. Planel and V. Thierry-Mieg, *Time resolved spontaneous emission of excitons in a microcavity: Behavior of the individual exciton-photons mixed states*, Phys. Rev. B **53**, 16 516 (1996).

[Sham, 1966] L. J. Sham, and T. M. Rice, *Many particle derivation of the effective mass equation for the Wannier exciton*, Phys. Rev. **144** 708 (1966).

[Shultheis, 1986] L. Schultheis, A. Honold, J. Kuhl, K. Köler, and C. W. Tu, *Optical dephasing of homogeneously broadened two-dimensional exciton transitions in GaAs quantum wells* , Phys. Rev. B **34**, 9027 (1986).

[Stanley, 1998] R. P. Stanley, C. Piermarocchi, R. Houdré, F. Tassone, U. Osterle, and M. Ilegems, *Inhibited acoustic phonon scattering of*

*cavity polaritons in semiconductor microcavities, Unpublished* (1998).

[Stolz, 1979] H. Stolz, and R. Zimmermann, *Correlated pairs and a Mass action law in two component Fermi systems*, phys. stat. solidi (b) **94**, 135 (1979).

[Stolz, 1989] H. Stolz, D. Schwarze, W. von der Osten, and G. Weimann, *Transient optical alignment and relaxation of excitons in GaAs/AlGaAs quantum wells*, Superlatt. Microstruct. **6**, 271 (1989).

[Strobel, 1991] R. Strobel, R. Eccelston, J. Kuhl, and K. Köler,*Measurement of exciton formation time and electron and hole tunneling times in a double quantum well structure* Phys. Rev. B **43**, 12564 (1991).

[Sumi, 1975] H. Sumi, *On the exciton luminescence at low temperatures: Importance of the polariton viewpoint*, J. Phys, Soc. Jpn. **21**, 1936 (1975).

[Tassone, 1996] F. Tassone, C. Piermarocchi, V. Savona, A. Quattropani, and P. Schwendimann, *Photoluminescence decay times in strong coupling semiconductors microcavities*, Phys. Rev. B **53**, R7642 (1996).

[Tassone, 1997] F. Tassone, C. Piermarocchi, V. Savona, A. Quattropani, and P. Schwendimann, *Bottleneck effects in the relaxation and photoluminescence of microcavity polaritons*, Phys. Rev. B **56**, 7554 (1997).

[Tassone, 1998] F. Tassone, and C. Piermarocchi,*Electron-hole correlation effects in the emission of light from quantum wires* Cond-mat/9808156 (1998).

[Tassone, 1998b] F. Tassone, R. Huang, and Y. Yamamoto,*Evidence for stimulated scattering of excitons into microcavity polaritons* Cond-mat/9801157 (1998).

[Toyozawa, 1959] Y. Toyozawa, *On the dynamical behavior of an exciton*, Progr. Theor. Phys. Suppl. **12**, 111 (1959).

[Trankle, 1987] G. Tränkle, H. Leier, A. Forchel, H. Haug, C. Ell, and G. Weimann, *Dimensionality dependence of the band gap renormalization in two and three dimensional electron hole plasmas in GaAs.* Phys. Rev. Lett. **58**, 419 (1987).

[Triques, 1997] A. L. C. Triques, and José A. Brum, *Exciton center of mass dispersion in semiconductor quantum wells*, Phys. Rev. B **56**, 2094 (1997).

[Wainstain, 1998] J. Wainstain, C. Delalande, D. Gendt, M. Voos, J. Bloch, V. Thierry-Mieg, and R. Planel, *Dynamics of polaritons in a semiconductor multiple quantum well microcavity*, Phys. Rev. B **58**, 7269 (1998).

[Wannier, 1937] G. H. Wannier,*The structure of electronic excitation levels in insulating crystals*, Phys. Rev. **52** , 191 (1937).

[Weisbuch, 1979] C. Weisbuch, and R. Ulbrich, *Spatial and spectral features of polariton fluorescence*, J. of Lumin., **18/19**, 27 (1979).

[Welber, 1975] B. Welber, M. Cardona, C. K. Kim, and S. Rodriguez, *Dependence of the direct energy gap of GaAs on hydrostatic pressure*, Phys. Rev. B **12**, 5729 (1975).

[Whittaker, 1998] D. M. Whittaker, *What determines inhomogeneous linewidths in semiconductor microcavities?*, Phys. Rev. Lett. **80**, 4791 (1998).

[Wolfe, 1970] E. M. Wolfe, G. E. Stilmann, and W. T. Lindley, *Electron mobility in high-purity GaAs*, J. Appl. Phys. **41**, 3088(1970).

[Yoon, 1996] H. W. Yoon, D. R. Wake, J. P. Wolfe,*Effect of exciton carrier thermodynamics on the GaAs quantum well photoluminescence*, Phys. Rev. B **55**, 2763 (1996).

[Yu, 1995] H. Yu, C. Roberts, and R. Murray, *Exciton recombination dynamics in $In_xGa_{1-x}As/GaAs$ quantum wells*, Phys. Rev. B **52**, 1493 (1995).

[Yura, 1994] F. Yura, and E. Hanamura, *Coherent light emission from condensing polaritons*, Phys. Rev. B **50**, 15 457 (1994).

[Zimmermann, 1988] R. Zimmermann, *Many particle theory of highly excited semiconductors*, Teubner, Liepzig (1988).

# Curriculum Vitæ

## Carlo Piermarocchi

Birth date: 10th of May 1969. Birth place Fermo, Italy.

### Education

- 1988: Secondary school diploma ("Maturità Classica") at the Liceo-Ginnasio "Annibal Caro", in Fermo, Italy, with the mark 60/60
- 1994: Degree in theoretical physics, University of Pisa, with the mark 110/110 cum laude. Degree thesis "Electronic structure of silicon and germanium superlattices", under the supervision of Prof. G. Grosso

### Activity

- 1995: Starts his activity as PhD student and assistant at the Ecole Polytechnique Fédérale de Lausanne, Switzerland, in the group of Prof. Antonio Quattropani
- 1995-1998: Teaching assistant in the courses of Classical mechanics and Quantum mechanics
- Partecipation to international conferences:

  1995: Optics of Excitons in Confined Systems, Cortona, Italy

  1996: European Physical Society/Condensed Matter, Stresa, Italy; Epioptics 4, Erice, Italy.

  1997: Hot carriers in Semiconductors, Berlin, Germany; Nonlinear Optics and Excitation Kinetics in Semiconductors, Graal-Müritz, Germany.

  1997: (15th Sept-31st Oct) Invited by Prof. Yamamoto at Stanford University, USA.

  1998: Symposium on Microcavities: Quantum electrodynamics and devices (invited), Loveno, Italy.

- Post degree formation:

  1995: Transports in solids (Prof. P. B. Allen, New York University)

  1996: Chaos et phénomènes non linéaires (Prof. H. Kunz, Ecole Polytechnique, Lausanne)

**Address:**
DP-IPT
Ecole Polytechnique Fédérale de Lausanne
PHB-Ecublens, CH-1015 Lausanne
Switzerland
ph: ++41-21-693 3419
fax: ++41-21-693 5419
e-mail Carlo.Piermarocchi@epfl.ch

**Private address:**
Avenue de Provence, 84
CH-1007 Lausanne
Switzerland
ph: ++41-21-624 08 79

## Publications

- C. Piermarocchi, F. Tassone, V. Savona, A. Quattropani, and P. Schwendimann, *Effect of the scattering by phonons on the temperature dependence of the free QW excitons radiative lifetimes*, Il Nuovo Cimento **17** D, 1663 (1995).

- G. Grosso, and C. Piermarocchi, *Tight-binding model and interaction scaling laws for silicon and germanium*, Phys. Rev. B **51**, 16772 (1995).

- V. Savona, F. Tassone, C. Piermarocchi, A. Quattropani, P. Schwendimann, and L. C. Andreani, *Light emission from quantum well excitons in semiconductor microcavities*, Il Nuovo Cimento **17** D, 1713 (1995).

- C. Piermarocchi, F. Tassone, V. Savona, A. Quattropani, and P. Schwendimann, *Nonequilibrium dynamics of free quantum well excitons in time resolved photoluminescence*, Phys. Rev B **53**, 15 834 (1996).

- F. Tassone, C. Piermarocchi, V. Savona, A. Quattropani, and P. Schwendimann, *Photoluminescence decay times in strong coupling semiconductors microcavities*, Phys. Rev. B **53**, R7642 (1996).

- V. Savona, F. Tassone, C. Piermarocchi, A. Quattropani and P. Schwendimann, *Theory of polariton photoluminescence in arbitrary semiconductor microcavity structures*,Phys. Rev. B **53**, 13 051 (1996).

- G. Grosso, G. Pastori Parravicini, and C. Piermarocchi, *Valley splitting in triangular Si(001) quantum wells*, Phys. Rev. B **54**, 16 393 (1996).

- F. Tassone, C. Piermarocchi, V. Savona, A. Quattropani, and P. Schwendimann, *Theory of photoluminescence of microcavity exciton-polaritons in the strong coupling regime*, QELS '96.Summaries of Papers Presented at the Quantum Electronics and Laser Science Conference. Vol.10 1996 Technical Digest Series. Conference Edition Opt. Soc. America, Washington, DC, USA, p.159 (1996).

- C. Piermarocchi, F. Tassone, V. Savona, A. Quattropani, and P. Schwendimann, *Exciton formation rates in GaAs quantum wells* Phys. Rev B **55**, 1333 (1997).

- C. Piermarocchi, V. Savona, A. Quattropani, P. Schwendimann, and F. Tassone, *Photoluminescence and carrier dynamics in GaAs quantum wells*, phys. stat. solidi (a) **164**, 221 (1997).

- C. Piermarocchi, V. Savona, A. Quattropani, P. Schwendimann,and F. Tassone, *Role of carrier phonon interaction on the exciton formation in quantum wells*, phys. stat. solidi (b) **204**, 191 (1997).
- V. Savona, and C. Piermarocchi *Microcavity polaritons: Homogeneous and Inhomogeneous broadening in the strong coupling regime*, phys. stat. solidi (a) **164**, 45 (1997).
- V. Savona, C. Piermarocchi, A. Quattropani, F. Tassone, and P. Schwendimann, *Microscopic theory of motional narrowing of microcavity polaritons in a disordered potential*, Phys. Rev. Lett. **78**, 4470 (1997).
- V. Savona, F. Tassone, C. Piermarocchi, A. Quattropani, and P. Schwendimann, *Influence of disorder on the optical properties of microcavity embedded quantum wells*, 23rd International Conference on the Physics of Semiconductors.World Scientific, Singapore, 3115 1996.
- F. Tassone, C. Piermarocchi, V. Savona, A. Quattropani, and P. Schwendimann, *Bottleneck effects in the relaxation and photoluminescence of microcavity polaritons*, Phys. Rev. B **56**, 7554 (1997).
- M. Di Ventra, G. Grosso, G. Pastori Parravicini, and C. Piermarocchi, *Electronic structure of n-i-p-i Si superlattices*, Journal of Physics, Cond. Matt. **9**, L657 (1997).
- C. Piermarocchi, V. Savona, A. Quattropani, P. E. Selbmann, P. Schwendimann, and F. Tassone, *Photoluminescence spectra in semiconductor confined systems: effects of Coulomb correlation*, phys. stat. solidi (b) **206**, 455 (1998).
- F. Tassone, and C. Piermarocchi,*Electron-hole correlation effects in the emission of light from quantum wires* Cond-mat/9808156 (1998).
- C. Ciuti, V. Savona, C. Piermarocchi, A. Quattropani, and P. Schwendimann, *Role of the exchange of carriers in elastic exciton-exciton scattering in quantum wells*, Phys. Rev. B **58** 7926 (1998).
- C. Ciuti, V. Savona, C. Piermarocchi, A. Quattropani, and P. Schwendimann, *Threshold behavior in the collision broadening of microcavity polaritons*, Phys. Rev. B **58**, R10 123 (1998).
- V. Savona, C. Piermarocchi, A. Quattropani, P. Schwendimann, and F. Tassone, *Optical properties of microcavity polaritons*, Phase Transitions (1998).